

## An Improved HR Diagram for the Orion Trapezium Cluster

MIN FANG,<sup>1,2</sup> JINYOUNG SERENA KIM,<sup>1,2</sup> ILARIA PASCUCCI,<sup>3,2</sup> AND DÁNIEL APAI<sup>1,3,2</sup>

<sup>1</sup>*Department of Astronomy, University of Arizona, 933 North Cherry Avenue, Tucson, AZ 85721, USA*

<sup>2</sup>*Earths in Other Solar Systems Team, NASA Nexus for Exoplanet System Science*

<sup>3</sup>*Department of Planetary Sciences, University of Arizona, 1629 East University Boulevard, Tucson, AZ 85721, USA*

### ABSTRACT

In this paper, we present a study of the Trapezium cluster in Orion. We analyze flux-calibrated VLT/MUSE spectra of 361 stars to simultaneously measure the spectral types, reddening, and the optical veiling due to accretion. We find that the extinction law from Cardelli et al. (1989) with a total-to-selective extinction value of  $R_V = 5.5$  is more suitable for this cluster. For 68% of the sample the new spectral types are consistent with literature spectral types within 2 subclasses, but as expected, we derive systematically later types than the literature by one to two subclasses for the sources with significant accretion levels. Here we present an improved Hertzsprung-Russell (H-R) diagram of the Trapezium cluster, in which the contamination by optical veiling on spectral types and stellar luminosities has been properly removed. A comparison of the locations of the stars in the H-R diagram with the non-magnetic and magnetic pre-main sequence evolutionary tracks indicates an age of 1–2 Myr. The magnetic pre-main sequence evolutionary tracks can better explain the luminosities of the low-mass stars. In the H-R diagram, the cluster exhibits a large luminosity spread ( $\sigma(\text{Log } L_*/L_\odot) \sim 0.3$ ). By collecting a sample of 14 clusters/groups with different ages, we find that the luminosity spread tends to be constant ( $\sigma(\text{Log } L_*/L_\odot) \sim 0.2\text{--}0.25$ ) after 2 Myr, which suggests that age spread is not the main cause of the spread. There are  $\sim 0.1$  dex larger luminosity spreads for the younger clusters, e.g., the Trapezium cluster, than the older clusters, which can be explained by the starspots, accretion history and circumstellar disk orientations.

*Keywords:* accretion, accretion disks — planetary systems: protoplanetary disks — stars: pre-main sequence

### 1. INTRODUCTION

T Tauri stars (TTSs) are low-mass pre-main sequence (PMS) stars, characterized by large variability and strong emission lines (Joy 1945). They are classified as either classical T Tauri stars (CTTSs) or weak-lined T Tauri stars (WTTSs) based on the strength of their H $\alpha$  emission line (e.g., Herbig & Bell 1988): CTTSs exhibit broad and strong H $\alpha$  emission lines attributed to accretion, while WTTSs show narrow and weak H $\alpha$  emission lines due to chromospheric activity (White & Basri 2003).

For CTTSs, accretion produces not only strong permitted emission lines, such as the hydrogen Balmer series, but also ultraviolet/optical excess continuum emissions (Calvet & Gullbring 1998), which veil the photospheric absorption features in stellar spectra (White & Hillenbrand 2004). Without accounting for this veiling effect, the estimated spectral types (of the veiled spectra) tend to appear earlier than the actual

spectral types (e.g. Herczeg & Hillenbrand 2014). This effect further complicates the analysis of the extinction and luminosity of young stars. Brightness variability of young stars is another complicating factor when deriving extinction and stellar luminosity from broadband photometry observed at different times, and this variability affects both CTTSs and WTTSs (see extreme cases like the CTTS GI Tau in Guo et al. 2018 and the WTTS LkCa 4 in Gully-Santiago et al. 2017).

Both spectral type (SpT), which is converted to an effective temperature ( $T_{\text{eff}}$ ) via a SpT- $T_{\text{eff}}$  relation (e.g., Pecaú & Mamajek 2013), and stellar luminosity ( $L_*$ ) are necessary to place young stars in the H-R diagram. From their locations in the H-R diagram compared to theoretical isochrones, ages and masses of young stars are determined (e.g. Hillenbrand 1997). Errors in measuring SpT and  $L_*$  could result in luminosity scatter in H-R diagram, which may be wrongly interpreted as an age spread (Hillenbrand et al. 2008; Soderblom et al. 2014). Simultaneous measurements of extinction,

ultraviolet/optical excess continuum emission, SpT, and  $L_*$  have been performed on flux-calibrated optical spectra of young stars in nearby low-mass star-forming regions, e.g. Taurus, Lupus, Chamaeleon I, etc. (Herczeg & Hillenbrand 2014; Alcalá et al. 2014, 2017; Manara et al. 2016, 2017b). In this work, we perform a similar study for the massive Orion Trapezium Cluster.

The Trapezium Cluster in the heart of the Orion nebula, at an age of  $\sim 1\text{--}2$  Myr (Hillenbrand 1997; Da Rio et al. 2010), is one of the nearest ( $388 \pm 10$  pc Kounkel et al. 2017) massive clusters, and has been an excellent laboratory for studying critical aspects of star and planet formation, e.g., initial mass function, cluster formation, protoplanetary disk evolution (Hillenbrand 1997; Hillenbrand & Carpenter 2000; Luhman et al. 2000; Slesnick et al. 2004; Da Rio et al. 2010, 2012; Hillenbrand et al. 1998; Lada et al. 2000; Eisner et al. 2018).

Here, we simultaneously derive the extinction, veiling, SpT, and  $L_*$  of young stars in the Trapezium Cluster, based on wide field spectroscopic data generated by the integral field spectrograph MUSE on the VLT (Bacon et al. 2014). In §2, we describe our data and spectral extraction. In §3, we present our analysis, which includes spectral typing and measurements of stellar properties. In §4, we discuss the suitable extinction law in the Trapezium cluster. In §5, we compare our measurements with those in the literature, and construct the H-R diagram of the cluster in §6. We discuss the implications of our results in §7 and summarize our findings in §8.

## 2. DATA

The data were taken with the Multi-Unit Spectroscopic Explorer (MUSE). MUSE is the second-generation Integral Field Unit (IFU) mounted on the Very Large Telescope (VLT) at the Nasmyth B focus of the Yepun (the VLT UT4 telescope) in Paranal, Chile. The observations were carried out during the first commissioning run (Bacon et al. 2014), under photometric conditions with the DIMM (Differential Image Motion Monitor) seeing ranging from  $0''.67$  to  $1''.25$ , and airmass changing from 1.067 to 1.483 (Weilbacher et al. 2015). The observations are performed in Wide Field Mode with a field of view (FoV) covering  $1' \times 1'$  and a pixel size of  $0''.2 \times 0''.2$ . A total of 30 pointings over a 6-by-5 mosaic are taken to cover the Orion Trapezium Cluster with a field of  $5.9 \times 4.9$ .

The data have been reduced with the public MUSE pipeline by Weilbacher et al. (2015), which provides two versions of wavelength and flux-calibrated IFU datacubes with a sampling of  $1.25 \text{ \AA}$  and  $0.85 \text{ \AA}$  and a

spectral resolution of  $\sim 3,000$ . These are publicly available<sup>1</sup>. In this work, we take advantage of the reduced dataset with a sampling of  $1.25 \text{ \AA}$  to characterize the properties of young stars in the cluster.

We extract the spectra by performing aperture photometry on each wavelength plane of the reduced IFU datacubes. For isolated sources, we adopt an aperture of  $0''.8$  and a sky annulus from  $2''.0$  to  $3''.0$ , while an aperture of  $0''.6$  is used for objects that have nearby sources with separations less than  $3''.0$ . For objects that appear near bright sources, we adopt both a smaller aperture ( $0''.6$ ) and smaller sky annulus ( $0''.8$  to  $1''.6$ ), in order to reduce the contamination. We apply wavelength-dependent aperture correction for each source. Due to variations of the seeing and airmass during the observations, we have divided the field into 30 sub-fields, and obtained the aperture corrections in each sub-field. The aperture corrections for individual sources are obtained using the isolated bright point sources by comparing their fluxes extracted using the apertures used for the targets and a large aperture of  $2''.0$  and sky annulus from  $3''.0$  to  $4''.0$ . Figure 1 shows the distribution of sources with extracted spectra within the cluster, and Table 1 list these sources.

The relative flux calibration of MUSE data is expected to be accurate to at least 5% (Weilbacher et al. 2015). We check the absolute flux calibration using the bright HD 37042, see Figure 1. A comparison between the MUSE spectra for HD 37042 and the best-fit model atmosphere suggests that the flux is underestimated only by  $\sim 5\%$ ; see the detailed description in Appendix A. Therefore, we adjust the flux calibration levels using the ratio between the observed spectra and the best-fit model of HD 37042. We use the star HD 37021, adopting  $T_{\text{eff}} = 18500 \text{ K}$ , in the field to test our flux calibration. We correct the spectrum of HD 37021 using the wavelength-dependent factor obtained from HD 37042, and compare it with its best-fit model atmosphere. The median difference between them is about 2%.

## 3. SPECTRAL FITTING AND STELLAR PROPERTIES

### 3.1. Pre-main sequence spectral templates

In Appendix B, we list the WTTSSs with X-shooter spectra that we used as PMS spectral templates. These sources are from the  $\eta$  Cha cluster, the TW Hydrae Association, the Lupus star-forming region, the  $\sigma$  Ori cluster, Upper Sco, Taurus, and the Cha I star-forming

<sup>1</sup> The reduced data are downloadable via the link <http://MUSE-vlt.eu/science/m42/>

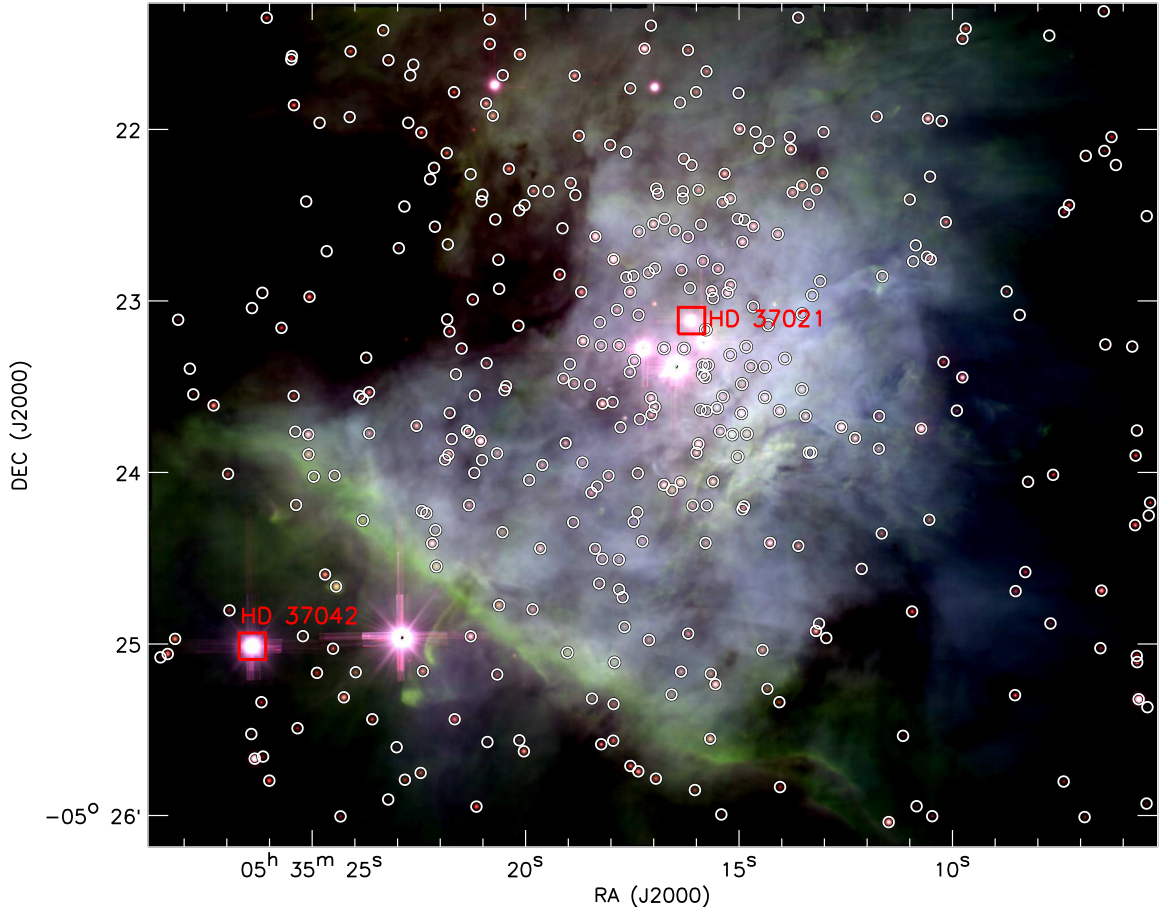


**Figure 1.** Three-color image of the Trapezium Cluster created with the MUSE data integrated over 5,000-6,000Å (blue), 6,000-7,000Å (green), and 7,500-8,500Å (red). The white open circles mark the sources for which spectra are extracted for the study in this work. Red squares show the two sources, HD 37042 and HD 37021, which were used to set and to verify the flux calibration levels.

region. Most of the sources we used for this study have been already published (Manara et al. 2013, 2017a; Rugel et al. 2018).

We extract the spectra of these sources from the X-shooter phase III data archive. The X-shooter phase III spectral data are flux calibrated, but not corrected for the slit losses. We re-calibrate these spectra using the standard star observed closest in time to each source and with the similar airmass to the source and the same instrumental setting as the source. For each standard star, we obtain the BOSZ Kurucz model atmosphere (Mészáros et al. 2012) corresponding to its spectral type. Next, we fit its broad-band photometry using the aforementioned model with two free parameters, extinction and stellar angular radius as in Fang et al. (2009, 2013a). Then, we shift and rotationally broaden the best-fit model atmosphere and degrade it to the X-shooter spectral resolution of the standard star. In the optical bands (UVB and VIS arm), the ratio be-

tween the X-shooter phase III spectrum and model spectrum is fitted with a 5-order polynomial function, from which we obtain the flux correction as a function of wavelengths. Implementing the correction, we obtain the flux-corrected spectra of the source and the standard star in the same wavelength. We divide the flux-corrected spectrum of the standard star by its model spectrum to obtain the telluric spectrum. The telluric spectrum is then scaled to match the telluric absorption in the spectrum of the source, and the scaled telluric spectrum is then applied for telluric correction of the spectrum of the source by dividing the flux-corrected spectrum by the scaled telluric spectrum. In the near-infrared bands (NIR arm), we directly implement the ratio between the X-shooter phase III spectrum and model spectrum of the standard star to correct the X-Shooter phase III spectrum of the source. In this way, we can correct for both the telluric absorption and flux.

All of the WTTSSs used as stellar templates have been previously classified in the literature (see Appendix B). In the Appendix B, we also describe how we determine the spectral types of individual sources used in this work as well as their visual extinction. The majority of the sources have negligible extinction based on their photometry in optical and near-infrared bands. For the sources with measurements of extinction, we list their visual extinction and deredden their X-shooter spectra using the visual extinction with the extinction law from Cardelli et al. (1989), adopting a total-to-selective extinction value of  $R_V = 3.1$ . All the X-shooter templates have been then degraded to the spectral resolution ( $\sim 3000$ ) of the MUSE spectra. For the X-shooter spectra with the same spectral types, we obtain one mean spectrum from their degraded spectra and use it as the X-shooter template with that spectral type. This set of the X-shooter templates have been employed to do the spectral classification of young stars in the North America and Pelican Nebulae Region (Fang et al. 2020).

### 3.2. Spectral typing

We determine the spectral types of the targets with MUSE spectra by fitting their spectra over  $\sim 5,500$ – $9,000 \text{ \AA}$  with the spectral templates constructed with X-shooter spectra. For one source (Source 133) in our sample with an early-G type, earlier than the ones of X-shooter templates, we fit it with the model atmosphere with a solar abundance and surface gravity  $\log g = 4.0$  from Husser et al. (2013). Our fitting procedure employs three free parameters: the spectral type, the extinction ( $A_V$ ) in the  $V$  band, and the veiling due to accretion. Given that the spectral resolution of MUSE is relatively low ( $\sim 3,000$ ), we do not consider the rotational broadening of the stars in the fitting. A Markov Chain Monte Carlo (MCMC) procedure is used to find the best-fit model parameters. When running the MCMC procedure, the used spectral templates are interpolated over spectral types using the grid of our spectral templates. Then an excess flux is added to the spectral template, which is parameterized as  $r_{7465} = \frac{F_{\text{excess}, 7465}}{F_{\text{phot}, 7465}}$ , where  $r_{7465}$  is the veiling at  $7465 \text{ \AA}$ ,  $F_{\text{excess}, 7465}$  is the excess flux at  $7465 \text{ \AA}$ , and  $F_{\text{phot}, 7465}$  is the photospheric emission at  $7465 \text{ \AA}$ . We choose  $7465 \text{ \AA}$  since at this wavelength there are no telluric absorption features and no strong absorption photospheric features. We adopt two types of the Accretion Continuum Spectrum. One is the same as in Herczeg & Hillenbrand (2014), and is approximated by a constant over  $5500$ – $9000 \text{ \AA}$ , and the other is assumed to be a blackbody spectrum with  $T = 7000 \text{ K}$  as in Da Rio et al. (2010). The veiled spectral template is then reddened with a visual extinction  $A_V$  using the

extinction law from Cardelli et al. (1989) with  $R_V = 3.1$  (typical of interstellar medium dust) and  $5.5$ . The resulting template is normalized at  $7465 \text{ \AA}$ , and compared with the normalized spectrum of each object. In Fig. 2, we show the posterior distributions with the best-fit parameters and their uncertainties for Source 68 as an example. With different assumptions, its spectral type,  $A_V$  and  $r_{7465}$  range from M2.2 to M2.7, 1.20 to 1.96 mag, and 0.23 to 0.48, respectively.

In total, we measure spectral types for 361 sources. Among them, 360 are determined with X-Shooter templates, and one (Source 133) uses the model atmosphere. There is no significant systematic difference (median  $\Delta \text{SpT} \lesssim 0.15$  subclass) in the spectral type derived based on different extinction  $R_V$  and the shapes of Accretion Continuum Spectrum. For more than 96% of the sources the spectral types agree well with each other within one subclass. Larger differences are seen mostly among the K or G type sources and/or with large veiling. For the constant Accretion Continuum Spectrum case, there are 3 sources with differences around 1 subclasses between  $R_V = 3.1$  and  $5.5$ . Two of them are G spectral type sources, and one is mid-K spectral type. In these cases the weak photospheric features from their spectra make their spectral types poorly constrained.

### 3.3. Stellar properties

We convert the spectral types to effective temperatures ( $T_{\text{eff}}$ ) using the conversions in Fang et al. (2017a), which are from Pecaut & Mamajek (2013) for stars earlier than M4 and from Herczeg & Hillenbrand (2014) for stars later than M4 type. We obtain the stellar luminosity ( $L_\star$ ) using the  $T_{\text{eff}}$  and the photospheric flux at  $7510 \text{ \AA}$  from the best-fit templates described above and the Bolometric Corrections from Herczeg & Hillenbrand (2014). A distance of  $388 \pm 10 \text{ pc}$  measured from the multi-epochs observations with the Very Large Baseline Array (Kounkel et al. 2017), confirmed by the *GAIA* measurement ( $389 \pm 3 \text{ pc}$ , Kounkel et al. 2018), is used for computing the bolometric luminosity  $L_\star$ .

Among the different  $R_V$  values and the shapes of Accretion Continuum Spectrum, there are systematic differences on the derived  $L_\star$ . Based on these comparisons we find that (1) for a given  $R_V$ , the  $L_\star$  obtained under the assumption of constant Accretion Continuum Spectrum is systematically lower by  $\sim 0.07$  dex compared to the  $L_\star$  assuming the Accretion Continuum Spectrum as a black body emission with  $T = 7000 \text{ K}$ ; (2) for a given shape of the Accretion Continuum Spectrum, the stellar luminosity from  $R_V = 3.1$  is systematically lower by  $\sim 0.1$  dex than that assuming  $R_V = 5.5$ .



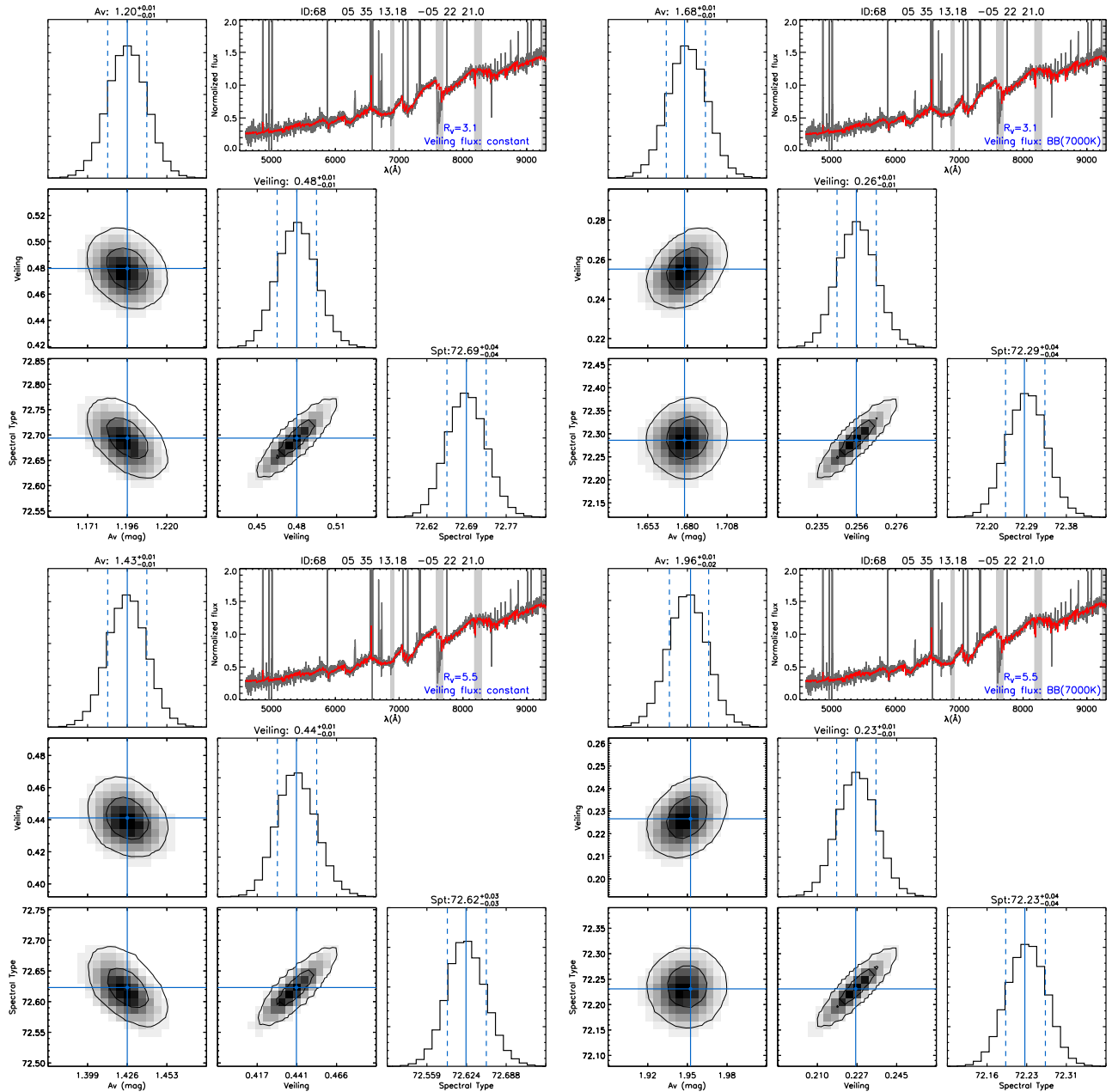


**Figure 2.** Corner plot showing the posterior distributions from the MCMC fit of the MUSE spectra for Source 68 for the four sets of parameters with different  $R_V$  and the shapes of Accretion Continuum Spectrum. The vertical dashed lines are the 16 and 85 percentiles, respectively. The solid lines indicate the medians of the posterior distributions. The best-fit templates (red) are overlapped on the observed MUSE spectra (grey).

In Table 1, we list the spectral types,  $L_*$ ,  $A_V$ , and veiling  $r_{7465}$  for different values of  $R_V$  and shapes of Accretion Continuum Spectrum for all the sources discussed in this work.

#### 4. EXTINCTION LAW

In this work, we use the extinction law from Cardelli et al. (1989), and take  $R_V=3.1$  and 5.5. As discussed in Appendix A, the value of  $R_V=5.5$  can fit

the spectral energy distribution of HD 37042 in near-infrared bands better than  $R_V=3.1$ .  $R_V=5.5$  has been considered more appropriate for the Orion nebula cluster (Johnson 1965a; Lee 1968; Costero & Peimbert 1970; Greve 2010). We further test if  $R_V=5.5$  is appropriate for our targets by comparing the observed 2MASS  $J$ -band photometry and synthetic 2MASS  $J$ -band photometry derived from the best-fit PMS spectral tem-

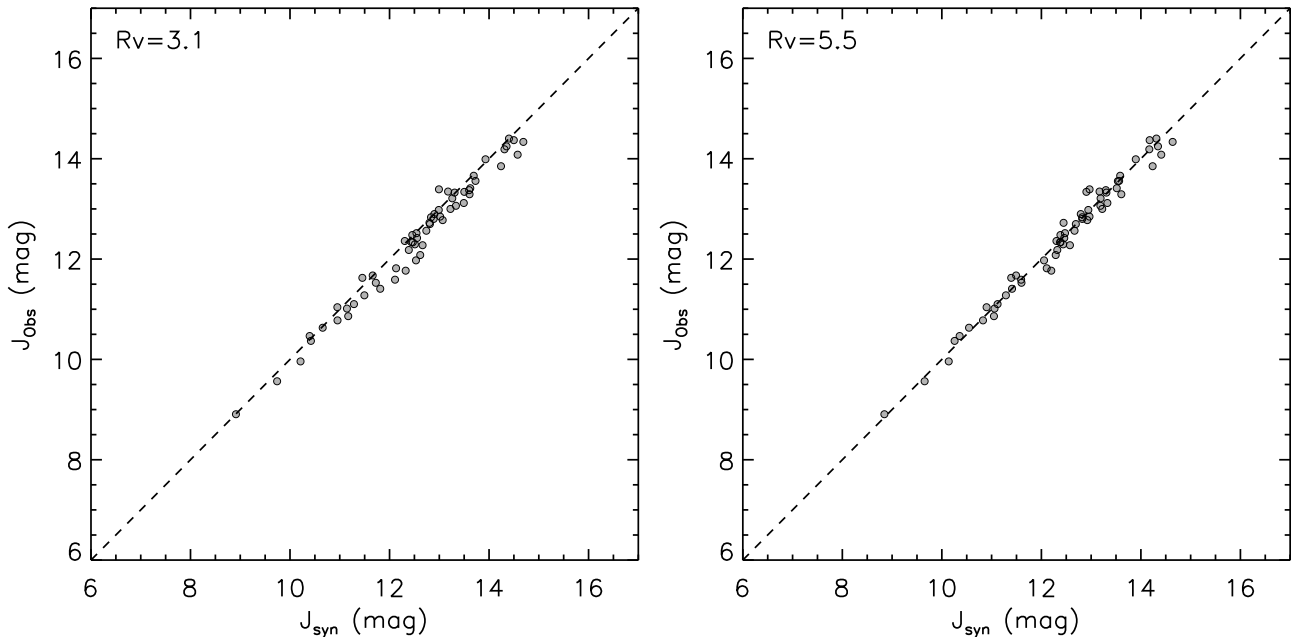


**Figure 3.** Comparison of the observed 2MASS J-band photometry and synthetic 2MASS J-band photometry derived from the best-fit PMS spectral templates for the diskless stars in the field. The dashed line in each panel shows the 1:1 relation.

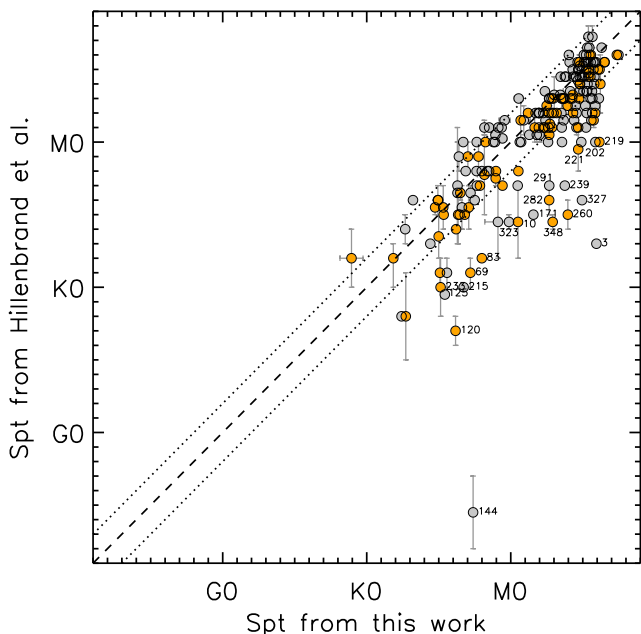


**Figure 4.** Comparison of the spectral types from the literature (Hillenbrand 1997; Hillenbrand et al. 2013) and from this work with  $R_V=5.5$  and constant Accretion Continuum Spectrum. The dashed line in each panel shows the 1:1 relation, and the dotted lines indicate the two subclass differences from the dashed line. The gray-color filled circles are for the sources with  $r_{\text{ex},7465} < 0.2$  and the orange-color filled circles are for those with  $r_{\text{ex},7465} \geq 0.2$ . The sources with spectral-type difference larger than five subclasses are marked with their identification numbers in Table 1.

plates for the diskless stars in the field; see Fig. 3. We select diskless stars which show no excess emission in mid-infrared bands (Muench et al. 2001; Megeath et al. 2012; Robberto et al. 2005; Smith et al. 2005).

The comparisons show that the synthetic photometry derived from the best-fit PMS templates with  $R_V=5.5$  agrees well with the observed photometry with the mean difference of less than 1%, while the comparisons with  $R_V=3.1$  underestimate the flux in  $J$  band by  $\sim 15\%$ . This indicates that  $R_V=5.5$  is a better choice for our targets. In the following sections, we will include two  $R_V$  values and two types of the Accretion Continuum Spectrum only in Sect. 6 and also in Table 1 in order to show how the different  $R_V$  affects the results in determining the stellar parameters, and adopt  $R_V=5.5$  and constant Accretion Continuum Spectrum in other sections.

## 5. COMPARISON WITH LITERATURE

### 5.1. Spectral type

Hillenbrand (1997) carried out the first extensive spectroscopic survey of young stars in the Orion nebula cluster, which are further enhanced by Hillenbrand et al. (2013). Figure 4 compares the spectral types of 203 common sources from the literature (Hillenbrand 1997; Hillenbrand et al. 2013) and this study. For the sources with the spectral types from both Hillenbrand (1997) and Hillenbrand et al. (2013), we only show the spectral types from the latter one in Figure 4. Among these

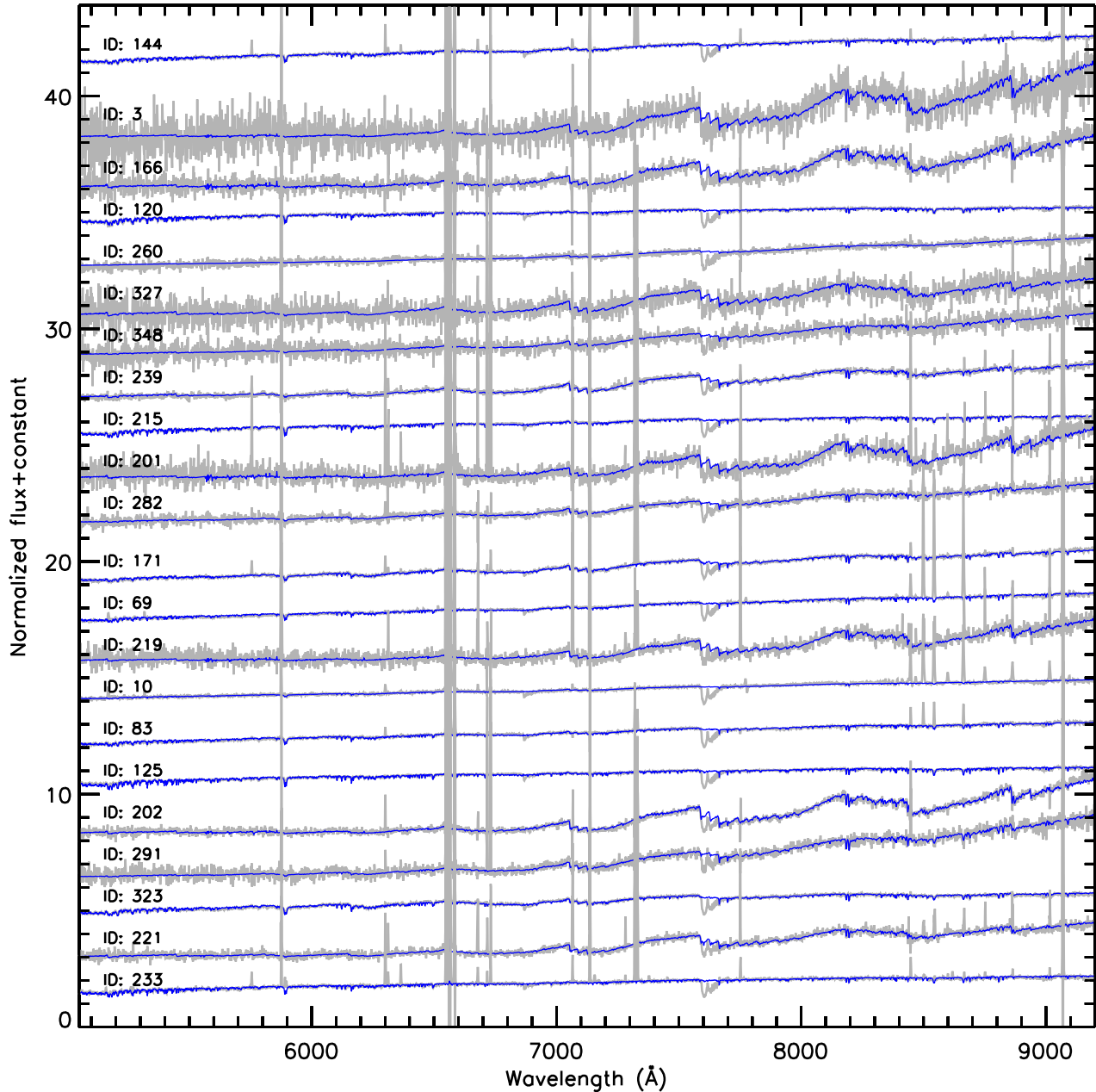


**Figure 5.** Best-fit spectral templates (blue) over-plotted on the MUSE spectra (gray) of 22 sources which have spectral type differences larger than five subclasses between the ones from Hillenbrand et al. (2013) and this work. From top to bottom, the spectral type difference decreases, and the identification number of each source is the same as in Table 1.

common sources, 40% of them show spectral-type differences of less than one subclass, and  $\sim 68\%$  with spectral-type differences of less than two subclasses. There are 22 sources with differences larger than five subclasses. In particular, Source 144 has a spectral type of F2–F7 in Hillenbrand (1997), a spectral type of K0–K7 in Luhman et al. (2000), and a spectral type of K7 in this work. In Fig. 5, we over-plot the best-fit spectral template on the MUSE spectrum of Source 144. We

find that the template fits the observed spectrum very well. In the figure, we also show the 21 other sources with spectral type difference larger than five subclasses. For each source, the best-fit template can reproduce the observation reasonably well.

Beside the extreme cases discussed above, literature spectral types for a number of sources in the cluster are actually very uncertain. In Table 1, we list all the known spectral types of individual sources collected from

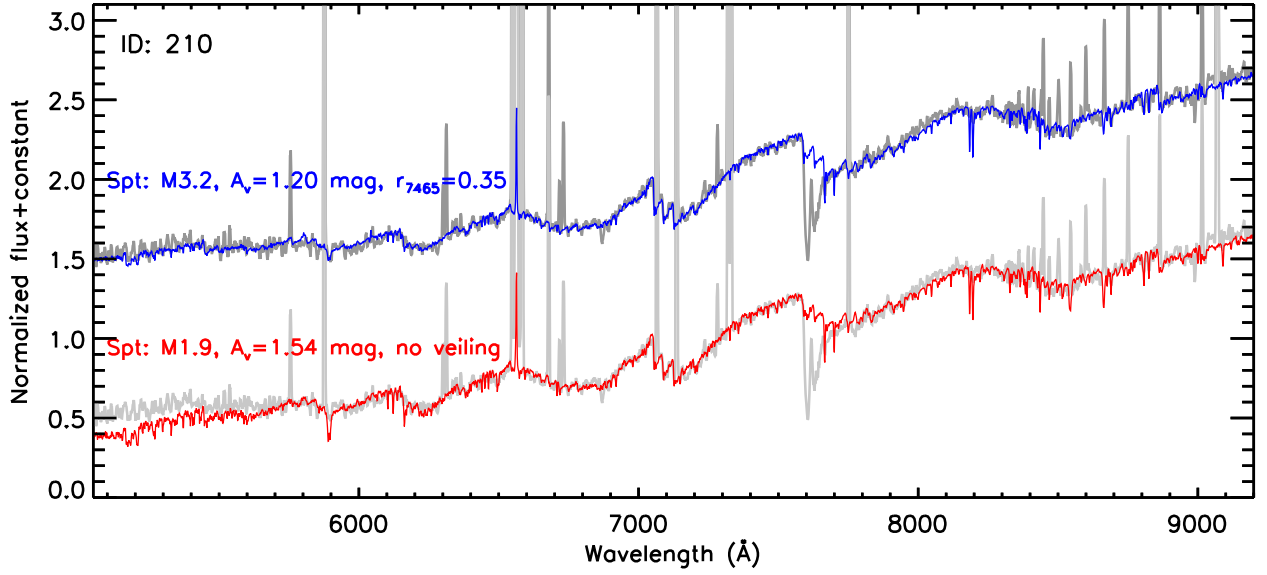


**Figure 6.** Best-fit spectral templates over-plotted on the MUSE spectra (gray) of Source 210. The best-fit templates are obtained in two cases: with constant Accretion Continuum Spectrum (blue) and without veiling (red), assuming  $R_V = 5.5$ .

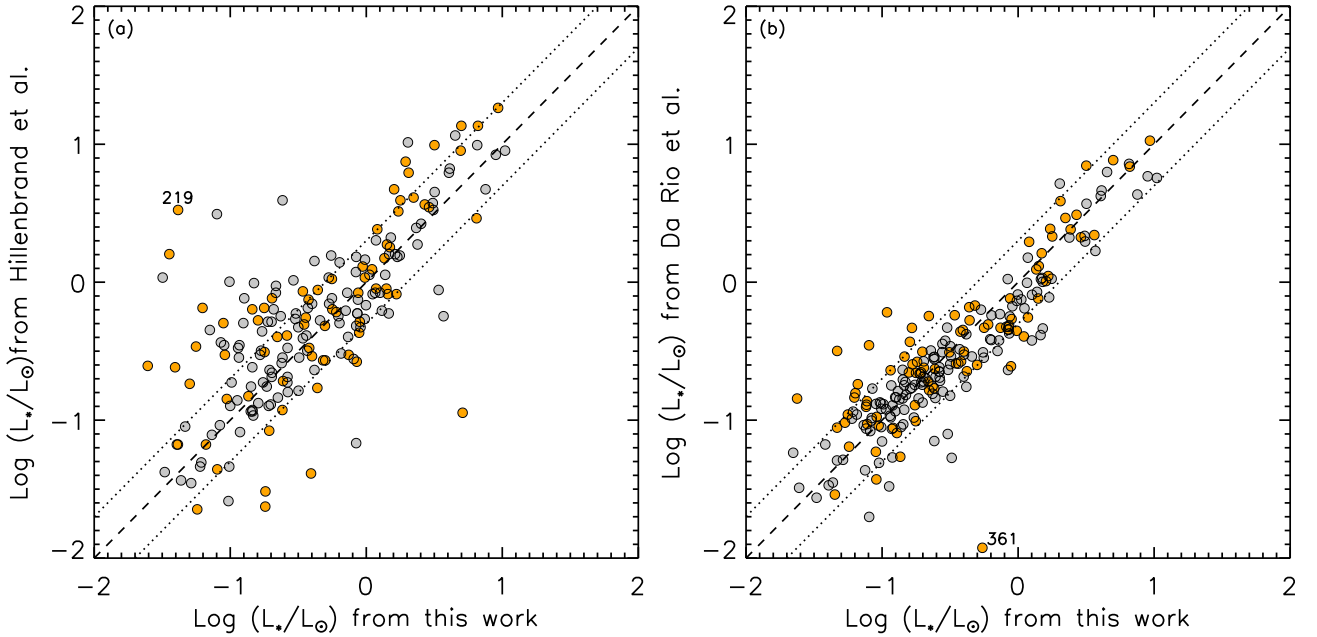


**Figure 7.** Comparison of the stellar luminosity from this work with those from Hillenbrand (1997) (a) and from Da Rio et al. (2012) (b). In each panel, the dashed line shows the 1:1 relation, and the dotted lines indicate the difference in the stellar luminosity by a factor of 2. The gray-color filled circles are for sources with  $r_{7465} < 0.2$  and the orange-color filled circles for those with  $r_{7465} \geq 0.2$ . The stellar luminosity from this work are derived taking  $R_V=5.5$  and assuming a constant Accretion Continuum Spectrum.



Hillenbrand et al. (2013). There can be 2–3 subclass differences between the literature values and our work. The differences are mostly due to (1) differences in the spectral ranges used for spectral typing and (2) whether veiling has been considered. For an accreting source, the Accretion Continuum Spectrum affects the blue part of the spectrum much more significantly than the red part. Therefore, fitting just the blue part of the spectrum results in earlier spectral type than using the red part, if veiling is not considered. For example, Figure 6 shows the effect of veiling for Source 210. Not accounting for veiling leads to a M1.9 spectral type, very similar to the M2 spectral type reported in Hillenbrand (1997). When veiling is considered, however, the derived spectral type is one subclass later. It is also clear that the best-fit template with veiling reproduces the observations much better at wavelengths  $\lesssim 6200 \text{ \AA}$  than that the template without veiling. However, the difference between the two best-fit templates is minor at longer wavelengths, illustrating the importance of broad wavelength range for accurate spectral classification. A similar example can be found in Figure 15 in Herczeg & Hillenbrand (2014).

### 5.2. Stellar luminosity

Figure 7(a) compares  $L_\star$  from this work with those in Hillenbrand (1997). There are 199 common sources between the two works. The  $L_\star$  from this work are derived using  $R_V=5.5$  and assuming a constant Accretion Continuum Spectrum. The  $L_\star$  from Hillenbrand (1997) have been scaled from 470 pc to the new distance of 388 pc (Kounkel et al. 2017) which is also used in our work. The mean difference on the  $L_\star$  between two works is 0.26 dex. There are 37% of common sources with difference larger than a factor of two. The largest difference comes from Source 219 with  $\text{Log}(L_\star/L_\odot)=0.52$  from Hillenbrand (1997) and  $\text{Log}(L_\star/L_\odot)=-1.38$  from this work. This object also has very different spectral types between both works: M0 from Hillenbrand (1997) and M6 from this work; see Fig. 5. The synthetic photometry of our best-fit template for this source is 13.74 mag in  $J$  band, which is fainter than the observed one 13.20–13.47 mag Robberto et al. (2010). This difference can be due to infrared excess emission from the circumstellar disk, which is suggested by its infrared color ( $K-L=0.82$  mag from Muench et al. 2002) and strong optical veiling (see Table 1).

Da Rio et al. (2012) complemented the sources with the spectral types from Hillenbrand (1997) by utilizing the photometry in  $I$  band and two medium-band filters at  $\lambda \sim 7530$  and  $7700 \text{ \AA}$  to derive the spectral types for M-type stars. In Figure 7(b) we compare  $L_\star$  from this work with the ones from Da Rio et al. (2012) for

the 227 sources in common. The  $L_\star$  from our work are same as above, and the  $L_\star$  from Da Rio et al. (2012) have been scaled to the distance we adopted (388 pc). The mean difference of the  $L_\star$  between two works is 0.16 dex, and only 16% of the common sources have differences larger than a factor of two. Among them, source 361 shows the largest difference:  $\text{Log}(L_\star/L_\odot)=-1.897$  from Da Rio et al. (2012) and  $\text{Log}(L_\star/L_\odot)=-0.262$  from our work. This is mainly due to the difference of the spectral types used in the two analyses: G4–K5 used in Da Rio et al. (2012) which was taken from Luhman et al. (2000) and K8.3 in our work. The difference is mainly due to its strong veiling ( $r_{7465}$ ) with large infrared excess emission ( $K-L=1.33$  mag from Muench et al. 2002).

Both Hillenbrand (1997) and Da Rio et al. (2012) take  $R_V=3.1$ . If we take the same  $R_V=3.1$  and assume a constant Accretion Continuum Spectrum, the mean difference on  $L_\star$  from our work and Hillenbrand (1997) becomes even larger (0.31 dex) with 46% of common sources with difference larger than a factor of two. However, the mean difference on  $L_\star$  from our work and Da Rio et al. (2012) becomes smaller (0.14 dex) with 18% of common sources with difference larger than a factor of two.

### 5.3. Extinction

In Figure 8 (a, b), we compare the  $A_V$  from this work with those in Da Rio et al. (2012). In these figures, the  $A_V$  from this work are derived assuming a constant Accretion Continuum Spectrum and taking  $R_V=3.1$  in Figure 8(a) and  $R_V=5.5$  in Figure 8(b). In Da Rio et al. (2012) they adopted the extinction law from Cardelli et al. (1989) with  $R_V=3.1$  and derived the extinction in optical bands. In Figure 8(a), the mean difference between the two works is 0.18 mag with the standard deviation of 0.81 mag, and in Figure 8(b) these are  $-0.10$  mag and  $0.87$  mag, respectively. The main sources of difference in extinction are (1) the differences in the assigned SpT, (2) whether one includes veiling in deriving the extinction, (3) whether the photometry of the sources are obtained simultaneously. In general, the  $A_V$  differences found here agree well with those discussed in the literature (see e.g. Herczeg & Hillenbrand 2014).

Figure 8 (c, d) compare the  $A_V$  from this work with those from Hasenberger et al. (2016). The extinction in Hasenberger et al. (2016) are derived using the photometry in near-infrared  $J, H, K_s$  bands and spectral types from Hillenbrand et al. (2013), adopting the extinction law from Cardelli et al. (1989) with  $R_V=3.1$ . The  $A_V$  measured from the photometry in near-infrared bands

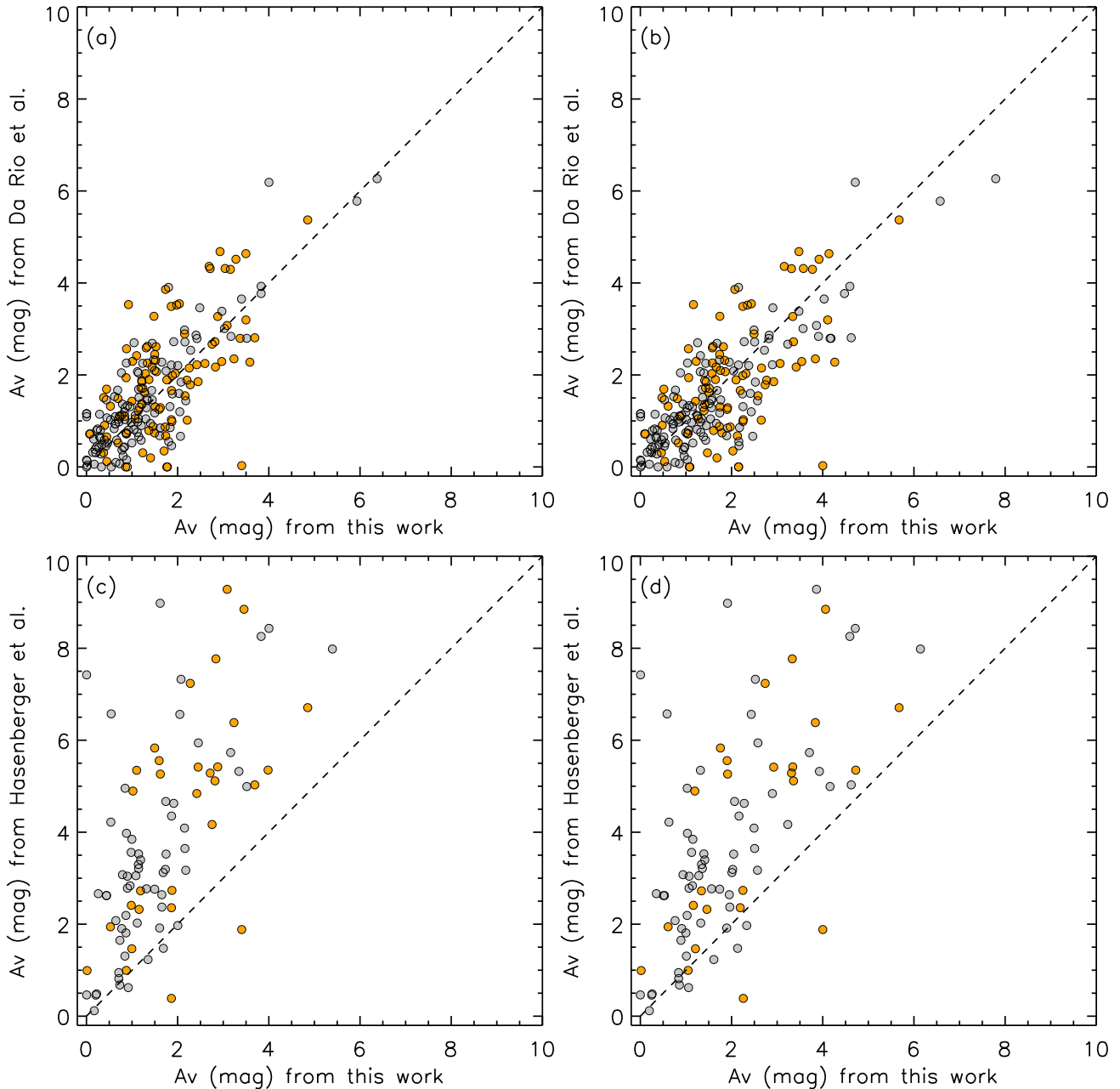


**Figure 8.** Comparisons of the extinction from this work with those from [Da Rio et al. \(2012\)](#) (a, b) and [Hasenberger et al. \(2016\)](#) (c, d). The extinction from this work are derived assuming a constant Accretion Continuum Spectrum and taking  $R_V=3.1$  in Panel (a, c) and  $R_V=5.5$  in Panel (b, d). In each panel, the dashed line shows the 1:1 relation. The gray-color filled circles are for sources with  $r_{7465} < 0.2$  and the orange-color filled circles for those with  $r_{7465} \geq 0.2$ .

are significantly higher than those derived at optical wavelengths. The large differences on the extinction derived at optical wavelengths and near-infrared wavelengths have been noted in literature ([McJunkin et al. 2014](#); [Herczeg & Hillenbrand 2014](#)), and could be caused by the large near-infrared excess emitted from the inner regions of circumstellar disks ([Herczeg & Hillenbrand 2014](#)).

## 6. HERZSPRUNG-RUSSELL DIAGRAM

With the derived  $T_{\text{eff}}$  and bolometric luminosities for different values of  $R_V$  and shapes of Accretion Continuum Spectrum, we place the stars in the H-R diagram in Figure 9. As a comparison, we show the nonmagnetic evolutionary tracks from [Feiden \(2016\)](#) and from [Baraffe et al. \(2015\)](#). A combination of the two evolutionary tracks has been used in [Pascucci et al. \(2016\)](#)

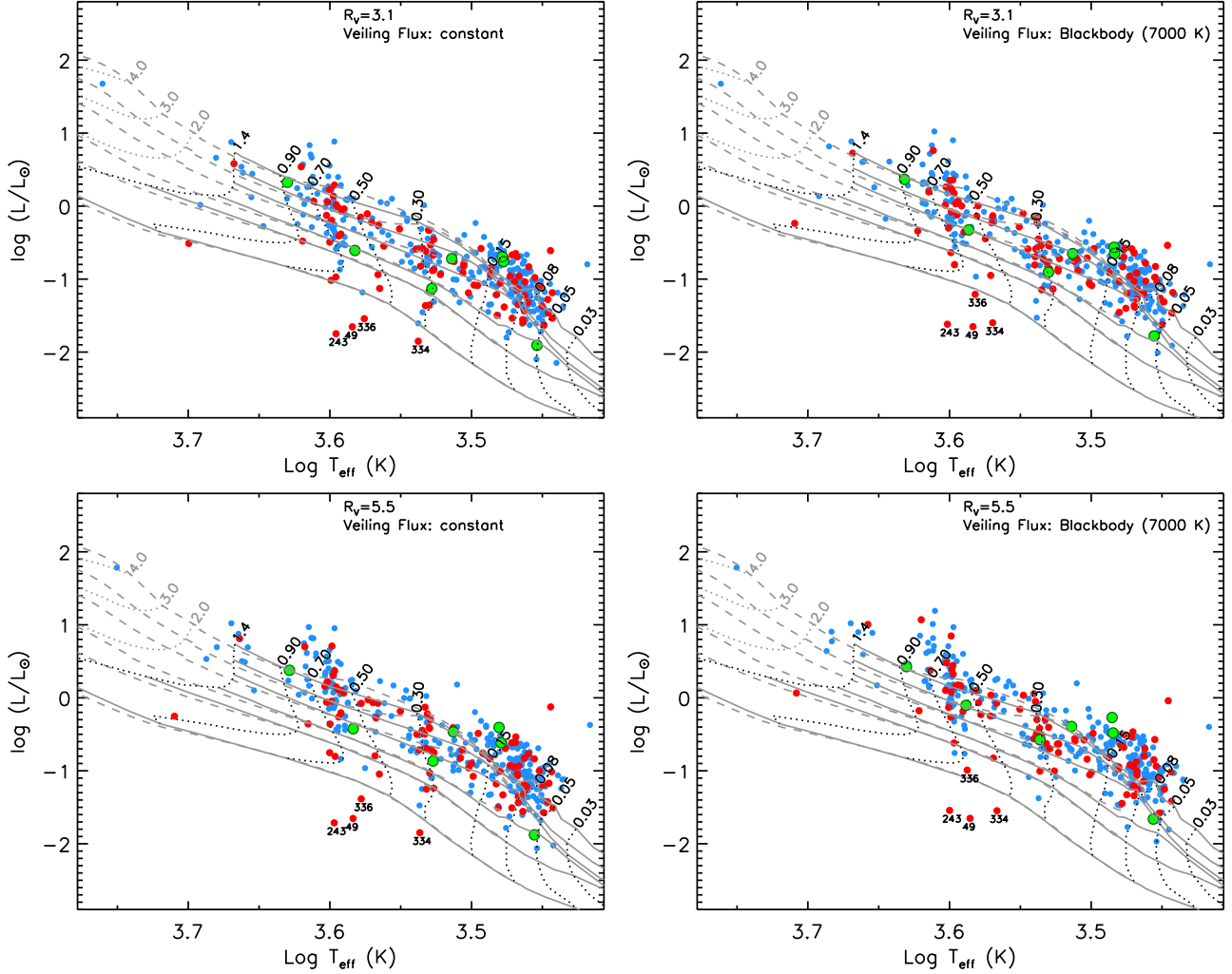


**Figure 9.** HR diagrams for the sources in the Trapezium cluster. The stellar parameters are derived with different values of  $R_V$  and shapes of Accretion Continuum Spectrum and shown in different panels. In each panel, the red-color filled circles are sources with proplyds, green-color filled circles are ones with silhouette disks, and blue-color filled circles are other sources in our sample. Four sublumines proplyds are marked with their identification numbers in Table 1. The nonmagnetic evolutionary tracks (dashed lines) from Feiden (2016) and the evolutionary tracks (solid lines) from Baraffe et al. (2015) are shown as a comparison. The isochrones are at ages of 0.5, 1, 2, 5, 10, and 50 Myr from top to bottom.

and can match empirical stellar loci of nearby young associations in H-R diagram better than older models (Herczeg & Hillenbrand 2015). We match our sample with those in Ricci et al. (2008), and find 89 sources with externally ionized protoplanetary disks (proplyds), as well as 7 sources with disks seen only in absorption against the bright nebular background (silhouette disks). In Figure 9, all these sources are shown with different symbols. There are a few proplyds, which appear sublumines compared to the sources of the same spectral types. We will discuss these sublumines sources in Section 7.2

In Figure 9, depending on the adopted  $R_V$  and the shapes of Accretion Continuum Spectrum, there are

73%–89% of the sources above the 2 Myr isochrone, and 56%–72% of the sources are above the 1 Myr isochrone. Including all the sources, the comparison with the PMS evolutionary tracks suggest that the cluster should be very young, i.e., younger than  $\sim 1$  Myr. However, we note that there are many sources located above the 0.5 Myr isochrone, which have  $\text{Log } T_{\text{eff}} \leq 3.49$ , corresponding to stellar masses  $\leq 0.15 M_{\odot}$ . If excluding the sources with  $\text{Log } T_{\text{eff}} \leq 3.49$ , a median age of  $\sim 1$  Myr can be derived for the cluster.

The over-dense population with  $\text{Log } T_{\text{eff}} \leq 3.49$  which appear above 0.5 Myr in H-R diagram can be better fit if we use the magnetic evolutionary tracks from Feiden (2016); see Figure 10. Feiden (2016) include the effect

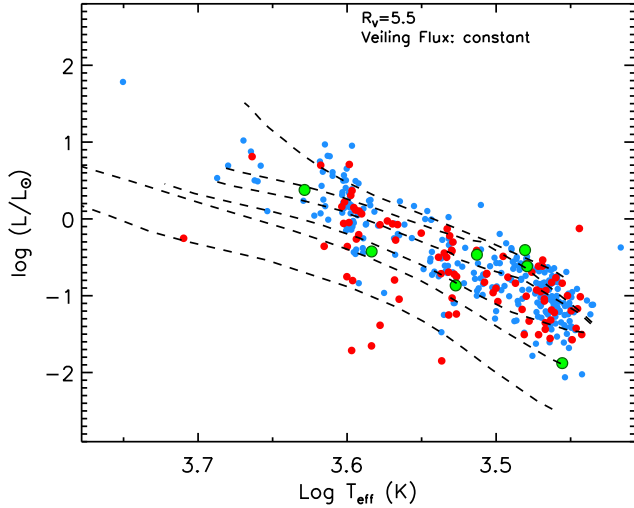


**Figure 10.** HR diagram for the sources in Trapezium cluster. The PMS evolutionary tracks are from Feiden (2016), in which the influence by the presence of magnetic fields are included in the calculation. The black dash lines show isochrones for 0.1, 1, 2, 5, 10, and 50 Myr, from top to bottom.

of magnetic fields on the stellar structure, which can inhibit the convection and thereby slow down contraction rates and result in larger stellar radii, which then results in larger luminosities, especially for the very low-mass stars. A comparison with their isochrones suggest a median age of  $\sim 2$  Myr for the Trapezium cluster.

## 7. DISCUSSION

### 7.1. Luminosity Spreads

The H-R diagrams in Fig. 9 show large spreads in luminosities ( $\sigma(\log L_*/L_\odot) \sim 0.3$ ) for sources with similar spectral types, which is much larger than that found in coeval loose associations like TW Hya and MBM 12 (Herczeg & Hillenbrand 2014). The luminosity spread in the H-R diagram has been usually attributed to an intrinsic age spread (see e.g. Jeffries et al. 2011; Fang et al. 2017b). If we assume that the luminosity dispersion in the Trapezium cluster is only due to the age spread, there is an age dispersion of  $\sim 2$  Myr in this cluster. However, other factors like veiling, binarity, starspots, and circumstellar disk orientations can contribute to the observed spread. As we have accounted for veiling in our study and still see large luminosity spreads, we can exclude that veiling contributes to most of the observed scatter.

We also argue that binaries are not the main contributor to the scatter. In an extreme case, if we assume half of the cluster population to have equal-mass binary companions, and the other half to be single stars, the

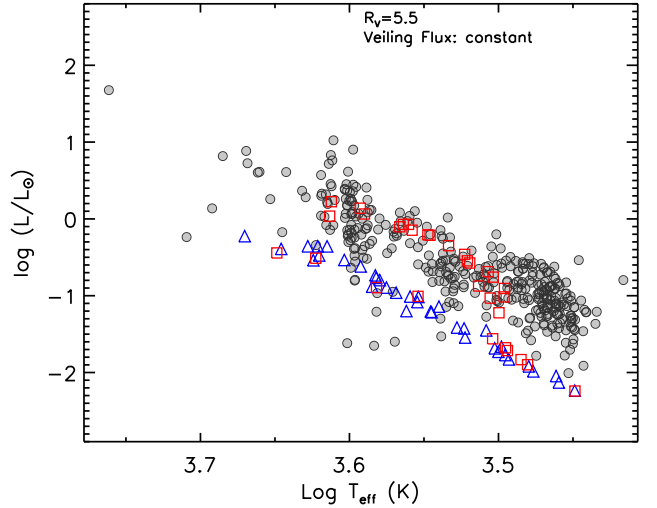


**Figure 11.** HR diagram for the sources (grey-color filled circles) in Trapezium cluster, compared with the position of 1 Myr-old cold models (blue open triangles) and 1 Myr-old hybrid models (red open squares) from Baraffe et al. (2017).

luminosity dispersion would be only  $\sim 0.15$ . Realistically, the contribution of the binaries in the luminosity spread should be much less than 0.15 dex, since the suggested companion mass ratios have a flat distribution (Kraus et al. 2011; Goodwin 2013). Hence, binaries are not the major cause of the luminosity spread.

Starspots can contribute to the luminosity spread (Gully-Santiago et al. 2017). It is well known that low-mass young stars have large spot coverage and show strong magnetic fields (Johns-Krull & Valenti 1996). Heavily spotted models (50% coverage) of 0.1-1.2  $M_\odot$  stars could have inflated stellar radii by a factor of 10% during the PMS stage (Somers & Pinsonneault 2015), and induce a luminosity difference between the heavily spotted models and spot-free models by a factor of two. A precise evaluation of the contribution of the starspots in our sample requires high spectral resolution data to estimate the spot coverage as done in Gully-Santiago et al. (2017).

Theoretical studies have argued that episodic accretion during the phase of protostellar evolution can strongly affect the structure and evolution of low-mass stars during the PMS stages. It can also introduce large luminosity spreads in observed H-R diagrams without any age spreads (Baraffe & Chabrier 2010; Baraffe et al. 2012). Baraffe et al. (2017) performed self-consistent calculations by coupling models of collapsing pre-stellar cores and stellar evolution models of accreting objects. In their calculation, they denote  $\alpha$ , the fraction of accreting internal energy absorbed by the central proto-stars. They consider two scenarios: (1) a cold accretion

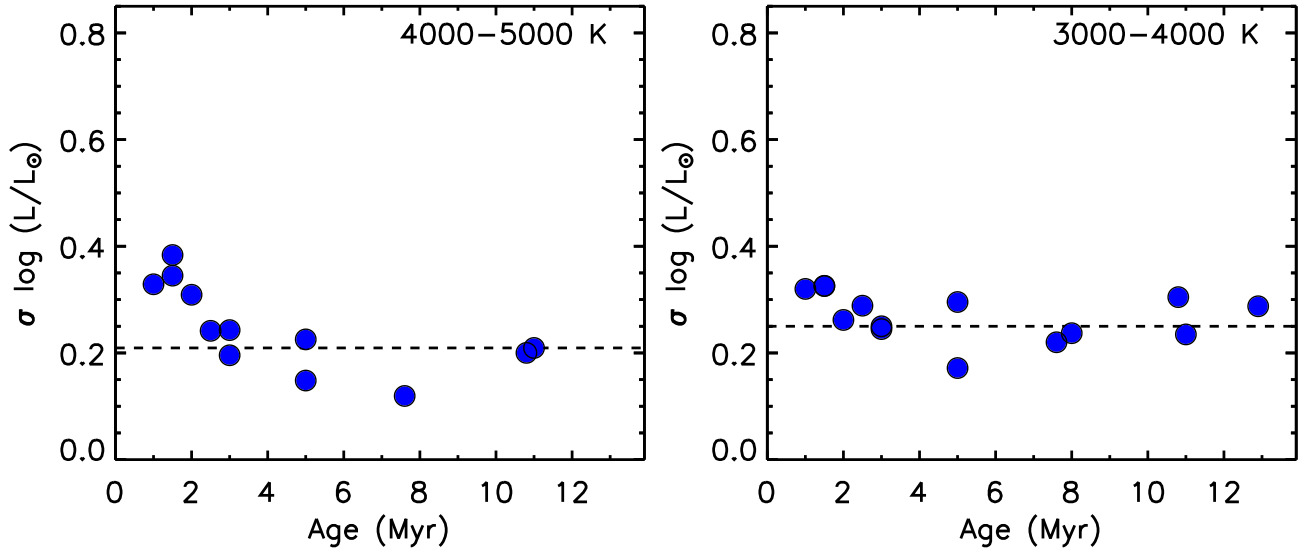


**Figure 12.** Luminosity spreads as a function of cluster/group ages within two  $T_{\text{eff}}$  bins, 4000–5000 K and 3000–4000 K.

**Table 2.** Luminosity spreads within different temperature bins

Regions	Age	4000–5000 K		3000–4000 K		References
		$\sigma(\text{Log } L_*/L_\odot)$	N	$\sigma(\text{Log } L_*/L_\odot)$	N	
Trapezium	1 Myr	0.33	35	0.32	204	1
Taurus	1.5 Myr	0.38	20	0.33	127	2
NGC2068/2071	1.5 Myr	0.34	23	0.33	105	3
Cha I	2 Myr	0.31	18	0.26	153	4
IC 348	2.5 Myr	0.24	20	0.29	203	5
NGC 2264	3 Myr	0.20	181	0.25	298	6
$\sigma$ Ori	3 Myr	0.24	20	0.24	122	7
NGC 2362	5 Myr	0.15	27	0.17	62	8
Upper Sco	11 Myr	0.21	65	0.23	562	9
Ori OB1b	5 Myr	0.23	63	0.30	412	10
25 Ori	7.6 Myr	0.12	16	0.22	172	10
HD 35762	8 Myr			0.24	74	10
Ori OB1a	10.8 Myr	0.20	68	0.30	653	10
HR 1833	12.9 Myr			0.29	54	10

References–1. This work, 2. [Herczeg & Hillenbrand \(2014\)](#), 3. [Fang et al. \(2009\)](#), 4. [Luhman \(2007\)](#), 5. [Luhman et al. \(2003\)](#), 6. [Venuti et al. \(2018\)](#), 7. [Hernández et al. \(2014\)](#), 8. [Dahm \(2005\)](#), 9. [Luhman et al. \(2018\)](#), 10. [Briceño et al. \(2019\)](#)

model with  $\alpha=0$ , meaning all accretion energy is radiated away; (2) a hybrid accretion model with  $\alpha=0$ , when accretion rates are smaller than a critical value ( $\dot{M}_{\text{cr}}$ ), and  $\alpha=0.2$  when accretion rates are larger than a critical value. Figure 11 compares the models with our data. A striking feature is seen in the comparison: the cold accretion model fits quite well a group of sub-luminous sources, which appear below the pre-main sequence loci. In this figure, the models tend to show a bimodal distribution, since the  $\dot{M}_{\text{cr}}$  is fixed ( $\dot{M}_{\text{cr}} = 10^{-5} M_\odot \text{ yr}^{-1}$ )

in the calculations. A variation of  $\dot{M}_{\text{cr}}$  can fill the gap and reproduce the observed luminosity spread when  $\text{Log}T_{\text{eff}} \gtrsim 3.5$ . However, the models fail to reproduce the luminosity spread when  $\text{Log}T_{\text{eff}} \lesssim 3.5$ .

Such luminosity spreads are commonly seen even for clusters with different ages. Figure 12 shows the luminosity spreads as a function of cluster/group ages within two temperature bins: 4000–5000 K and 3000–4000 K. In order to remove the contribution of the luminosity spreads from the  $\text{Log}L_*\text{--Log}T_{\text{eff}}$  relation, we first fit



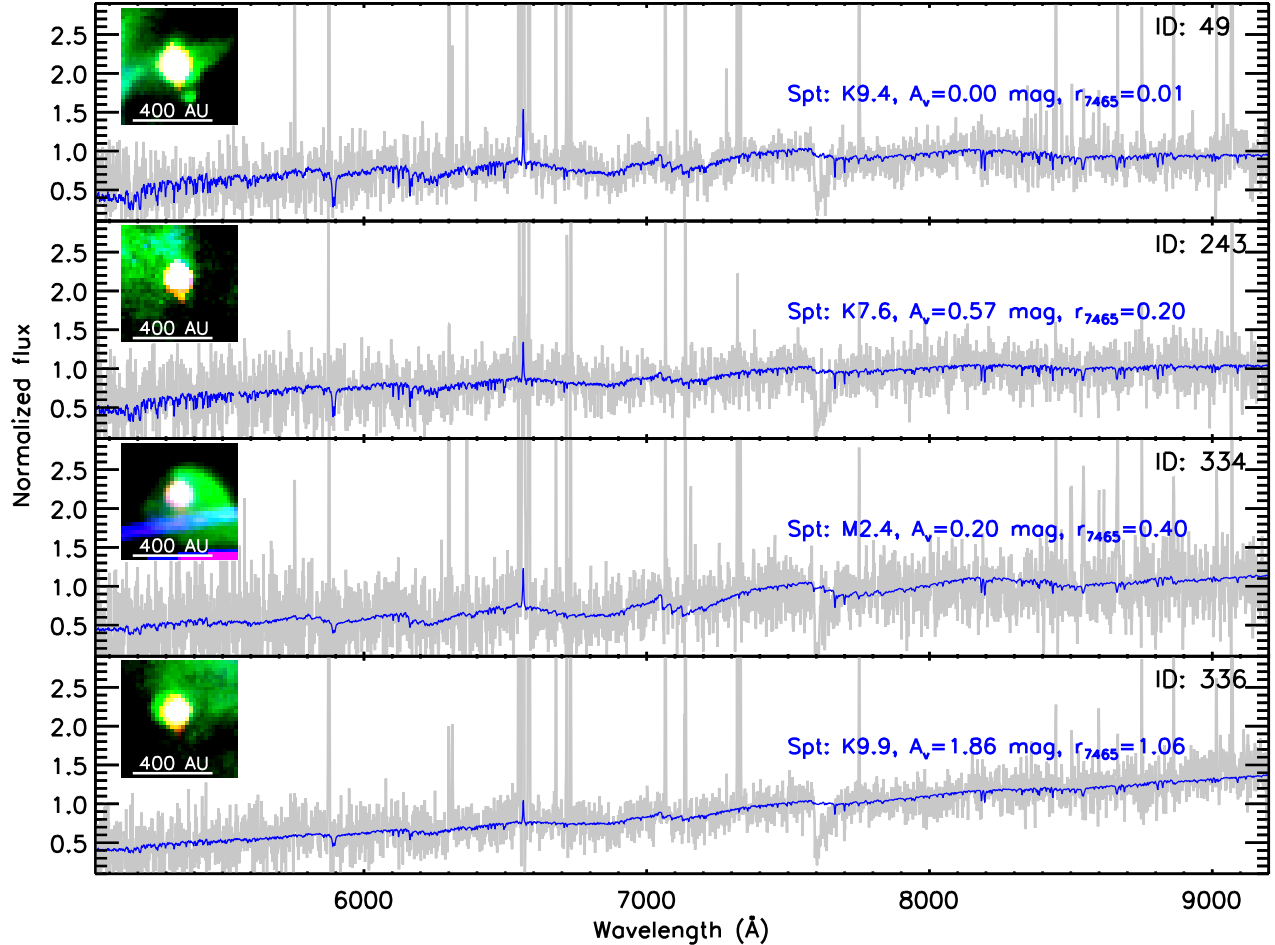


**Figure 13.** MUSE spectra of four sub-luminous objects, numbered sources in Fig. 9, are overplotted with their best-fit spectral templates. The best-fit templates are obtained with a constant Accretion Continuum Spectrum and  $R_V = 5.5$ . In each panel, the inset is the HST ACS color-composite image of the proplyd; HST image data were taken from Ricci et al. (2008). The tails of these four proplyds are obvious in the HST image in the F658N band.

the  $\text{Log}L_\star\text{--}\text{Log}T_{\text{eff}}$  relation with a linear function for each cluster within each temperature bin, and then subtract the calculated  $\text{Log}L_\star$  at  $\text{Log}T_{\text{eff}}$  using the fitted linear function from observed  $\text{Log}L_\star$ . We then calculate the standard deviation among the residual luminosity and use it as the luminosity spreads. The plotted clusters/groups include the Trapezium cluster, the Taurus star-forming region, NGC 2068/2071, the Cha I star forming region, IC 348, NGC 2264,  $\sigma$  Ori, NGC 2362, Upper Sco, and Orion OB associations including Ori OB1a, Ori OB1b, 25 Ori, HD 35762, and HR 1833. In Table 2, we list the luminosity spread and number of stars within each temperature bin, the age of each cluster/group, as well the references. The luminosity spreads are calculated only when the number of stars in each temperature bins are larger than 10. For the Upper Sco and Orion OB associations, no stellar luminosities are listed in tables in Luhman et al.

(2018) and Briceño et al. (2019). We calculate the stellar luminosity for each source using the method described in Fang et al. (2017a) taking its spectral type and extinction from the literature (Luhman et al. 2018; Briceño et al. 2019). Beside the Trapezium cluster and Taurus, the veiling effect has not been considered in deriving the spectral types and stellar luminosities. However, it should only affect the young clusters, such as NGC 2068/2071 and Cha I where more than 50% of sources are still accreting (Fedele et al. 2010).

Figure 12 shows that the large  $\sigma(\log L_\star/L_\odot)$  perseveres even in the old clusters, such as Upper Sco within the two temperature bins. The  $\sigma(\log L_\star/L_\odot)$  tends to flatten ( $\sim 0.20\text{--}0.25$ ) after  $\sim 2$  Myr. If this is due to the age spread,  $\sigma(\log L_\star/L_\odot) = 0.20$  at  $\sim 2$  Myr require an age dispersion of  $\sim 2$  Myr, and the same dispersion at  $\sim 11$  Myr require an age dispersion of  $\sim 7$  Myr, according to PMS evolutionary tracks from Baraffe et al.

(2015). Thus, increasing age spreads with increasing cluster ages are required to reproduce the constant  $\sigma(\text{Log}L_*/L_\odot)$ . This argues against age spread being the main contribution of luminosity spread. Figure 12 also shows  $\sim 0.1$  dex larger in luminosity spreads for the younger regions, like the Trapezium cluster and Taurus, than those older regions. While the binarity induces a similar luminosity spread for clusters at different ages, other factors, e.g., starspots, accretion history and circumstellar disk orientations, can induce a larger luminosity spread for young clusters than older ones (Morris 2020; Baraffe et al. 2017; Guarcello et al. 2010).

### 7.2. Proplyds

Proplyds are protoplanetary disks being photoevaporated by ultraviolet radiation from nearby massive stars and show cometary structures with tails pointing away from the massive stars (O'dell et al. 1993). In the Orion nebula, there are more than a hundred known proplyds. In Figure 9 there are about ten proplyds, which appear sub-luminous compared to other young stars with the same spectral types. In particular, four proplyds (Souresces 49, 243, 334, 336) in Figure 9(a,b,c) and three proplyds in Figure 9(d) appear below the isochrone of 50 Myr. In Fig. 13 we show their MUSE spectra as well their best-fit spectral templates. We find that for each object, the best-fit template can fit the observation well. Such sub-luminous young stars are often found in young star-forming regions (Fang et al. 2009, 2013a; Comerón et al. 2003; White & Hillenbrand 2004; Fang et al. 2013b). They are explained as young stars with highly inclined disks. The stellar light is reduced due to attenuation by the dusty disk and the observed light mainly comes from photons scattered off the disk surface. However, we cannot exclude the possibility that the stellar parameters of those sub-luminous objects are not well determined, since their spectra are rather noisy.

Furthermore, we can test if there is any difference on the stellar properties between the proplyds and other sources. It is clear that in the H-R diagram the majority of the proplyds are well-mixed among other sources; see Figure 9. The Kolmogorov-Smirnov tests on the distributions of the luminosity and the spectral types of the proplyds and other young stars return a high probability ( $P=0.51$  and  $0.27$  for luminosity and spectral type, respectively) for both the proplyds and other sources to be drawn from the same parent population. Since the stellar ages and masses are derived from the stellar luminosity and spectral types, we conclude that the proplyds have similar ages and show similar mass function to other sources in the cluster. This suggests that the

majority of the proplyds formed as other stars in the cluster.

## 8. SUMMARY

We present a spectroscopic study of 361 young stars in the Trapezium cluster, and analyze their flux-calibrated optical spectra to derive their spectral type, extinction, and optical veiling due to the accretion simultaneously. Based on this enhanced spectroscopic analysis, we update the H-R diagram of the Trapezium cluster, and present the main results as follows.

- We improve the spectral classification of young stars in the Trapezium cluster using the X-shooter spectra of WTTSs as templates.
- In the Trapezium cluster, the optical total-to-selective extinction ratio ( $R_V$ ) is suggested to be 5.5.
- With the derived spectral type and stellar luminosity, we present an improved H-R diagram of the Trapezium cluster. The age of the Trapezium cluster is estimated to be  $\sim 1$  Myr with the non-magnetic PMS evolutionary tracks and  $\sim 2$  Myr with the magnetic PMS evolutionary tracks. .
- We find the magnetic PMS evolutionary tracks can better explain the over-luminous low-mass young stars with  $\text{Log } T_{\text{eff}} \leq 3.49$  in H-R diagram than the non-magnetic PMS evolutionary tracks.
- In the H-R diagram, there are about ten sources that appear below the 10 Myr isochrone, which can be explained by high-inclination disks or the cold accretion model from Baraffe et al. (2017).
- The Trapezium cluster shows a large luminosity spread,  $\sigma(\text{Log}L_*/L_\odot) \sim 0.3$ , in the H-R diagram. We collect a sample of 14 clusters/groups at different ages, and find that the luminosity spread remains in older ( $\sim 10$  Myr) cluster and the luminosity spread tend to be constant after 2 Myr. This suggests that the age spread is not the main contributor to the luminosity spread.
- There are no significant difference on the spectral types and stellar luminosity between the proplyds and other members in the cluster.

Our work further stress the importance of accounting for veiling when deriving spectral types of accreting young stars.

Many thanks to the anonymous referee for comments that help to improve this paper. This material is

based upon work supported by the National Aeronautics and Space Administration under Agreement No. NNX15AD94G for the program "Earths in Other Solar Systems". The results reported herein benefited from collaborations and/or information exchange within NASA Nexus for Exoplanet System Science (NExSS) research coordination network sponsored by NASA's Science Mission Directorate.

*Facilities:* VLT: (MUSE)

**Table 1.** A List of the Sources in This Work, as well as Their Spectral types and stellar luminosities

ID	RA	DEC	$R_V = 3.1^a$										$R_V = 5.5^b$										Star <sup>c</sup>	SpT
			Constant					BB(7000 K)					Constant					BB(7000 K)						
			SpT	Log $L_\star$	$A_V$	$r_{7465}$	$(L_\odot)$ (mag)	SpT	Log $L_\star$	$A_V$	$r_{7465}$	$(L_\odot)$ (mag)	SpT	Log $L_\star$	$A_V$	$r_{7465}$	$(L_\odot)$ (mag)	SpT	Log $L_\star$	$A_V$	$r_{7465}$	$(L_\odot)$ (mag)		
1 05 35 05.37	-05 24 10.6	K7.6	-0.347	3.40	0.19	K7.1	-0.246	3.64	0.10	K7.6	-0.042	4.03	0.12	K7.0	0.033	4.16	0.02	265				M0(H97)		
2 05 35 05.40	-05 24 15.1	M4.5	-0.983	2.88	0.23	M4.3	-0.922	3.06	0.15	M4.3	-0.776	3.34	0.21	M4.1	-0.719	3.49	0.13	266				M1.5(H13)M2.5(H13)		
3 05 35 05.43	-05 25 22.1	M5.9	-1.315	1.86	0.02	M6.0	-1.303	1.89	0.02	M5.9	-1.195	2.09	0.02	M5.9	-1.150	2.27	0.02	267				K3e(H13)		
4 05 35 05.45	-05 22 30.4	M7.4	-1.396	1.88	0.35	M7.1	-1.216	2.61	0.29	M7.4	-1.242	2.25	0.35	M7.1	-1.031	2.97	0.26	5096				M6(H13)M6.5(H97)M7.25(Luc01)M6.75(RRL)>M9.5(WLR)		
5 05 35 05.45	-05 25 55.8	M5.3	-1.319	0.39	0.09	M5.2	-1.272	0.54	0.06	M5.3	-1.287	0.46	0.09	M5.2	-1.227	0.64	0.06	270				M3.5(H97)		
6 05 35 05.64	-05 25 19.3	K1.8	0.662	0.36	0.40	K1.5	0.817	1.00	0.45	K1.8	0.694	0.43	0.40	K1.6	0.906	1.18	0.43	273				K0(WSH)K0-K3e(H97)A0V+K1V(?)A0V(vA)K0:e(J)K4eIV(W)K3(CK)K2(Ste)		
7 05 35 05.68	-05 23 45.4	M2.5	-1.454	2.59	0.34	M2.2	-1.299	3.02	0.21	M2.5	-1.250	3.05	0.34	M1.9	-1.086	3.45	0.17	274				M5:(H13)<M0e(H97)		
8 05 35 05.68	-05 25 04.2	M4.9	-0.616	0.00	0.00	M4.9	-0.615	0.00	0.00	M4.9	-0.617	0.00	0.00	M4.9	-0.616	0.00	0.00							
9 05 35 05.71	-05 23 54.1	M4.8	-0.510	0.22	0.00	M4.8	-0.510	0.22	0.00	M4.8	-0.493	0.26	0.00	M4.8	-0.493	0.26	0.00	276				M5-M5.5(H13)M4-4.5(H97)		
10 05 35 05.72	-05 24 18.4	M0.6	-0.938	1.34	2.82	M1.9	-0.587	2.84	3.53	M0.5	-0.796	1.60	2.55	M0.3	-0.249	3.32	2.27	278				K2-K7e(H97)		
11 05 35 05.79	-05 23 16.0	M5.4	-1.276	0.77	0.03	M5.4	-1.262	0.81	0.02	M5.5	-1.221	0.88	0.03	M5.4	-1.203	0.93	0.02	279				M6.5e(H13)M5.5e(H97)		
12 05 35 05.67	-05 25 06.4	M0.6	-0.281	0.90	0.10	M0.5	-0.219	1.07	0.06	M0.6	-0.197	1.09	0.09	M0.5	-0.132	1.25	0.04							
13 05 35 06.17	-05 22 12.5	M4.0	-0.908	4.85	1.08	M3.7	-0.626	5.74	0.80	M3.9	-0.506	5.67	0.93	M3.3	-0.175	6.76	0.72	3064				M2.5(H13)M4(H97)		
14 05 35 06.28	-05 22 02.7	K5.1	0.259	5.93	0.06	K4.9	0.301	6.11	0.08	K6.4	0.568	6.58	0.15	K5.1	0.755	7.01	0.01	286				K5(H97)		
15 05 35 06.42	-05 23 15.2	M7.5	-1.214	1.15	0.00	M7.5	-1.209	1.15	0.00	M7.5	-1.117	1.38	0.00	M7.5	-1.134	1.32	0.00	289				M6(H13)		
16 05 35 06.44	-05 22 07.5	M5.1	-1.214	0.01	0.06	M5.0	-1.182	0.10	0.04	M5.1	-1.213	0.01	0.06	M5.1	-1.175	0.11	0.04	287				M5.5-M6.5e(H13)M3.5e(H97)		
17 05 35 06.46	-05 21 18.7	M5.2	-1.158	0.16	0.03	M5.2	-1.138	0.22	0.02	M5.2	-1.135	0.22	0.03	M5.2	-1.114	0.28	0.02	288				M5(H97)		
18 05 35 06.54	-05 25 01.5	M4.3	-1.054	0.63	0.10	M4.3	-1.032	0.68	0.06	M4.3	-1.007	0.73	0.09	M4.2	-0.983	0.78	0.05	292				M4.5(H13)M4(H97)M4.5(H97)		
19 05 35 06.51	-05 24 41.4	K9.0	-0.123	0.73	0.00	K9.0	-0.123	0.73	0.00	K9.1	-0.066	0.86	0.00	K9.1	-0.066	0.86	0.00	291				M1(H97)K4-M0(Sam)K6(Ste)		
20 05 35 06.88	-05 22 09.3	M5.6	-1.405	0.06	0.03	M5.6	-1.389	0.11	0.02	M5.6	-1.393	0.10	0.03	M5.6	-1.383	0.12	0.02	298				M1.5(H13)M6(H97)M5(Luc01)M6(RRL)M6(WLR)		
21 05 35 06.91	-05 26 00.6	M4.8	-1.057	0.61	0.07	M4.8	-1.029	0.68	0.04	M4.8	-1.007	0.72	0.06	M4.7	-0.980	0.79	0.04	299				M3.5(H13)		
22 05 35 07.27	-05 22 26.5	M4.9	-0.712	0.22	0.03	M4.9	-0.698	0.26	0.02	M4.9	-0.694	0.26	0.03	M4.9	-0.679	0.30	0.02	300				M4.5(H13)M2-M4:(H97)M6(SHC-ir)		
23 05 35 07.39	-05 22 28.9	M5.0	-0.984	0.19	0.02	M5.0	-0.980	0.20	0.01	M5.0	-0.972	0.22	0.02	M5.0	-0.966	0.23	0.01	302				M5-M5.5(H13)M6(SHC-ir)		
24 05 35 07.40	-05 25 48.1	M5.7	-1.071	0.00	0.03	M5.7	-1.066	0.00	0.02	M5.7	-1.072	0.00	0.03	M5.7	-1.066	0.00	0.02	303				M6.5-M8e(H13)		
25 05 35 07.64	-05 24 00.9	M3.5	-0.753	0.66	0.03	M3.4	-0.741	0.69	0.02	M3.4	-0.702	0.78	0.03	M3.4	-0.689	0.81	0.02	305				M3-M3.5(H97)		
26 05 35 07.70	-05 24 52.9	M5.8	-1.364	0.00	0.00	M5.8	-1.364	0.00	0.00	M5.8	-1.362	0.00	0.00	M5.8	-1.362	0.00	0.00	306				M4(H97)M6.5(RRL)M6(WLR)		
27 05 35 07.73	-05 21 27.2	M7.2	-2.148	0.59	0.47	M7.0	-1.912	1.54	0.48	M7.0	-2.023	0.96	0.43	M6.8	-1.805	1.78	0.45							
28 05 35 08.23	-05 24 03.3	M4.8	-0.815	2.40	0.02	M4.8	-0.803	2.44	0.02	M4.8	-0.629	2.82	0.02	M4.7	-0.617	2.86	0.02	314				M4.5(H13)M4.75(RRL)		
29 05 35 08.29	-05 24 34.9	M5.2	-0.872	0.32	0.04	M5.2	-0.852	0.38	0.03	M5.2	-0.849	0.37	0.04	M5.2	-0.819	0.45	0.03	317				M5.5e(H13)		
30 05 35 08.43	-05 23 04.9	M6.4	-1.287	2.85	0.00	M6.4	-1.294	2.85	0.00	M6.4	-1.095	3.26	0.00	M6.4	-1.073	3.33	0.00							
31 05 35 08.52	-05 24 41.5	M5.1	-0.879	0.56	0.03	M5.0	-0.856	0.63	0.02	M5.1	-0.831	0.67	0.03	M5.0	-0.810	0.73	0.02	322				M4.5(H97)		
32 05 35 08.53	-05 25 17.9	M2.0	-0.524	1.14	0.08	M1.8	-0.476	1.25	0.02	M2.0	-0.430	1.34	0.07	M1.8	-0.382	1.45	0.02	323				M2(H97)		
33 05 35 08.73	-05 22 56.7	K9.5	-0.315	5.20	0.01	K9.3	-0.285	5.31	0.01	K9.6	0.094	6.11	0.01	K9.4	0.108	6.16	0.00	3072				M1.5(H13)		
34 05 35 09.69	-05 21 24.8	M3.7	-0.860	0.07	0.06	M3.6	-0.820	0.20	0.03	M3.7	-0.847	0.11	0.06	M3.6	-0.803	0.24	0.03	332				M3(H13)M3.5(H97)		
35 05 35 09.77	-05 21 28.3	K4.7	0.246	6.15	0.17	K4.9	0.328	6.58	0.26	K4.9	0.747	7.28	0.15	K4.8	0.851	7.64	0.16	336				MM0(H13),K5-K7(H13)		
36 05 35 09.90	-05 23 38.4	M5.7	-1.226	0.63	0.06	M5.6	-1.201	0.70	0.04	M5.6	-1.186	0.71	0.06	M5.6	-1.143	0.83	0.04							
37 05 35 09.77	-05 23 26.7	K9.0	0.091	0.45	0.36	K9.1	0.248	0.93	0.28	K9.0	0.134	0.53	0.34	K9.0	0.326	1.09	0.26	337				K8(H97)K4-M0(Sam)K4(Ste)		
38 05 35 10.16	-05 22 32.4	M2.2	-0.588	1.12	0.00	M2.2	-0.586	1.13	0.00	M2.3	-0.499	1.32	0.00	M2.3	-0.500	1.31	0.00	340				M2(H13)		
39 05 35 10.21	-05 23 21.4	K6.7	0.227	6.14	0.26	K6.8	0.350	6.56	0.24	K7.1	0.708	7.16	0.22	K7.0	0.847	7.56	0.17	341				K4-K7(H97)		
40 05 35 10.25	-05 21 57.1	M5.6	-1.017	1.15	0.01	M5.5	-1.007	1.18	0.00	M5.5	-0.923	1.36	0.01	M5.5	-0.907	1.41	0.00	342				M5.5(H13)M5(SHC-ir)M5.75(RRL)		
41 05 35 10.48	-05 26 00.3	M5.9	-1.095	0.28	0.01	M5.9	-1.089	0.31	0.01	M5.9	-1.078	0.32	0.01	M5.9	-1.062	0.38	0.02	3104				M5.5(H13)		
42 05 35 10.53	-05 22 16.5	M3.8	-0.395	6.37	0.01	M3.8	-0.359	6.50	0.01	M3.6	0.181	7.79	0.00	M3.6	0.199	7.85	0.00							
43 05 35 10.54	-05 24 16.6	K7.9	-0.971	1.76	0.36	K7.7	-0.803	2.25	0.25	K7.8	-0.803	2.10	0.30	K7.6	-0.619	2.60	0.19	349				K8-M0(H13)K:(H97)		
44 05 35 10.60	-05 22 44.6	M3.0	-0.845	0.90	0.57	M2.6	-0.635	1.44	0.32	M3.0	-0.769	1.06	0.54	M2.4	-0.509	1.69	0.26	350				M2(H13)		
45 05 35 10.51	-05 22 45.5	M1.2	0.101	0.92	0.00	M1.2	0.101	0.92	0.00	M1.3	0.168	1.06	0.00	M1.3	0.169	1.06	0.00	345				M0.5(H97)M0-M2(Sam)K6(Ste)		

Table 1 continued

Table 1 (continued)

ID	RA	DEC	$R_V = 3.1^a$								$R_V = 5.5^b$								Star <sup>c</sup>	SpT
			Constant				BB(7000 K)				Constant				BB(7000 K)					
			SpT	Log $L_\star$	$A_V$	$r_{7465}$	SpT	Log $L_\star$	$A_V$	$r_{7465}$	SpT	Log $L_\star$	$A_V$	$r_{7465}$	SpT	Log $L_\star$	$A_V$	$r_{7465}$		
			$(L_\odot)$ (mag)				$(L_\odot)$ (mag)				$(L_\odot)$ (mag)				$(L_\odot)$ (mag)					(Literature <sup>d</sup> )
46 05 35	10.58 -05 21 56.2	K6.3 -0.127	0.69	0.29	K6.2	0.013	1.11	0.20	K6.3	-0.059	0.83	0.26	K6.3	0.101	1.28	0.18	347		K3-K7(H97)M0(H97)M2(E)K2-K4(Sam)K5(Ste)	
47 05 35	10.84 -05 25 56.8	M5.4 -1.047	2.07	0.13	M5.3	-0.984	2.26	0.08	M5.3	-0.861	2.52	0.12	M5.2	-0.785	2.73	0.08	3102		M6.5(H13)	
48 05 35	10.86 -05 22 40.6	M6.2 -1.043	4.24	0.03	M6.1	-0.970	4.51	0.03	M6.3	-0.690	5.03	0.03	M6.0	-0.679	5.14	0.03				
49 05 35	10.92 -05 22 46.2	K9.4 -1.654	0.00	0.01	K9.4	-1.651	0.01	0.00	K9.4	-1.653	0.00	0.01	K9.3	-1.651	0.01	0.00	355		M0-M0.5(H13)mid-K::(H97)	
50 05 35	10.95 -05 24 48.7	M4.3 -0.423	1.44	0.23	M4.0	-0.384	1.51	0.12	M4.3	-0.317	1.66	0.21	M3.9	-0.263	1.80	0.11	356		M3e(H97)M3(SHC-ir)	
51 05 35	10.73 -05 23 44.7	K7.6	0.884	0.82	K7.4	0.902	0.84	0.00	K7.6	0.953	0.97	0.02	K7.5	0.968	0.99	0.00	352		K8(H97)M0.1(P)M1(E)K2V(HT)K5IV(Ham)K2-K3(Sam)K5(Ste)	
52 05 35	11.00 -05 22 24.5	M4.5 -0.683	3.83	0.00	M4.5	-0.683	3.83	0.00	M4.4	-0.400	4.48	0.00	M4.4	-0.400	4.47	0.00				
53 05 35	11.16 -05 25 32.2	M4.7 -1.099	2.18	0.00	M4.7	-1.098	2.18	0.00	M4.7	-0.925	2.57	0.00	M4.7	-0.924	2.57	0.00	3098		M5(H13)M4.75(RRL)	
54 05 35	11.64 -05 22 51.4	M5.2 -1.045	0.31	0.13	M5.1	-0.979	0.52	0.09	M5.2	-1.016	0.37	0.13	M5.1	-0.933	0.62	0.08				
55 05 35	11.66 -05 24 21.4	M5.4 -0.959	0.25	0.08	M5.4	-0.918	0.37	0.05	M5.4	-0.932	0.31	0.07	M5.4	-0.878	0.47	0.05	366		M4.5-M5e(H97)	
56 05 35	11.49 -05 26 02.3	K6.6	0.407	1.23	K6.4	0.451	1.33	0.02	K6.6	0.503	1.43	0.06	K6.4	0.557	1.54	0.00	365		K2-K3(Sam)K4(Ste)	
57 05 35	11.72 -05 23 40.3	M5.4 -0.699	0.02	0.00	M5.4	-0.697	0.03	0.00	M5.4	-0.696	0.03	0.00	M5.4	-0.699	0.02	0.00	9008		M4.5(H97)	
58 05 35	11.72 -05 23 51.7	M0.7 -1.128	0.86	0.35	M0.3	-0.949	1.38	0.23	M0.7	-1.046	1.07	0.36	M0.5	-0.825	1.69	0.24	368		M0-M3(H13)	
59 05 35	11.77 -05 21 55.5	M5.4 -0.852	0.31	0.06	M5.3	-0.819	0.41	0.04	M5.4	-0.829	0.35	0.06	M5.3	-0.785	0.49	0.04	369		M5.5(H13)M6(SHC-ir)	
60 05 35	12.13 -05 24 33.7	M5.8 -1.321	1.29	0.37	M5.4	-1.157	1.87	0.27	M5.8	-1.219	1.53	0.36	M5.4	-1.002	2.23	0.26	376		M1-M2e(H13)M5.5(RRL)M7(WLR)	
61 05 35	12.28 -05 23 48.0	K9.5	0.101	0.81	K9.3	0.115	0.83	0.01	K9.4	0.177	0.96	0.01	K9.3	0.183	0.97	0.00				
62 05 35	12.60 -05 23 44.1	K4.9	0.571	0.68	K4.9	0.571	0.68	0.00	K5.1	0.614	0.77	0.00	K5.0	0.614	0.77	0.00	385		K1V(HT)<K7(P)<M0(Sam)K4(Ste)	
63 05 35	12.96 -05 24 57.9	M5.1 -1.240	2.03	0.00	M5.1	-1.224	2.09	0.00	M5.1	-1.089	2.37	0.00	M5.1	-1.058	2.46	0.00				
64 05 35	13.02 -05 22 00.9	M5.2 -0.953	0.71	0.05	M5.2	-0.930	0.78	0.03	M5.2	-0.897	0.84	0.05	M5.2	-0.861	0.95	0.03	395		M5.5(H13)M2(H97)	
65 05 35	13.05 -05 22 15.2	M3.9 -0.692	0.85	0.15	M3.7	-0.615	1.09	0.09	M3.8	-0.616	1.03	0.14	M3.7	-0.525	1.30	0.09	9029		M4.5(H97)	
66 05 35	13.10 -05 22 53.1	M5.6 -1.612	0.07	0.34	M5.4	-1.469	0.49	0.23	M5.6	-1.606	0.08	0.34	M5.3	-1.436	0.58	0.24	9030		mid-M::(H13)M2:(H97)	
67 05 35	13.13 -05 24 52.9	M5.9 -1.629	1.37	0.28	M5.7	-1.528	1.70	0.20	M5.8	-1.532	1.56	0.27	M5.7	-1.404	1.97	0.19				
68 05 35	13.18 -05 22 21.0	M2.7 -0.813	1.20	0.48	M2.3	-0.620	1.68	0.26	M2.6	-0.704	1.43	0.44	M2.2	-0.483	1.96	0.23				
69 05 35	13.20 -05 24 55.4	K7.4	0.084	2.00	K6.8	0.236	2.32	0.11	K7.2	0.289	2.41	0.20	K6.7	0.422	2.65	0.04	401		K0-K2e(H97)<M0(Sam)	
70 05 35	13.29 -05 22 58.0	M6.2 -1.414	0.01	0.60	M5.9	-1.237	0.59	0.43	M6.2	-1.413	0.01	0.60	M5.9	-1.187	0.70	0.42	9038		M2-M6(H13)cont(H97)	
71 05 35	13.31 -05 23 53.1	M6.5 -1.633	0.81	0.06	M6.5	-1.625	0.87	0.06	M6.5	-1.574	0.94	0.05	M6.3	-1.579	0.99	0.05				
72 05 35	13.37 -05 22 26.2	M4.3 -0.827	0.98	0.11	M4.2	-0.808	1.02	0.07	M4.3	-0.759	1.12	0.10	M4.2	-0.734	1.18	0.06	404		M4.5-M5.5(H97)	
73 05 35	13.37 -05 23 53.1	M8.5 -0.797	5.41	0.00	M8.6	-0.796	5.33	0.00	M8.6	-0.372	6.29	0.00	M8.6	-0.398	6.22	0.00				
74 05 35	13.52 -05 23 04.6	M5.7 -0.894	2.00	0.00	M5.7	-0.908	1.95	0.00	M5.7	-0.743	2.33	0.00	M5.7	-0.745	2.33	0.00	9045		M3(H13)late-K:(H97)	
75 05 35	13.53 -05 23 30.9	M3.1 -0.764	0.00	0.00	M3.7	-0.757	0.00	0.07	M3.6	-0.774	0.00	0.09	M3.7	-0.757	0.00	0.07	412		M3(H97)	
76 05 35	13.44 -05 23 40.3	M0.8 -0.353	1.36	0.73	M0.0	-0.078	2.13	0.46	M0.7	-0.214	1.65	0.66	K9.8	0.092	2.44	0.38	409		<M0(Sam)K4(Ste)	
77 05 35	13.61 -05 24 25.7	K8.9 -0.538	1.11	0.03	K9.0	-0.519	1.18	0.03	K8.9	-0.440	1.33	0.02	K9.0	-0.427	1.37	0.02	417		M0.5(H97)	
78 05 35	13.61 -05 21 20.9	M4.5 -1.351	0.21	0.09	M4.4	-1.324	0.28	0.06	M4.5	-1.331	0.25	0.09	M4.4	-1.309	0.31	0.06				
79 05 35	13.52 -05 22 19.6	M0.4 -0.223	1.84	0.19	M0.4	-0.132	2.12	0.15	M0.4	-0.065	2.17	0.16	M0.3	0.036	2.47	0.12	411		M1.4(P)K-M(LR)	
80 05 35	13.75 -05 22 22.0	M1.9 -0.169	2.15	0.18	M0.9	-0.029	2.46	0.00	M2.0	-0.009	2.49	0.18	M1.0	0.156	2.86	0.00	420		M2e(H13)M1.5(H97)>G6(LR)	
81 05 35	13.81 -05 22 02.7	M5.3 -1.174	1.80	0.00	M5.3	-1.167	1.82	0.00	M5.2	-1.022	2.16	0.00	M5.2	-1.012	2.20	0.00	424		M1(H13)	
82 05 35	13.93 -05 23 20.2	M5.4 -1.351	0.00	0.35	M5.4	-1.270	0.15	0.23	M5.4	-1.352	0.00	0.35	M5.4	-1.255	0.18	0.22				
83 05 35	13.79 -05 22 06.9	K8.0	0.021	1.41	K7.6	0.175	1.83	0.23	K8.0	0.148	1.68	0.32	K7.4	0.325	2.10	0.17	423		K2e(H)M0,M4(Sam)G4-K3(LR)K5(Ste)	
84 05 35	14.04 -05 25 50.1	M5.5 -0.888	0.44	0.00	M5.5	-0.888	0.43	0.00	M5.5	-0.849	0.53	0.00	M5.5	-0.853	0.52	0.00	3099		M6(H13)M4.5(H97)	
85 05 35	14.06 -05 25 20.4	M5.6 -0.790	1.62	0.22	M5.4	-0.695	1.92	0.16	M5.6	-0.660	1.91	0.22	M5.4	-0.532	2.30	0.15	3093		M6(H13)	
86 05 35	14.05 -05 23 38.5	M2.6	0.012	0.54	M2.5	0.017	0.55	0.00	M2.7	0.024	0.59	0.05	M2.5	0.062	0.65	0.00	431		M3(H97)<M0(Sam)	
87 05 35	14.09 -05 22 36.6	M4.1 -0.232	0.46	0.10	M3.9	-0.201	0.55	0.05	M4.1	-0.196	0.54	0.09	M3.9	-0.153	0.67	0.05	432		M3.1(P)K5-M2(LR)	
88 05 35	14.31 -05 22 04.2	M5.4 -1.241	1.87	0.00	M5.4	-1.237	1.89	0.00	M5.4	-1.065	2.30	0.00	M5.3	-1.073	2.29	0.00				
89 05 35	14.32 -05 23 08.5	M5.6 -1.039	2.94	0.57	M5.5	-0.877	3.42	0.45	M5.6	-0.801	3.47	0.55	M5.5	-0.571	4.14	0.44	9061		mid-M:(H97)K5-M2(LR)	
90 05 35	14.34 -05 25 15.7	M5.9 -0.898	1.14	0.05	M5.9	-0.876	1.21	0.04	M5.9	-0.803	1.36	0.05	M5.8	-0.779	1.45	0.04				
91 05 35	14.40 -05 23 23.1	M5.9 -1.143	2.42	0.00	M5.8	-1.115	2.54	0.00	M5.9	-0.911	2.98	0.00	M5.9	-0.902	3.02	0.00				
92 05 35	14.45 -05 25 02.1	M2.7 -0.693	0.87	0.24	M2.3	-0.566	1.17	0.10	M2.6	-0.612	1.05	0.22	M2.2	-0.471	1.37	0.08	443		M2(H97)K5(Ste)	

Table 1 continued



Table 1 (continued)

ID	RA	DEC	$R_V = 3.1^a$								$R_V = 5.5^b$								Star <sup>c</sup>	SpT
			Constant				BB(7000 K)				Constant				BB(7000 K)					
			SpT	Log $L_\star$	$A_V$	$r_{7465}$	SpT	Log $L_\star$	$A_V$	$r_{7465}$	SpT	Log $L_\star$	$A_V$	$r_{7465}$	SpT	Log $L_\star$	$A_V$	$r_{7465}$		
$(L_\odot)$ (mag)				$(L_\odot)$ (mag)				$(L_\odot)$ (mag)				$(L_\odot)$ (mag)				(Literature <sup>d</sup> )				
93 05 35	14.28	-05 24 24.6	K7.6	0.288	0.90	0.13	K7.3	0.359	1.07	0.07	K7.6	0.367	1.07	0.12	K7.4	0.443	1.24	0.06	437	K7(H97)K4,M0-M1(Sam)K5(Ste)
94 05 35	14.40	-05 23 33.7	K9.2	0.114	1.62	0.01	K9.2	0.119	1.63	0.00	K9.4	0.246	1.91	0.00	K9.4	0.248	1.92	0.00	441	M1(H97)K5-M2(LR)
95 05 35	14.52	-05 22 06.5	M3.8	-0.896	2.03	0.00	M3.8	-0.895	2.04	0.00	M3.7	-0.732	2.41	0.00	M3.7	-0.720	2.45	0.00	442	M3(H97)
96 05 35	14.61	-05 22 00.9	M6.9	-0.610	6.01	0.02	M6.7	-0.537	6.32	0.01	M6.9	-0.125	7.11	0.02	M6.8	-0.041	7.42	0.01	9066	K:(H97)
97 05 35	14.67	-05 23 02.0	M1.2	-0.483	3.69	0.26	M1.3	-0.369	4.07	0.24	M0.9	-0.074	4.62	0.15	M0.9	-0.011	4.78	0.11	9069	M0.5-M2.5(H97)M0-M3(LR)
98 05 35	14.82	-05 23 46.5	M2.6	-0.758	0.84	0.13	M2.5	-0.691	1.01	0.08	M2.5	-0.683	1.00	0.12	M2.5	-0.611	1.18	0.07	453	K6-M4(LR)
99 05 35	14.72	-05 23 22.9	M0.9	-0.548	2.46	0.17	M0.1	-0.446	2.72	0.06	M0.5	-0.276	3.06	0.08	K9.9	-0.230	3.13	0.00	451	M3e(H97)K-M(LR)
100 05 35	14.83	-05 23 16.1	M4.4	-0.849	0.71	0.00	M4.4	-0.850	0.71	0.00	M4.4	-0.797	0.82	0.00	M4.4	-0.796	0.83	0.00		
101 05 35	14.87	-05 22 31.7	M3.0	-1.308	2.60	0.61	M2.6	-1.083	3.21	0.37	M2.9	-1.096	3.06	0.57	M2.4	-0.811	3.77	0.29	452	K-M:(H13)
102 05 35	14.66	-05 22 33.9	K8.5	0.288	1.95	0.27	K9.0	0.408	2.40	0.29	K8.5	0.462	2.32	0.23	K8.8	0.601	2.76	0.21	448	K7(P)K3-K4,M0-M1.5(Sam)K5-M2(LR)
103 05 35	14.88	-05 24 11.9	M4.8	-0.588	0.90	0.00	M4.8	-0.588	0.90	0.00	M4.8	-0.517	1.06	0.00	M4.8	-0.517	1.06	0.00	9077	M4(H97)
104 05 35	14.92	-05 24 12.9	M4.1	-0.640	0.87	0.02	M4.1	-0.636	0.87	0.01	M4.1	-0.577	1.00	0.01	M4.0	-0.572	1.00	0.00	9080	M5.5(H97)
105 05 35	14.93	-05 23 29.1	M4.3	-0.581	1.28	0.07	M4.1	-0.582	1.27	0.04	M4.2	-0.488	1.49	0.06	M4.0	-0.488	1.47	0.03	455	K-M(LR)
106 05 35	15.01	-05 21 47.3	M5.6	-1.436	1.61	0.19	M5.3	-1.362	1.89	0.13	M5.6	-1.317	1.87	0.18	M5.2	-1.203	2.29	0.15		
107 05 35	15.03	-05 22 31.3	M5.3	-1.035	1.09	0.00	M5.3	-1.032	1.10	0.00	M5.2	-0.948	1.29	0.00	M5.2	-0.942	1.31	0.00	9086	M6(H97)M6(H97)
108 05 35	15.03	-05 23 54.5	M6.3	-1.266	0.38	0.00	M6.3	-1.260	0.38	0.00	M6.3	-1.242	0.41	0.00	M6.3	-1.241	0.41	0.00		
109 05 35	14.95	-05 23 39.3	K7.0	0.219	1.28	0.07	K6.9	0.261	1.39	0.04	K7.0	0.340	1.53	0.04	K6.9	0.368	1.60	0.02	456	K5-M2(LR)
110 05 35	14.92	-05 22 39.3	K6.2	0.216	1.37	0.39	K6.2	0.380	1.92	0.34	K6.2	0.348	1.65	0.34	K6.2	0.540	2.23	0.29	454	K4(H97)K7(E)K4-M0(Sam)K5-M2(LR)K3(Ste)
111 05 35	15.16	-05 23 46.8	M2.0	-0.771	0.54	0.16	M1.8	-0.687	0.73	0.07	M2.0	-0.727	0.63	0.16	M1.8	-0.634	0.84	0.07	464	M0-M1(H13)K5-M2(LR)
112 05 35	15.20	-05 22 54.5	K4.8	0.150	2.97	0.52	K5.1	0.318	3.68	0.60	K5.0	0.430	3.54	0.41	K5.2	0.636	4.26	0.43	463	K2-K5(H97)G4-K5(LR)
113 05 35	14.99	-05 21 59.9	K6.4	0.074	1.21	0.23	K6.5	0.175	1.56	0.22	K6.4	0.174	1.41	0.21	K6.5	0.301	1.80	0.18	457	K3-K4(Sam)K5-M2(LR)K5(Ste)
114 05 35	15.20	-05 23 18.9	M4.7	-1.496	0.01	0.19	M4.8	-1.455	0.13	0.19	M4.7	-1.506	0.00	0.23	M4.8	-1.447	0.13	0.19		
115 05 35	15.39	-05 22 25.5	M2.8	-0.533	1.43	0.02	M2.8	-0.519	1.46	0.00	M2.8	-0.408	1.70	0.00	M2.8	-0.404	1.72	0.00	9096	M0-M3(LR)
116 05 35	15.38	-05 23 33.5	M5.3	-0.659	0.72	0.06	M5.3	-0.631	0.81	0.04	M5.3	-0.587	0.90	0.05	M5.2	-0.554	1.00	0.04	5177	M2e(H97)M0-M3(LR)
117 05 35	15.21	-05 22 24.2	K4.9	-0.116	1.86	0.34	K5.0	0.027	2.39	0.33	K5.0	0.072	2.26	0.27	K5.0	0.232	2.77	0.25	467	K6(H13)K7(H97)K5-M2(LR)
118 05 35	15.42	-05 25 59.7	M6.1	-1.611	0.01	0.00	M6.1	-1.612	0.01	0.00	M6.1	-1.610	0.01	0.00	M6.1	-1.602	0.04	0.00	3103	M6.5(RRL)
119 05 35	15.44	-05 23 45.6	M3.0	-0.417	1.26	0.45	M2.6	-0.241	1.71	0.25	M2.9	-0.304	1.51	0.41	M2.3	-0.086	2.01	0.18	475	M1e(H97)K0-K7(LR)
120 05 35	15.27	-05 22 57.1	K6.2	0.226	0.88	0.39	K6.2	0.392	1.43	0.34	K6.2	0.311	1.05	0.36	K6.2	0.511	1.66	0.30	468	G6-G8(H97)K0-K7(LR)
121 05 35	15.49	-05 22 48.7	M1.7	-0.107	1.33	0.07	M1.3	-0.050	1.46	0.00	M1.7	-0.002	1.56	0.06	M1.4	0.061	1.70	0.00	476	M2(H97)K5-M2(LR)
122 05 35	15.52	-05 23 37.5	M6.7	-1.279	0.98	4.80	M6.1	-0.828	2.75	4.44	M6.8	-1.170	1.24	4.78	M6.1	-0.571	3.38	4.43	5178	K(LR)
123 05 35	15.34	-05 22 15.5	K2.8	0.539	3.17	0.13	K2.8	0.604	3.43	0.15	K2.7	0.877	3.91	0.04	K2.7	0.899	4.02	0.06	470	K3-K5(H97)<=K5(P)G4-K5(LR)K3e(Sta)
124 05 35	15.61	-05 22 59.0	M6.8	-1.067	1.42	0.00	M6.9	-1.063	1.43	0.00	M6.8	-0.911	1.84	0.00	M6.8	-0.910	1.85	0.00		
125 05 35	15.64	-05 22 56.6	K5.3	0.707	1.44	0.00	K5.2	0.716	1.48	0.00	K5.4	0.816	1.68	0.00	K5.4	0.818	1.69	0.00	479	G8-K1(H97)K0-K7(LR)K3(Ste)
126 05 35	15.66	-05 25 10.5	M3.7	-0.844	1.21	0.15	M3.4	-0.764	1.51	0.09	M3.7	-0.724	1.51	0.14	M3.4	-0.638	1.78	0.07	9108	M1.5(H97)
127 05 35	15.68	-05 25 33.2	M0.4	-0.561	1.01	1.68	M0.5	-0.189	2.34	1.61	M0.5	-0.466	1.23	1.67	M0.5	0.032	2.90	1.67	482	K8e(H97)<M0(Sam)
128 05 35	15.73	-05 23 22.5	K5.4	0.068	1.96	0.21	K5.2	0.195	2.32	0.13	K6.1	0.159	2.15	0.26	K5.3	0.378	2.65	0.07		
129 05 35	15.76	-05 21 39.7	M2.8	-0.756	0.77	0.00	M2.8	-0.754	0.78	0.00	M2.8	-0.695	0.91	0.00	M2.8	-0.694	0.91	0.00	481	M3(H97)
130 05 35	15.76	-05 23 38.5	M2.2	-0.853	2.10	0.04	M1.9	-0.822	2.18	0.00	M2.1	-0.687	2.46	0.03	M2.0	-0.653	2.55	0.00		
131 05 35	15.75	-05 24 11.6	M6.5	-1.572	0.01	0.00	M6.5	-1.569	0.01	0.00	M6.5	-1.570	0.01	0.00	M6.5	-1.570	0.01	0.00		
132 05 35	15.55	-05 25 14.1	K8.2	0.398	1.04	0.03	K8.0	0.417	1.06	0.00	K8.2	0.493	1.24	0.01	K8.1	0.501	1.25	0.00	478	M0.4(P)K4,K7-M1(Sam)K4(Ste)
133 05 35	15.78	-05 23 10.1	G2.8	1.677	1.57	0.00	G2.7	1.676	1.57	0.00	G3.9	1.783	1.81	0.00	G3.9	1.784	1.81	0.00	1864	B5-B8+G0-G5(Par)G4-K3(LR)
134 05 35	15.78	-05 24 24.7	M4.0	-0.967	1.08	0.39	M3.9	-0.825	1.48	0.26	M4.0	-0.879	1.26	0.37	M3.8	-0.704	1.75	0.25		
135 05 35	15.79	-05 23 26.7	M2.8	-1.356	1.14	3.70	M3.1	-0.890	2.76	3.52	M3.0	-1.238	1.41	3.67	M3.1	-0.634	3.39	3.57	489	G4-K5(LR)
136 05 35	15.61	-05 24 03.2	K6.3	0.067	1.00	0.00	K6.3	0.067	1.00	0.00	K6.4	0.139	1.15	0.00	K6.4	0.143	1.16	0.00	480	K8-M0(H97)<M0(Sam)K5(Ste)
137 05 35	15.84	-05 22 46.1	M3.6	-0.468	0.78	0.11	M3.3	-0.412	0.96	0.04	M3.6	-0.398	0.94	0.10	M3.3	-0.337	1.13	0.04	492	M3e(H97)K6-M4(LR)
138 05 35	15.84	-05 23 22.5	K6.5	0.056	1.74	0.49	K6.3	0.261	2.36	0.37	K6.5	0.222	2.13	0.47	K6.4	0.480	2.88	0.36		
139 05 35	15.85	-05 23 25.7	M2.9	-0.883	1.73	0.01	M2.8	-0.859	1.83	0.00	M2.9	-0.720	2.13	0.01	M2.8	-0.697	2.21	0.00	489	G4-K5(LR)

Table 1 continued

Table 1 (continued)

ID	RA	DEC	$R_V = 3.1^a$								$R_V = 5.5^b$								Star <sup>c</sup>	SpT
			Constant				BB(7000 K)				Constant				BB(7000 K)					
			SpT	Log $L_\star$	$A_V$	$r_{7465}$	SpT	Log $L_\star$	$A_V$	$r_{7465}$	SpT	Log $L_\star$	$A_V$	$r_{7465}$	SpT	Log $L_\star$	$A_V$	$r_{7465}$		
			$(L_\odot)$ (mag)				$(L_\odot)$ (mag)				$(L_\odot)$ (mag)				$(L_\odot)$ (mag)					(Literature <sup>d</sup> )
140 05 35	15.90	-05 23 38.1	M5.2	-1.536	0.38	0.29	M4.9	-1.400	0.81	0.20	M5.2	-1.508	0.45	0.29	M5.0	-1.327	0.97	0.20		
141 05 35	15.95	-05 22 21.2	K9.5	-0.608	1.88	0.85	K9.2	-0.326	2.73	0.64	K9.4	-0.424	2.25	0.74	K9.0	-0.104	3.13	0.52	496	K7e(H97)K-M(LR)
142 05 35	15.89	-05 22 33.3	M5.6	-1.169	1.43	0.30	M5.5	-1.061	1.79	0.25	M5.6	-1.050	1.71	0.30	M5.5	-0.924	2.11	0.26		M4-M6e(H13)M2.5:e(H97)
143 05 35	16.00	-05 21 47.0	M4.7	-0.663	1.07	0.04	M4.6	-0.648	1.11	0.03	M4.6	-0.579	1.26	0.03	M4.6	-0.562	1.30	0.02	500	M5.5(H97)
144 05 35	16.00	-05 23 53.1	K7.4	0.136	1.80	0.18	K7.2	0.228	2.04	0.11	K7.4	0.306	2.15	0.13	K7.2	0.391	2.36	0.07	503	F2-F7e(H97)K0-K7(LR)
145 05 35	16.03	-05 25 51.1	M5.3	-1.014	0.84	0.12	M5.3	-0.947	1.05	0.08	M5.3	-0.942	1.01	0.11	M5.2	-0.865	1.23	0.08	9124	M4(H97)
146 05 35	16.09	-05 24 11.6	M4.6	-0.734	0.87	0.12	M4.5	-0.687	1.01	0.08	M4.6	-0.664	1.03	0.12	M4.5	-0.609	1.17	0.08	505	M2-M4:(H13)M2(H97)
147 05 35	16.11	-05 22 12.5	M5.4	-1.109	1.07	0.01	M5.4	-1.109	1.07	0.00	M5.4	-1.012	1.30	0.00	M5.4	-1.010	1.31	0.00		
148 05 35	16.15	-05 22 55.5	M6.8	-1.436	2.26	0.01	M6.6	-1.447	2.32	0.02	M6.6	-1.215	2.86	0.01	M6.6	-1.211	2.89	0.02	9128	M0-M3(LR)
149 05 35	15.95	-05 23 50.1	K4.8	0.539	1.53	1.11	K5.4	0.762	2.64	1.53	K5.0	0.699	1.82	0.96	K4.8	1.070	3.09	0.99	499	K0:e(H97)G5:(HT)G4-K5(LR)K3(Ste)M0.5+M2(Dae)
150 05 35	16.20	-05 22 37.6	M5.6	-0.751	1.08	0.00	M5.6	-0.751	1.08	0.00	M5.6	-0.664	1.28	0.00	M5.6	-0.664	1.28	0.00	9132	M3.5(H97)
151 05 35	16.19	-05 21 32.3	M3.8	-0.820	1.32	0.18	M3.6	-0.722	1.63	0.12	M3.8	-0.711	1.56	0.17	M3.6	-0.591	1.93	0.11	507	M4.5(H13)M3e(H97)
152 05 35	16.29	-05 22 10.3	M4.7	-0.900	1.48	0.24	M4.5	-0.818	1.72	0.15	M4.7	-0.780	1.74	0.23	M4.4	-0.696	1.98	0.14		
153 05 35	16.31	-05 22 24.2	M2.3	-1.606	1.43	0.03	M2.3	-1.529	1.72	0.03	M2.4	-1.475	1.73	0.02	M2.4	-1.376	2.07	0.02		
154 05 35	16.32	-05 22 21.7	M5.4	-1.153	0.98	0.00	M5.4	-1.146	1.01	0.00	M5.4	-1.069	1.18	0.00	M5.4	-1.061	1.21	0.00	9140	M3e(H13)>=M2(H97)K-M(LR)
155 05 35	16.35	-05 22 49.2	M2.5	-0.581	1.60	0.30	M2.3	-0.450	1.93	0.17	M2.5	-0.445	1.89	0.27	M2.3	-0.299	2.24	0.15	513	M2e,M3e(H13),M1.5e(H97)K4-M2(LR)
156 05 35	16.36	-05 25 09.7	M2.6	-0.620	1.35	0.15	M2.5	-0.540	1.55	0.08	M2.6	-0.500	1.61	0.13	M2.4	-0.417	1.81	0.06	516	M0(H13)M1.5(H97)
157 05 35	16.37	-05 24 03.5	K6.6	0.269	1.48	0.19	K6.5	0.367	1.78	0.14	K6.6	0.403	1.77	0.16	K6.5	0.508	2.05	0.10	515	K4-K7(H97)<M0(Sam)K4(Ste)
158 05 35	16.38	-05 21 50.6	M5.9	-1.226	1.00	0.20	M5.7	-1.156	1.26	0.15	M5.9	-1.150	1.17	0.19	M5.7	-1.059	1.47	0.14	9142	M2.5(H97)
159 05 35	16.29	-05 23 16.7	M0.2	-0.107	0.95	0.23	K9.7	0.005	1.24	0.13	M0.2	-0.027	1.12	0.22	K9.6	0.101	1.42	0.10	512	cont(H97)K0-K7(LR)
160 05 35	16.19	-05 24 56.4	M5.1	-0.774	1.31	1.05	M4.2	-0.543	2.03	0.62	M5.1	-0.656	1.58	1.02	M4.0	-0.405	2.29	0.55		
161 05 35	16.57	-05 24 06.2	M5.3	-0.649	0.38	0.12	M5.2	-0.585	0.58	0.08	M5.3	-0.615	0.46	0.12	M5.2	-0.537	0.69	0.08	521	M3.5e(H13)M0(H97)
162 05 35	16.58	-05 25 17.7	M3.5	-0.721	3.16	0.15	M3.5	-0.651	3.35	0.11	M3.5	-0.466	3.71	0.13	M3.5	-0.393	3.92	0.10	9147	M2(H97)
163 05 35	16.50	-05 22 35.3	M4.8	-0.661	0.98	0.22	M4.6	-0.584	1.22	0.14	M4.8	-0.583	1.16	0.21	M4.6	-0.486	1.44	0.13		
164 05 35	16.74	-05 22 31.4	M4.9	-0.760	1.86	0.34	M4.6	-0.649	2.20	0.22	M4.8	-0.617	2.19	0.33	M4.6	-0.481	2.57	0.21	9151	M4(H97)K-M(LR)
165 05 35	16.90	-05 22 22.5	K7.3	0.066	1.41	0.00	K7.2	0.068	1.41	0.00	K7.4	0.181	1.67	0.00	K7.4	0.182	1.67	0.00	529	M0(Sam)K5-M2(LR)K5(Ste)
166 05 35	16.94	-05 22 20.7	M6.3	-1.530	0.26	0.19	M6.1	-1.450	0.54	0.14	M6.3	-1.497	0.35	0.19	M6.1	-1.413	0.61	0.14		K7(H97)
167 05 35	16.95	-05 25 47.1	M3.8	-0.725	0.84	0.23	M3.0	-0.621	1.17	0.07	M3.0	-0.579	1.25	0.09	M3.0	-0.529	1.38	0.07	535	M2e,M4.5e(H13),M2.5(H)
168 05 35	16.97	-05 22 48.6	M5.4	-1.132	1.00	0.79	M4.9	-0.830	2.01	0.57	M5.4	-1.042	1.21	0.79	M4.8	-0.650	2.45	0.57	532	M0:(H13)<K7(H97)K5-M2(LR)
169 05 35	16.98	-05 23 37.1	M1.1	-0.398	1.76	1.26	M0.7	-0.031	2.94	1.00	M1.2	-0.250	2.15	1.34	M0.5	0.243	3.61	1.00	534	M2e(H97)K3(Ste)
170 05 35	16.76	-05 24 04.3	K7.6	0.291	1.07	0.34	K7.4	0.445	1.52	0.25	K7.6	0.386	1.27	0.32	K7.4	0.566	1.75	0.21		
171 05 35	17.05	-05 23 39.7	M1.5	-0.313	1.57	0.06	M1.5	-0.284	1.65	0.04	M1.6	-0.185	1.84	0.05	M1.6	-0.156	1.92	0.03	537	K5e(H13)K8e(H97)K4-M2(LR)
172 05 35	17.06	-05 21 23.7	M5.1	-1.048	1.43	0.00	M5.1	-1.045	1.44	0.00	M5.0	-0.936	1.69	0.00	M5.1	-0.935	1.69	0.00	9163	M3.5(H97)
173 05 35	17.01	-05 22 33.1	K5.1	0.095	1.52	0.27	K5.2	0.217	1.94	0.25	K5.1	0.251	1.85	0.22	K5.1	0.384	2.27	0.20	536	K0-K2(H97)<M0(Sam)K5-M3(LR)K3(Ste)
174 05 35	17.12	-05 22 50.1	M3.1	-0.680	0.73	0.01	M3.1	-0.680	0.73	0.00	M3.1	-0.622	0.86	0.01	M3.1	-0.622	0.85	0.00	539	M1(H13)M4.5(H97)K6-M4(LR)
175 05 35	17.11	-05 24 58.7	M5.5	-0.685	0.71	0.00	M5.5	-0.686	0.71	0.00	M5.5	-0.629	0.84	0.00	M5.5	-0.626	0.85	0.00	540	M4.5(H13)M5(H97)
176 05 35	17.06	-05 23 34.1	K5.4	0.404	2.29	0.07	K5.3	0.453	2.45	0.06	K5.6	0.608	2.72	0.04	K5.4	0.646	2.79	0.00	538	K0-K2(H97)K0-K7(LR)K3(Ste)
177 05 35	17.21	-05 21 31.7	K5.3	0.665	1.54	0.40	K5.4	0.831	2.12	0.38	K5.3	0.821	1.86	0.34	K5.4	1.010	2.47	0.31	544	K4-K7(H97)K5:III(HT)K7(E)K4II(Ham)K3(Sam)K4(Ste)
178 05 35	17.26	-05 24 24.1	M4.6	-1.068	0.00	0.16	M4.6	-1.041	0.00	0.12	M4.6	-1.069	0.00	0.17	M4.7	-1.040	0.00	0.12	9171	M0.5-M1.5(H97)
179 05 35	17.32	-05 23 41.4	M3.9	-1.189	2.74	1.16	M3.6	-0.881	3.74	0.91	M3.9	-0.960	3.20	1.06	M3.6	-0.560	4.44	0.81		M2.5(H97)K-M(LR)
180 05 35	17.35	-05 23 04.9	M7.0	-1.187	1.69	0.00	M7.0	-1.183	1.69	0.00	M6.9	-1.013	2.13	0.00	M6.9	-1.015	2.13	0.00		M4-M6(H97)M4-M6(LR)M7(H97)
181 05 35	17.36	-05 25 44.6	K9.8	-0.199	1.20	0.12	M0.8	-0.155	1.40	0.17	K9.8	-0.087	1.45	0.10	K9.9	-0.021	1.64	0.08		
182 05 35	17.37	-05 24 00.3	K8.8	-0.525	5.29	0.18	K7.8	-0.382	5.58	0.02	K9.1	-0.074	6.27	0.14	K8.2	0.030	6.46	0.01	549	G4-K5(LR)K2-K7(H97)
183 05 35	17.38	-05 24 13.9	M6.1	-0.979	1.56	0.00	M6.1	-0.975	1.57	0.00	M6.1	-0.838	1.90	0.00	M6.0	-0.849	1.87	0.00	9176	M5(H97)
184 05 35	17.34	-05 22 35.7	K0.2	-0.511	2.58	0.75	G9.0	-0.237	3.28	0.43	G8.9	-0.252	3.17	0.68	G9.2	0.065	4.04	0.46	548	K0-K2,K2-K4(H13)<=K5(H97)<=K5(P)<M0(Sam)cont+emis(CK)G4-K5(LR)
185 05 35	17.45	-05 23 21.0	K8.9	-0.423	1.78	0.92	K8.9	-0.132	2.69	0.74	K9.0	-0.253	2.12	0.83	K8.9	0.093	3.12	0.64	9180	K7-K8e(H97)K0-K7(LR)
186 05 35	17.47	-05 24 17.3	M6.2	-1.257	0.08	0.32	M5.9	-1.146	0.47	0.23	M6.2	-1.252	0.09	0.32	M5.9	-1.104	0.56	0.22	9179	M5e(H97)

Table 1 continued

Table 1 (continued)

ID	RA	DEC	$R_V = 3.1^a$								$R_V = 5.5^b$								Star <sup>c</sup>	SpT
			Constant				BB(7000 K)				Constant				BB(7000 K)					
			SpT	Log $L_\star$	$A_V$	$r_{7465}$	SpT	Log $L_\star$	$A_V$	$r_{7465}$	SpT	Log $L_\star$	$A_V$	$r_{7465}$	SpT	Log $L_\star$	$A_V$	$r_{7465}$		
$(L_\odot)$ (mag)				$(L_\odot)$ (mag)				$(L_\odot)$ (mag)				$(L_\odot)$ (mag)				(Literature <sup>d</sup> )				
187 05 35 17.48 -05 22 51.3	M2.6	-1.364	1.24	0.54	M2.5	-1.146	1.82	0.32	M2.7	-1.251	1.47	0.49	M2.4	-1.005	2.11	0.30	9181	M0-M1(H13)K5-M2(LR)		
188 05 35 17.55 -05 21 45.6	M4.7	-0.839	2.84	2.04	M3.8	-0.493	3.91	1.32	M4.5	-0.604	3.33	1.84	M3.0	-0.167	4.63	1.02				
189 05 35 17.54 -05 25 42.7	K8.5	-0.383	2.05	0.05	K8.9	-0.355	2.20	0.08	K8.5	-0.205	2.43	0.02	K8.8	-0.185	2.53	0.05	557	K8(H13)K8(H97)		
190 05 35 17.56 -05 23 24.9	M2.8	-1.169	1.52	1.21	M2.2	-0.806	2.53	0.75	M2.8	-1.030	1.84	1.19	M2.2	-0.558	3.14	0.75	554	>G6(LR)		
191 05 35 17.55 -05 22 56.8	K7.0	0.039	1.73	0.48	K7.0	0.231	2.34	0.39	K7.0	0.205	2.07	0.41	K7.0	0.422	2.69	0.31				
192 05 35 17.64 -05 22 51.7	M5.6	-1.594	1.90	1.93	M5.0	-1.193	3.22	1.48	M5.4	-1.437	2.25	1.85	M4.8	-0.946	3.75	1.35	9188	K5-M2(LR)		
193 05 35 17.64 -05 22 07.9	M6.5	-1.153	1.65	0.00	M6.5	-1.151	1.66	0.00	M6.5	-1.021	1.96	0.00	M6.5	-1.006	2.01	0.00	9187	M5.5e(H13)>=M2(H97)		
194 05 35 17.68 -05 24 54.1	M5.8	-0.832	0.81	0.15	M5.7	-0.780	0.98	0.11	M5.8	-0.766	0.96	0.15	M5.7	-0.695	1.19	0.11	559	M5.5e(H97)		
195 05 35 17.73 -05 24 43.7	M6.4	-1.091	0.94	0.15	M6.2	-1.036	1.13	0.11	M6.3	-1.000	1.18	0.15	M6.2	-0.937	1.38	0.11	9192	M6.5e(H97)		
196 05 35 17.78 -05 23 44.2	M5.7	-0.924	1.19	0.04	M5.7	-0.909	1.24	0.02	M5.7	-0.826	1.41	0.03	M5.7	-0.803	1.48	0.02	9196	M5.5(H13)M3-M5(LR)		
197 05 35 17.81 -05 24 40.9	M7.0	-1.536	0.37	0.18	M7.0	-1.462	0.65	0.18	M7.0	-1.505	0.42	0.17	M6.9	-1.417	0.74	0.17				
198 05 35 17.81 -05 24 30.5	M6.4	-1.024	0.51	0.06	M6.3	-1.007	0.57	0.05	M6.4	-0.981	0.62	0.06	M6.3	-0.961	0.69	0.05				
199 05 35 17.86 -05 23 03.1	K7.9	-0.585	1.68	0.20	K7.7	-0.478	1.97	0.12	K8.0	-0.434	2.01	0.17	K7.6	-0.327	2.26	0.08	9201	K8(H97)K4-M2(LR)		
200 05 35 17.81 -05 23 15.6	M0.7	0.055	1.83	0.04	M0.6	0.083	1.90	0.01	M0.7	0.228	2.25	0.04	M0.6	0.260	2.33	0.01	562	M0(H97)K5-M2(LR)		
201 05 35 17.92 -05 25 06.5	M6.7	-1.448	0.01	0.36	M6.5	-1.292	0.57	0.28	M6.7	-1.448	0.02	0.37	M6.4	-1.236	0.71	0.28		M0(H97)		
202 05 35 17.94 -05 25 21.1	M5.9	-0.888	0.73	0.10	M5.8	-0.847	0.87	0.08	M5.9	-0.825	0.89	0.10	M5.8	-0.778	1.04	0.07	569	M0(H13)M3.5(H97)		
203 05 35 17.95 -05 25 33.9	M4.1	-0.637	0.83	0.10	M4.0	-0.601	0.94	0.07	M4.0	-0.574	0.98	0.09	M3.9	-0.519	1.13	0.06				
204 05 35 17.94 -05 22 45.5	K5.2	0.835	1.24	0.57	K5.5	1.023	1.94	0.57	K5.2	0.969	1.51	0.50	K5.5	1.192	2.26	0.50	567	late-G(H97)K3-4(HT)K4III(Ham)K2-K3(Sam)K5-M2(LR)K2(Ste)		
205 05 35 17.96 -05 23 35.4	M4.9	-0.742	1.75	0.00	M4.9	-0.743	1.74	0.00	M4.9	-0.607	2.05	0.00	M4.9	-0.610	2.04	0.00	9206	M0e(H13)K6-M4(LR)		
206 05 35 18.02 -05 22 05.5	K1.0	0.016	5.78	0.21	K1.0	0.137	6.22	0.20	K1.3	0.532	6.91	0.14	K1.4	0.640	7.29	0.15	9209	G-K7(H13)M0:(H97)K5-M2(LR)		
207 05 35 18.06 -05 24 01.1	M4.8	-0.620	0.79	0.09	M4.7	-0.586	0.90	0.06	M4.8	-0.556	0.94	0.09	M4.7	-0.516	1.05	0.05	575	M4-M5e(H13)		
208 05 35 18.21 -05 24 30.3	M5.7	-1.151	0.40	0.27	M5.4	-1.011	0.90	0.19	M5.7	-1.118	0.48	0.27	M5.4	-0.933	1.08	0.19				
209 05 35 18.23 -05 25 35.1	K8.4	-0.869	0.33	0.15	K7.8	-0.793	0.45	0.04	K8.5	-0.837	0.39	0.14	K7.7	-0.757	0.52	0.03	583	M1(H97)		
210 05 35 18.23 -05 23 15.6	M3.2	-0.914	1.02	0.34	M2.7	-0.779	1.34	0.15	M3.2	-0.838	1.20	0.35	M2.6	-0.670	1.57	0.14	582	M2(H97)K5-M3(LR)		
211 05 35 18.26 -05 23 07.5	M5.5	-1.239	0.53	0.30	M5.2	-1.096	0.99	0.21	M5.4	-1.204	0.61	0.30	M5.1	-1.015	1.18	0.20	9220	M5(H13)M4(H97)M4-M5(LR)		
212 05 35 18.28 -05 24 38.8	M4.5	-0.938	1.22	0.05	M4.5	-0.912	1.29	0.04	M4.5	-0.837	1.44	0.05	M4.5	-0.818	1.49	0.03	9219	M2.5(H97)		
213 05 35 18.32 -05 24 04.9	M2.9	-1.130	3.41	0.69	M2.8	-0.905	4.05	0.50	M3.0	-0.866	4.00	0.71	M2.4	-0.575	4.70	0.36	588	M3(H97)		
214 05 35 18.37 -05 24 26.7	M5.2	-0.762	0.96	0.07	M5.1	-0.723	1.07	0.05	M5.2	-0.681	1.14	0.07	M5.1	-0.629	1.30	0.04	9224	M2.5(H97)		
215 05 35 18.36 -05 22 37.5	K6.7	0.554	1.04	0.09	K6.6	0.615	1.19	0.04	K6.7	0.654	1.26	0.07	K6.6	0.706	1.37	0.03	589	K0(H97)G8-K0:(HT)K1IV(Ham)M0(E)K5-M2(LR)K3(Ste)		
216 05 35 18.20 -05 23 35.9	K3.2	0.443	2.04	0.53	K3.7	0.610	2.78	0.68	K3.0	0.692	2.57	0.39	K3.2	0.890	3.29	0.45	581	early-Ke(H97)<M0(Sam)G4-K3(LR)K4(Ste)		
217 05 35 18.45 -05 25 19.1	M5.6	-1.555	0.01	0.49	M5.3	-1.385	0.51	0.34	M5.6	-1.557	0.01	0.50	M5.3	-1.341	0.62	0.34				
218 05 35 18.46 -05 24 07.1	M2.7	-0.445	1.20	0.03	M2.7	-0.426	1.24	0.01	M2.7	-0.340	1.43	0.02	M2.6	-0.325	1.47	0.01	9228	M3e(H97)		
219 05 35 18.49 -05 23 29.3	M6.2	-1.413	0.47	0.55	M5.8	-1.246	1.07	0.39	M6.2	-1.383	0.55	0.54	M5.8	-1.156	1.29	0.40	9230	M0(H97)K-M(LR)		
220 05 35 18.66 -05 23 14.1	K2.5	0.581	2.39	0.37	K2.5	0.724	2.91	0.37	K2.7	0.811	2.92	0.36	K3.0	1.004	3.58	0.37	596	G5-K1(H13)K2-K5e(H97)		
221 05 35 18.67 -05 23 56.5	M4.7	-1.098	0.74	0.22	M4.5	-1.026	0.96	0.14	M4.7	-1.040	0.88	0.23	M4.4	-0.957	1.11	0.13	9232	K8-M0e,M1e(H13)M2(H97)M0-M3(LR)		
222 05 35 18.75 -05 22 02.3	M1.8	-0.204	2.54	0.00	M1.8	-0.201	2.56	0.00	M2.0	-0.011	2.96	0.00	M1.9	-0.011	2.96	0.00	600	M1(H13)M2.5(H97)K5-M2(LR)M1(SHC-ir)		
223 05 35 18.83 -05 22 23.0	M5.4	-1.074	2.93	0.52	M5.3	-0.888	3.56	0.44	M5.3	-0.835	3.48	0.50	M4.8	-0.579	4.33	0.37		M3(H97)K5-M3(LR)		
224 05 35 18.85 -05 21 41.2	K6.9	-0.199	1.47	0.10	K6.8	-0.141	1.64	0.07	K6.9	-0.069	1.75	0.08	K6.8	-0.013	1.89	0.04	603	K8(H13)		
225 05 35 18.86 -05 23 28.9	M3.0	-0.874	1.50	0.25	M2.7	-0.771	1.75	0.13	M3.0	-0.750	1.76	0.23	M2.7	-0.628	2.05	0.11	604	<M2:(H13)M0e(H97)K4-M2(LR)		
226 05 35 18.88 -05 24 17.5	M6.2	-1.124	0.44	0.00	M6.2	-1.135	0.40	0.00	M6.1	-1.098	0.51	0.00	M6.1	-1.095	0.51	0.00	9238	M3(H97)		
227 05 35 18.70 -05 22 56.9	K3.1	0.123	3.09	0.34	K3.2	0.257	3.63	0.38	K2.9	0.489	3.86	0.17	K2.9	0.596	4.25	0.19				
228 05 35 18.94 -05 22 18.8	K7.8	-0.384	3.98	0.33	K7.7	-0.243	4.45	0.28	K7.9	-0.027	4.72	0.23	K7.5	0.112	5.08	0.14	9243	K7(H97)K5-M2(LR)		
229 05 35 18.96 -05 23 22.1	M7.2	-1.186	3.01	0.01	M7.1	-1.213	2.96	0.01	M7.2	-1.062	3.16	0.01	M7.2	-0.937	3.60	0.02				
230 05 35 19.02 -05 25 03.0	M4.0	-1.240	0.47	0.23	M3.7	-1.125	0.87	0.16	M4.0	-1.201	0.55	0.24	M3.1	-1.084	1.04	0.15		K7(H97)		
231 05 35 19.12 -05 23 27.1	M0.3	-0.386	1.65	0.00	M0.3	-0.384	1.66	0.00	M0.5	-0.252	1.95	0.00	M0.5	-0.253	1.95	0.00	610	K7(H13)K8(H97)K5-M2(LR)M1(SHC-ir)		
232 05 35 19.13 -05 22 34.6	M5.8	-1.282	2.99	0.01	M5.7	-1.239	3.17	0.01	M5.8	-1.002	3.66	0.01	M5.7	-1.018	3.64	0.01				
233 05 35 19.06 -05 23 49.7	K4.9	-0.479	1.50	0.27	K4.7	-0.341	1.98	0.26	K5.1	-0.357	1.74	0.24	K4.8	-0.177	2.26	0.18	607	G8-K2(H97)<=K5(P)>G6(LR)		

Table 1 continued

Table 1 (continued)

ID	RA	DEC	$R_V = 3.1^a$								$R_V = 5.5^b$								Star <sup>c</sup>	SpT
			Constant				BB(7000 K)				Constant				BB(7000 K)					
			SpT	Log $L_\star$	$A_V$	$r_{7465}$	SpT	Log $L_\star$	$A_V$	$r_{7465}$	SpT	Log $L_\star$	$A_V$	$r_{7465}$	SpT	Log $L_\star$	$A_V$	$r_{7465}$		
$(L_\odot)$ (mag)				$(L_\odot)$ (mag)				$(L_\odot)$ (mag)				$(L_\odot)$ (mag)				(Literature <sup>d</sup> )				
234 05 35	19.20	-05 22 50.8	K5.3	-0.288	2.83	0.32	K5.3	-0.143	3.35	0.31	K5.3	-0.010	3.42	0.23	K5.2	0.143	3.88	0.19	9250	K5(H97)K8-M0(H97)K5-M2(LR)
235 05 35	19.46	-05 22 21.7	M5.1	-1.208	2.76	0.42	M4.8	-1.057	3.18	0.26	M4.1	-0.928	3.23	0.04	M4.2	-0.838	3.66	0.15	617	M3.5(H13) >= M6(H97)
236 05 35	19.61	-05 23 57.4	M1.6	-0.763	1.37	0.31	M1.7	-0.634	1.75	0.23	M1.7	-0.654	1.61	0.30	M1.7	-0.498	2.03	0.22	620	M0,M2(H13)K8(H97)
237 05 35	19.65	-05 24 26.6	M2.8	-0.332	1.24	0.49	M1.7	-0.101	1.74	0.13	M2.7	-0.220	1.47	0.45	M1.7	0.035	2.02	0.12	622	M0-M2.5e(H97)M0.5(P) < M0(Sam)
238 05 35	19.82	-05 22 21.6	K6.9	-1.016	2.21	2.41	K7.0	-0.637	3.73	2.67	K6.8	-0.753	2.65	1.87	K6.9	-0.266	4.29	1.87	624	late-M(H97)
239 05 35	19.84	-05 24 47.9	M3.8	-0.791	0.90	0.12	M3.2	-0.720	1.14	0.01	M3.8	-0.717	1.07	0.12	M3.1	-0.634	1.34	0.01	625	K7(H13)M1(H97)M6-M6.5(H97)
240 05 35	19.92	-05 24 02.7	M5.6	-1.041	0.44	0.20	M5.4	-0.943	0.77	0.14	M5.7	-1.006	0.51	0.20	M5.4	-0.875	0.92	0.14	9256	M2(H97)
241 05 35	20.03	-05 22 26.5	M4.5	-0.903	3.34	0.01	M4.5	-0.893	3.39	0.01	M4.4	-0.649	3.93	0.00	M4.4	-0.638	3.98	0.00	630	cont+emis(H13)M5(H97)
242 05 35	20.04	-05 25 37.6	M0.4	-0.167	1.30	0.00	M0.4	-0.166	1.31	0.00	M0.5	-0.061	1.54	0.00	M0.5	-0.061	1.54	0.00	636	M0.3(P)
243 05 35	20.15	-05 25 33.7	K7.9	-1.748	0.51	0.22	K6.5	-1.618	0.85	0.10	K7.6	-1.713	0.57	0.20	K6.8	-1.543	1.01	0.09	9260	M1(SHC-ir)M:(H97)
244 05 35	20.15	-05 22 28.3	M6.4	-1.370	1.86	0.24	M6.4	-1.263	2.29	0.25	M6.5	-1.196	2.25	0.23	M6.3	-1.083	2.69	0.23		M3(H13)
245 05 35	20.17	-05 23 08.7	M3.1	-0.653	3.50	0.46	M3.1	-0.491	4.00	0.39	M3.2	-0.377	4.11	0.47	M2.7	-0.170	4.63	0.26	3075	M2(SHC-ir)
246 05 35	20.13	-05 21 33.7	K9.1	0.082	1.93	0.00	K9.1	0.084	1.94	0.00	K9.3	0.237	2.28	0.00	K9.3	0.236	2.28	0.00	637	<M0(Sam)
247 05 35	20.39	-05 22 13.8	M1.0	0.036	2.45	0.00	M1.0	0.038	2.46	0.00	M1.8	0.102	2.58	0.12	M1.1	0.224	2.87	0.00	645	M0(H13)
248 05 35	20.46	-05 23 29.8	K8.5	-0.066	1.88	0.13	K8.6	0.003	2.11	0.12	K8.5	0.102	2.24	0.10	K8.5	0.169	2.43	0.07		
249 05 35	20.49	-05 23 31.2	M6.0	-1.348	1.68	0.36	M5.8	-1.239	2.11	0.32	M5.9	-1.212	2.00	0.36	M5.8	-1.061	2.54	0.32		
250 05 35	20.53	-05 21 41.1	M4.7	-1.217	1.34	0.61	M4.3	-1.052	1.79	0.38	M4.6	-1.111	1.58	0.59	M4.2	-0.934	2.03	0.36		
251 05 35	20.54	-05 24 20.9	M3.8	-0.915	1.17	0.11	M3.1	-0.856	1.37	0.00	M3.7	-0.825	1.37	0.10	M3.1	-0.751	1.60	0.00		
252 05 35	20.62	-05 22 55.8	M5.0	-1.727	0.92	0.33	M4.8	-1.580	1.44	0.28	M5.1	-1.625	1.16	0.32	M4.8	-1.475	1.68	0.27	656	M:(H97)M4-M8(SHC-ir)
253 05 35	20.62	-05 24 46.5	M3.0	-0.457	1.70	0.58	M2.3	-0.227	2.25	0.26	M2.8	-0.302	2.03	0.51	M2.2	-0.049	2.62	0.23	658	M2e(H97)
254 05 35	20.64	-05 22 45.6	M3.5	-1.004	2.97	0.17	M2.8	-0.943	3.09	0.01	M3.5	-0.781	3.48	0.17	M2.7	-0.709	3.60	0.00	657	M4.5(H13)M1(H97)
255 05 35	20.66	-05 25 10.7	M5.3	-1.145	0.38	0.25	M5.1	-1.024	0.76	0.18	M5.3	-1.110	0.46	0.25	M5.0	-0.959	0.92	0.17		
256 05 35	20.67	-05 23 53.3	M5.7	-0.665	0.28	0.11	M5.7	-0.622	0.43	0.08	M5.7	-0.642	0.34	0.11	M5.7	-0.586	0.51	0.08	659	M4-M6e(H13)
257 05 35	20.71	-05 22 31.5	M4.6	-0.846	3.03	0.00	M4.6	-0.847	3.02	0.00	M4.6	-0.608	3.57	0.00	M4.6	-0.607	3.57	0.00	9270	M2(H13)
258 05 35	20.77	-05 21 55.2	K6.6	-0.226	1.73	0.00	K6.6	-0.220	1.75	0.00	K6.7	-0.093	2.03	0.00	K6.7	-0.090	2.03	0.00	661	M0(H97)K5(Ste)
259 05 35	20.84	-05 21 30.1	M4.6	-0.594	1.15	0.14	M4.5	-0.548	1.27	0.09	M4.5	-0.498	1.36	0.13	M4.4	-0.453	1.48	0.08	663	M4.5(H97)
260 05 35	20.84	-05 21 21.5	M4.5	-1.449	1.87	4.11	M3.9	-1.004	3.43	3.46	M4.0	-1.298	2.18	3.61	M3.5	-0.712	4.20	3.40	662	K4-K6e(H13)K7(H97)
261 05 35	20.90	-05 25 34.3	M6.4	-1.722	0.23	0.00	M6.3	-1.703	0.32	0.00	M6.4	-1.681	0.35	0.00	M6.3	-1.683	0.37	0.00		
262 05 35	20.91	-05 23 21.8	M3.6	-1.009	1.14	0.07	M3.4	-0.963	1.28	0.03	M3.6	-0.904	1.39	0.06	M3.4	-0.864	1.51	0.03	9271	M0(H97)
263 05 35	20.92	-05 21 50.9	K7.7	-0.258	1.74	0.15	K7.0	-0.176	1.89	0.05	K7.7	-0.101	2.07	0.12	K7.0	-0.029	2.16	0.01	665	K-M1e(H13)M:e(H97)
264 05 35	21.01	-05 22 22.8	M5.9	-1.444	1.86	0.00	M5.8	-1.421	1.96	0.00	M5.8	-1.273	2.30	0.00	M5.8	-1.262	2.32	0.00		M3:(H97)
265 05 35	21.02	-05 23 55.7	M6.4	-1.075	1.07	0.00	M6.4	-1.065	1.11	0.00	M6.4	-0.974	1.32	0.00	M6.3	-0.985	1.29	0.00		
266 05 35	21.03	-05 22 25.1	M4.2	-1.087	2.49	0.14	M3.9	-1.055	2.60	0.09	M4.0	-0.903	2.91	0.12	M3.9	-0.841	3.07	0.07		
267 05 35	21.05	-05 23 49.0	K2.4	0.877	1.44	0.02	K2.4	0.884	1.53	0.07	K2.4	1.020	1.76	0.00	K2.4	1.021	1.78	0.01	669	G8(H97) <= K5(P)K3(CK)K1-K2(Sam)SB2(R)K2(Ste)
268 05 35	21.19	-05 23 33.1	M5.6	-1.135	1.51	0.21	M5.4	-1.027	1.89	0.16	M5.5	-1.025	1.75	0.21	M5.3	-0.876	2.22	0.15	9277	M4.5(H13)M6(H97)M6(SHC-ir)
269 05 35	21.20	-05 24 00.1	M5.7	-1.038	2.86	0.00	M5.7	-1.029	2.87	0.00	M5.6	-0.827	3.32	0.00	M5.7	-0.799	3.41	0.00	9276	M3::(H13)
270 05 35	21.24	-05 22 59.5	M3.0	-0.674	2.82	0.31	M2.8	-0.543	3.16	0.19	M2.8	-0.419	3.36	0.24	M2.6	-0.294	3.68	0.14	9280	M3(H97)M1.5-M4(SHC-ir)
271 05 35	21.15	-05 25 56.9	M0.7	-0.258	2.06	0.03	M0.4	-0.230	2.14	0.00	M0.6	-0.074	2.47	0.00	M0.6	-0.073	2.47	0.00	674	M0(H13)M0.5(H97)
272 05 35	21.29	-05 24 57.3	K6.2	-0.010	0.87	0.53	K6.5	0.177	1.52	0.50	K6.2	0.081	1.06	0.49	K6.4	0.310	1.79	0.44	678	K1-K2(Sam)K4(Ste)
273 05 35	21.29	-05 22 15.7	M5.7	-1.555	1.16	0.36	M5.6	-1.413	1.70	0.35	M5.6	-1.439	1.46	0.35	M5.6	-1.256	2.08	0.34		M1.5(H97)
274 05 35	21.32	-05 23 46.0	M4.9	-1.382	0.69	1.19	M3.0	-1.136	1.56	0.57	M4.9	-1.330	0.81	1.19	M3.0	-1.003	1.82	0.53		
275 05 35	21.33	-05 24 11.5	K8.7	-0.509	1.61	0.00	K8.7	-0.505	1.62	0.00	K8.9	-0.381	1.89	0.00	K8.9	-0.377	1.90	0.00	679	M0(H13)M0.5(H97)K7:(P)
276 05 35	21.37	-05 23 45.4	K6.6	-0.268	1.32	0.13	K6.6	-0.201	1.53	0.10	K6.7	-0.151	1.57	0.11	K6.6	-0.079	1.77	0.07		
277 05 35	21.50	-05 23 16.7	M5.4	-0.695	1.91	0.12	M5.3	-0.641	2.08	0.08	M5.3	-0.535	2.28	0.11	M5.2	-0.466	2.49	0.08	685	M3.5(H97)
278 05 35	21.63	-05 23 25.7	M6.5	-1.486	1.19	0.32	M6.4	-1.412	1.51	0.32	M6.5	-1.405	1.34	0.30	M6.4	-1.293	1.76	0.30	9285	M5.5(H97)
279 05 35	21.68	-05 21 47.0	K8.0	-0.402	3.58	0.52	K8.5	-0.205	4.25	0.47	K8.0	-0.052	4.26	0.35	K8.4	0.130	4.89	0.36		
280 05 35	21.66	-05 25 26.3	K8.2	-0.543	1.50	0.31	K8.6	-0.403	1.96	0.27	K8.2	-0.399	1.79	0.26	K8.6	-0.249	2.27	0.24	690	M0(H97)

Table 1 continued

Table 1 (continued)

ID	RA	DEC	$R_V = 3.1^a$								$R_V = 5.5^b$								Star <sup>c</sup>	SpT
			Constant				BB(7000 K)				Constant				BB(7000 K)					
			SpT	Log $L_\star$	$A_V$	$r_{7465}$	SpT	Log $L_\star$	$A_V$	$r_{7465}$	SpT	Log $L_\star$	$A_V$	$r_{7465}$	SpT	Log $L_\star$	$A_V$	$r_{7465}$		
			$(L_\odot)$ (mag)				$(L_\odot)$ (mag)				$(L_\odot)$ (mag)				$(L_\odot)$ (mag)				(Literature <sup>d</sup> )	
281 05 35	21.73	-05 23 48.3	M6.6	-1.178	2.64	0.00	M6.5	-1.149	2.76	0.00	M6.5	-0.953	3.17	0.00	M6.5	-0.967	3.13	0.00	9287	<M2(H97)
282 05 35	21.78	-05 23 39.2	M3.2	-0.938	2.28	0.60	M2.6	-0.725	2.76	0.27	M2.7	-0.693	2.74	0.38	M2.5	-0.509	3.20	0.23	694	K5-K7(H97)
283 05 35	21.78	-05 23 10.7	M4.5	-0.539	2.16	0.19	M4.3	-0.496	2.27	0.12	M4.4	-0.381	2.51	0.17	M4.2	-0.339	2.61	0.10	693	M1.5(H97)
284 05 35	21.82	-05 22 40.2	M6.5	-1.471	0.71	0.16	M6.4	-1.401	1.00	0.16	M6.5	-1.399	0.88	0.15	M6.4	-1.328	1.19	0.18		M0.5(H13)M0-M5(H97)
285 05 35	21.84	-05 23 06.5	M3.5	-0.759	4.72	0.01	M3.5	-0.756	4.73	0.01	M3.5	-0.410	5.49	0.01	M3.5	-0.384	5.57	0.00		M5(SHC-ir)
286 05 35	21.85	-05 22 08.3	M1.9	-0.668	1.50	0.08	M1.4	-0.592	1.69	0.00	M1.9	-0.553	1.74	0.07	M1.7	-0.492	1.87	0.00	697	M2(H97)
287 05 35	21.89	-05 23 55.5	M2.6	-0.903	1.15	0.50	M1.9	-0.681	1.66	0.20	M2.3	-0.748	1.46	0.37	M1.9	-0.554	1.93	0.18	9292	M1(H97)
288 05 35	21.81	-05 23 53.8	K4.3	0.326	0.64	0.06	K4.2	0.366	0.78	0.06	K4.4	0.377	0.74	0.06	K4.3	0.427	0.89	0.04	698	K3(H97)G6-K3(H97)K4(Ste)
289 05 35	22.09	-05 24 32.9	M5.2	-0.668	0.60	0.17	M4.9	-0.578	0.91	0.11	M5.1	-0.616	0.73	0.16	M4.9	-0.507	1.07	0.10		
290 05 35	22.11	-05 24 20.2	M5.5	-1.344	1.21	0.37	M5.3	-1.192	1.68	0.26	M5.5	-1.245	1.43	0.36	M5.2	-1.048	2.02	0.25		
291 05 35	22.12	-05 22 34.0	M2.9	-0.619	3.83	0.12	M2.8	-0.559	3.98	0.06	M2.7	-0.258	4.59	0.01	M2.7	-0.247	4.62	0.01	9297	K7(H97)
292 05 35	22.14	-05 22 13.4	M4.7	-1.492	0.17	0.01	M4.7	-1.489	0.18	0.01	M4.7	-1.482	0.20	0.02	M4.7	-1.465	0.24	0.01	9298	M5(H97)
293 05 35	22.24	-05 22 17.4	M6.5	-1.487	2.15	0.49	M6.3	-1.344	2.79	0.51	M6.4	-1.331	2.49	0.46	M6.3	-1.131	3.24	0.48		M4-M5(H97)
294 05 35	22.19	-05 24 24.8	K4.3	0.101	1.29	0.49	K4.4	0.282	1.98	0.51	K4.4	0.236	1.57	0.43	K4.4	0.464	2.31	0.40	707	K2-K3(H97)<K7(P)K4(Ste)
295 05 35	22.41	-05 25 09.5	M2.4	-0.569	0.64	0.04	M2.3	-0.546	0.71	0.03	M2.4	-0.515	0.76	0.04	M2.3	-0.491	0.82	0.02	713	M3.5(H13)
296 05 35	22.43	-05 24 13.5	M4.5	-1.346	0.37	0.00	M4.5	-1.349	0.37	0.00	M4.5	-1.323	0.42	0.00	M4.5	-1.316	0.44	0.00		M0.5-M1.5(H97)M0.1(P)K5(Ste)
297 05 35	22.44	-05 22 01.1	K4.7	-0.246	2.71	0.49	K5.1	-0.080	3.39	0.54	K4.7	0.042	3.31	0.36	K5.0	0.228	3.96	0.38	712	K5-K6(H13)K2-K4(H97)<K7(P)
298 05 35	22.46	-05 25 45.1	M4.2	-0.901	0.34	0.00	M4.2	-0.898	0.35	0.00	M4.2	-0.873	0.40	0.00	M4.2	-0.873	0.40	0.00		
299 05 35	22.33	-05 24 14.3	K8.2	-0.022	1.48	0.10	K7.9	0.031	1.60	0.04	K8.2	0.115	1.77	0.07	K7.9	0.158	1.85	0.02	710	M0.5-M1.5(H97)M0.1(P)K5(Ste)
300 05 35	22.56	-05 23 43.7	K4.9	0.028	1.87	0.00	K4.9	0.042	1.91	0.00	K5.2	0.165	2.16	0.00	K5.2	0.170	2.18	0.00	721	<=K7(H97)M0(E)<M0(Sam)
301 05 35	22.63	-05 21 37.3	M5.3	-1.299	2.42	0.02	M4.8	-1.287	2.59	0.02	M5.2	-1.125	2.82	0.02	M4.8	-1.087	3.03	0.01		
302 05 35	22.70	-05 21 41.1	M6.2	-2.097	0.04	0.02	M6.2	-2.008	0.43	0.07	M6.2	-2.062	0.15	0.02	M6.2	-1.969	0.55	0.08		
303 05 35	22.75	-05 21 57.7	M6.6	-1.404	3.01	0.04	M6.4	-1.327	3.38	0.05	M6.4	-1.152	3.63	0.04	M6.3	-1.058	4.02	0.05		
304 05 35	22.83	-05 25 47.5	M5.1	-0.956	0.36	0.00	M5.1	-0.957	0.36	0.00	M5.1	-0.926	0.43	0.00	M5.1	-0.919	0.45	0.00	724	M5.5(H13)
305 05 35	22.84	-05 22 27.0	M3.7	-1.318	2.99	0.01	M3.7	-1.275	3.14	0.01	M3.7	-0.989	3.83	0.00	M3.6	-0.996	3.83	0.00		K(H97)
306 05 35	22.97	-05 22 41.5	K5.7	-0.157	5.39	0.08	K5.5	-0.084	5.55	0.01	K6.3	0.212	6.14	0.07	K6.2	0.287	6.31	0.01	726	K3-M0(H13)K5-K7(H97)
307 05 35	23.02	-05 25 36.1	M6.2	-1.908	0.49	0.38	M6.1	-1.779	1.04	0.40	M6.1	-1.878	0.58	0.37	M6.0	-1.661	1.36	0.40		
308 05 35	23.21	-05 21 35.8	M4.2	-0.838	1.86	0.04	M4.2	-0.824	1.91	0.03	M4.1	-0.704	2.15	0.02	M4.1	-0.696	2.17	0.02	730	M3.5(H13)
309 05 35	23.33	-05 21 25.3	K8.4	-0.773	3.16	0.50	K7.8	-0.556	3.72	0.29	K8.2	-0.457	3.77	0.33	K7.8	-0.262	4.28	0.21	732	K5-M0.5e(H97)
310 05 35	23.59	-05 25 26.3	M4.5	-0.845	1.22	0.57	M3.9	-0.710	1.60	0.32	M4.3	-0.759	1.41	0.53	M3.8	-0.578	1.91	0.31	737	M3-M3.5e(H13)
311 05 35	23.66	-05 23 46.3	M3.6	-0.652	0.88	0.15	M3.2	-0.611	0.97	0.06	M3.5	-0.580	1.03	0.14	M3.2	-0.536	1.14	0.05	740	M1(H97)<K7(SHC-ir)
312 05 35	23.67	-05 23 32.0	K7.2	-0.310	2.00	0.04	K6.9	-0.277	2.06	0.00	K7.2	-0.133	2.38	0.01	K7.1	-0.122	2.40	0.00	738	K6-K7(H13)K5(H97)
313 05 35	23.73	-05 23 19.9	M3.5	-1.159	2.69	0.61	M2.4	-0.945	3.15	0.20	M3.5	-0.937	3.16	0.58	M2.4	-0.699	3.68	0.18	742	M3e(H97)
314 05 35	23.82	-05 23 34.3	M2.8	-0.328	2.16	0.41	M2.2	-0.146	2.59	0.18	M2.6	-0.129	2.58	0.34	M2.1	0.057	3.01	0.14	744	M1e(H13)M1e(H97)
315 05 35	23.81	-05 24 16.8	M3.9	-1.000	1.14	0.22	M3.7	-0.894	1.48	0.14	M3.9	-0.891	1.40	0.20	M3.7	-0.762	1.79	0.13		
316 05 35	23.89	-05 23 33.2	K***	-1.182	2.25	0.49	K9.6	-0.967	2.80	0.27	M0.1	-0.964	2.66	0.37	K8.9	-0.765	3.15	0.20		M1e(H13)M1e(H97)
317 05 35	23.98	-05 25 09.9	M4.7	-1.213	0.44	0.61	M4.0	-1.088	0.79	0.34	M4.7	-1.178	0.52	0.61	M4.0	-1.021	0.94	0.33	3087	M1(H97)
318 05 35	24.10	-05 21 32.7	M4.5	-0.644	1.12	0.14	M4.3	-0.617	1.19	0.08	M4.4	-0.558	1.31	0.12	M4.3	-0.536	1.36	0.07		
319 05 35	24.12	-05 21 55.7	M5.8	-1.161	1.47	0.15	M5.7	-1.110	1.63	0.11	M5.8	-1.045	1.73	0.14	M5.7	-0.979	1.93	0.10	9316	M4.5(H97)
320 05 35	24.34	-05 26 00.3	M5.7	-1.115	0.00	0.03	M5.7	-1.099	0.05	0.03	M5.7	-1.115	0.01	0.04	M5.7	-1.093	0.07	0.03		
321 05 35	24.44	-05 24 39.9	K8.8	-0.038	1.10	0.21	K8.2	0.068	1.34	0.10	K8.8	0.066	1.32	0.18	K8.2	0.175	1.56	0.08	756	M0e(H97)K7(H97)K6(Ste)
322 05 35	24.47	-05 24 01.1	M5.8	-1.157	0.83	0.11	M5.7	-1.113	0.98	0.08	M5.8	-1.087	1.00	0.11	M5.7	-1.034	1.17	0.08	757	M1-M3:(H13)
323 05 35	24.26	-05 25 18.7	K9.8	-0.152	0.87	0.03	K9.6	-0.138	0.89	0.00	K9.9	-0.076	1.03	0.02	K9.8	-0.067	1.05	0.00	750	K4-K5e(H97)K0-K2(Sam)K6(Ste)
324 05 35	24.51	-05 25 01.6	M2.4	-0.824	1.28	0.30	M2.2	-0.694	1.60	0.17	M2.4	-0.713	1.50	0.27	M2.1	-0.562	1.87	0.14	759	M1e(H97)
325 05 35	24.66	-05 22 42.6	M4.5	-0.841	4.00	0.01	M4.5	-0.812	4.20	0.07	M4.5	-0.522	4.71	0.01	M4.5	-0.487	4.93	0.07	761	M4.5(H13)M6:(H97)
326 05 35	24.70	-05 24 35.7	K7.0	-0.195	1.60	0.25	K7.0	-0.079	1.94	0.18	K7.0	-0.048	1.90	0.21	K7.0	0.076	2.24	0.14	762	K8,M0e(H13)M0e(H97)
327 05 35	24.82	-05 21 57.7	M5.0	-1.800	0.08	0.00	M5.0	-1.782	0.14	0.00	M4.9	-1.783	0.13	0.00	M5.0	-1.771	0.16	0.00	9320	K6(H97)

Table 1 continued



Table 1 (continued)

ID	RA	DEC	$R_V = 3.1^a$								$R_V = 5.5^b$								Star <sup>c</sup>	SpT
			Constant				BB(7000 K)				Constant				BB(7000 K)					
			SpT	Log $L_\star$	$A_V$	$r_{7465}$	SpT	Log $L_\star$	$A_V$	$r_{7465}$	SpT	Log $L_\star$	$A_V$	$r_{7465}$	SpT	Log $L_\star$	$A_V$	$r_{7465}$		
$(L_\odot)$ (mag)				$(L_\odot)$ (mag)				$(L_\odot)$ (mag)				$(L_\odot)$ (mag)				(Literature <sup>d</sup> )				
328 05 35 24.89 -05 25 10.1 M5.6 -0.923 0.43 0.07 M5.5 -0.882 0.56 0.05 M5.5 -0.883 0.53 0.07 M5.5 -0.838 0.66 0.05 764	M3(H13)M5(SHC-ir)																			
329 05 35 24.96 -05 24 01.5 M3.6 -1.205 2.42 1.66 M2.4 -0.813 3.48 0.89 M3.5 -1.000 2.85 1.56 M2.5 -0.555 3.98 0.81																				
330 05 35 25.06 -05 22 58.5 K5.4 0.302 3.04 0.28 K5.4 0.425 3.49 0.28 K5.6 0.560 3.58 0.22 K5.5 0.709 4.02 0.18																				
331 05 35 25.08 -05 23 53.7 M2.1 -0.613 0.93 0.70 M1.0 -0.317 1.68 0.32 M1.9 -0.516 1.12 0.63 M0.9 -0.176 1.96 0.27																				
332 05 35 25.09 -05 23 46.7 K7.3 0.020 0.62 0.07 K7.0 0.061 0.69 0.02 K7.4 0.071 0.73 0.07 K7.0 0.115 0.80 0.01 769	K2-K4(Sam)K5(Ste)																			
333 05 35 25.14 -05 22 25.2 M5.9 -1.018 3.28 0.52 M5.8 -0.833 3.97 0.46 M5.9 -0.742 3.92 0.48 M5.6 -0.528 4.69 0.45 770	M1.5-M2.5(H97)																			
334 05 35 25.22 -05 24 57.3 M2.3 -1.851 0.23 0.41 M0.4 -1.599 0.75 0.02 M2.4 -1.848 0.20 0.40 M0.6 -1.547 0.85 0.02 773	cont+emis(H13)<M1e(H97)																			
335 05 35 25.34 -05 25 29.5 M5.7 -0.911 0.88 0.10 M5.6 -0.872 1.00 0.07 M5.6 -0.844 1.03 0.10 M5.6 -0.792 1.18 0.07 3095	M5(SHC-ir)																			
336 05 35 25.38 -05 24 11.4 M0.0 -1.542 1.55 1.19 K9.6 -1.208 2.58 0.91 K9.9 -1.385 1.86 1.06 K9.1 -0.991 2.97 0.77 775	M1:(H97)																			
337 05 35 25.39 -05 23 45.7 M7.5 -1.371 1.99 0.00 M7.5 -1.366 2.00 0.00 M7.4 -1.119 2.68 0.00 M7.5 -1.120 2.66 0.00																				
338 05 35 25.43 -05 21 51.5 K7.4 -0.298 2.45 0.38 K7.7 -0.142 2.99 0.36 K7.3 -0.070 2.92 0.31 K7.8 0.102 3.48 0.30																				
339 05 35 25.43 -05 23 33.2 M2.6 -0.801 2.17 0.13 M2.6 -0.741 2.32 0.08 M2.5 -0.609 2.58 0.09 M2.5 -0.560 2.70 0.06																				
340 05 35 25.47 -05 21 34.4 K7.4 -0.440 3.52 0.11 K7.6 -0.390 3.75 0.14 K7.5 -0.140 4.16 0.07 K7.6 -0.093 4.30 0.06 777	K6(H97)																			
341 05 35 25.49 -05 21 35.5 K3.5 -0.273 3.37 0.23 K3.6 -0.173 3.78 0.26 K3.2 0.101 4.18 0.10 K3.3 0.171 4.44 0.12 777	K6(H97)																			
342 05 35 25.72 -05 23 09.4 K6.4 -0.373 3.24 0.65 K6.5 -0.148 4.02 0.61 K6.5 -0.070 3.84 0.52 K6.7 0.177 4.61 0.46 782	K6-K7e(H13)K8e(H97)																			
343 05 35 26.00 -05 25 47.8 K8.7 -0.189 2.42 0.23 K9.1 -0.083 2.78 0.21 K8.4 0.047 2.90 0.14 K8.9 0.136 3.20 0.15 792	K8(H97)M0.1(P)																			
344 05 35 26.06 -05 21 21.0 K5.6 0.170 4.78 0.15 K5.6 0.247 5.04 0.14 K6.3 0.497 5.45 0.15 K6.3 0.592 5.73 0.11 791	K3-K6(H13)																			
345 05 35 26.15 -05 25 39.4 M6.2 -1.186 0.61 0.19 M6.0 -1.115 0.85 0.13 M6.2 -1.134 0.72 0.19 M6.0 -1.044 1.01 0.13																				
346 05 35 26.17 -05 22 57.2 M4.8 -1.014 3.46 0.25 M4.7 -0.909 3.76 0.16 M4.8 -0.741 4.06 0.23 M4.6 -0.647 4.33 0.15 3069	<M3(H13)M5-M6(H97)																			
347 05 35 26.19 -05 25 20.4 M4.1 -1.082 0.14 0.04 M4.0 -1.071 0.17 0.02 M4.0 -1.076 0.15 0.04 M4.0 -1.056 0.21 0.02 3090	M6(H13)M4(H97)																			
348 05 35 26.41 -05 23 02.5 M3.0 -1.309 2.56 0.64 M2.8 -1.097 3.18 0.46 M2.9 -1.095 3.00 0.57 M2.7 -0.813 3.69 0.30 800	K4-K5,M0-M2:(H97)																			
349 05 35 26.43 -05 25 31.5 M6.8 -1.465 0.25 0.18 M6.6 -1.312 0.84 0.14 M6.7 -1.425 0.38 0.18 M6.6 -1.253 0.95 0.13 3096	K0-K2:(H13)																			
350 05 35 26.35 -05 25 40.1 K2.8 0.457 0.38 0.46 K2.9 0.612 1.08 0.59 K2.8 0.501 0.47 0.44 K1.6 0.774 1.32 0.34 799	G5(Par)G0III(HB)G-K:(GS)K1,M3(Sam)K2(Ste)																			
351 05 35 26.94 -05 24 48.2 M5.4 -1.039 0.53 0.00 M5.4 -1.038 0.54 0.00 M5.4 -0.990 0.65 0.00 M5.4 -0.990 0.65 0.00 806	M6.5(H97)M7-M8(H97)M5.5(SHC)M6.5(SHC-ir)																			
352 05 35 26.97 -05 24 00.5 M4.7 -0.849 0.70 0.06 M4.6 -0.823 0.78 0.04 M4.7 -0.794 0.83 0.06 M4.6 -0.764 0.91 0.04 807	M3.5,M5(H13),M6(H97)																			
353 05 35 27.31 -05 23 36.5 K7.1 -0.036 2.04 0.27 K7.2 0.089 2.45 0.23 K7.1 0.152 2.43 0.22 K7.2 0.284 2.83 0.18 810	K4(Sam)																			
354 05 35 27.78 -05 23 32.7 M5.1 -1.140 2.20 0.61 M4.6 -0.927 2.88 0.38 M4.9 -0.919 2.77 0.56 M4.3 -0.744 3.28 0.33																				
355 05 35 27.86 -05 23 23.7 M5.2 -1.437 1.98 0.41 M4.8 -1.295 2.45 0.28 M5.1 -1.273 2.35 0.39 M4.8 -1.093 2.88 0.26																				
356 05 35 28.14 -05 23 06.6 M4.8 -0.693 3.50 0.37 M4.6 -0.564 3.88 0.24 M4.8 -0.406 4.14 0.33 M4.6 -0.270 4.51 0.21 825	M3e(H97)																			
357 05 35 28.21 -05 24 58.2 K6.8 -0.493 1.46 0.45 K6.6 -0.300 2.04 0.34 K6.8 -0.360 1.73 0.41 K6.7 -0.133 2.35 0.27 826	K5e(H13)K6-K8e(H97)																			
358 05 35 28.55 -05 25 04.7 M6.5 -1.433 0.29 0.00 M6.5 -1.432 0.29 0.00 M6.5 -1.418 0.32 0.00 M6.5 -1.401 0.38 0.00																				
359 05 35 28.38 -05 25 03.5 M2.4 -0.313 0.45 0.11 M2.3 -0.258 0.60 0.06 M2.4 -0.273 0.54 0.10 M2.3 -0.210 0.70 0.06 830	M1.5(H97)M4(E)																			
360 05 35 23.22 -05 25 54.4 M6.0 -1.443 1.73 0.20 M5.9 -1.354 2.11 0.19 M6.0 -1.347 1.97 0.25 M5.8 -1.188 2.50 0.19 3100	M2:(H13)																			
361 05 35 16.76 -05 23 16.6 K8.3 -0.408 1.78 1.06 K8.2 -0.119 2.83 1.05 K8.3 -0.262 2.15 1.13 K8.5 0.150 3.52 1.10 524	G4-K5(LR)																			

<sup>d</sup> All the spectral types are collected from Hillenbrand et al. (2013). H97: Hillenbrand (1997); H13: Hillenbrand et al. (2013); Luc01: Lucas et al. (2001); RRL: Riddick et al. (2007a); WLR: Weights et al. (2009); WSH: Wolff et al. (2004); vA: van Altena et al. (1988); J: Johnson (1965b); W: Walker (1983); CK: Cohen & Kuhi (1979); Ste: H C. Stempels 2008, private communication, high dispersion spectra, taken from Hillenbrand et al. (2013); SHC-ir: infrared

<sup>a</sup> Fitting the MUSE spectra using the extinction law from Cardelli et al. (1989) with  $R_V = 3.1$ . Constant: During the fitting, Accretion Continuum Spectrum is taken as a constant. BB(7000 K): During the fitting, Accretion Continuum Spectrum is assumed to be a black body emission with  $T = 7000$  K.

<sup>b</sup> Same as <sup>a</sup> but for  $R_V = 5.5$ .

<sup>c</sup> Star identifier in Hillenbrand et al. (2013)

spectral types from Slesnick et al. (2004); Sam: A.E. Samuel 1993 unpublished PhD thesis, taken from Hillenbrand et al. (2013); E: Edwards et al. (1993); P: Prosser & Stauffer 1995, private communication, taken from Hillenbrand et al. (2013); HT: Herbig & Terndrup (1986) or reference therein; Ham: C. Hamilton 1994 unpublished masters thesis, taken from Hillenbrand et al. (2013); LR: Luhman et al. (2000); Sta: K. Stassun 2005, private communication, low dispersion spectra, taken from Hillenbrand et al. (2013); Par: Parenago (1954); Dae: Daemgen et al. (2012); CK: Cohen & Kuhi (1979); HB: Herbst et al. (2002); GS: Greenstein & Struve (1946); SHC: optical spectral types from Slesnick et al. (2004)

## REFERENCES

- Alcalá, J. M., Natta, A., Manara, C. F., et al. 2014, *A&A*, 561, A2
- Alcalá, J. M., Manara, C. F., Natta, A., et al. 2017, *A&A*, 600, A20
- Bacon, R., Vernet, J., Borisova, E., et al. 2014, *The Messenger*, 157, 13
- Baraffe, I., & Chabrier, G. 2010, *A&A*, 521, A44
- Baraffe, I., Elbakyan, V. G., Vorobyov, E. I., & Chabrier, G. 2017, *A&A*, 597, A19
- Baraffe, I., Homeier, D., Allard, F., & Chabrier, G. 2015, *A&A*, 577, A42
- Baraffe, I., Vorobyov, E., & Chabrier, G. 2012, *ApJ*, 756, 118
- Barrado y Navascués, D., Béjar, V. J. S., Mundt, R., et al. 2003, *A&A*, 404, 171
- Briceño, C., Calvet, N., Hernández, J., et al. 2019, *AJ*, 157, 85
- Caballero, J. A., Martín, E. L., Zapatero Osorio, M. R., et al. 2006, *A&A*, 445, 143
- Calvet, N., & Gullbring, E. 1998, *ApJ*, 509, 802
- Cardelli, J. A., Clayton, G. C., & Mathis, J. S. 1989, *ApJ*, 345, 245
- Cohen, M., & Kuhl, L. V. 1979, *ApJS*, 41, 743
- Comerón, F., Fernández, M., Baraffe, I., Neuhäuser, R., & Kaas, A. A. 2003, *A&A*, 406, 1001
- Costero, R., & Peimbert, M. 1970, *Boletín de los Observatorios Tonantzintla y Tacubaya*, 5, 229
- Covino, E., Alcalá, J. M., Allain, S., et al. 1997, *A&A*, 328, 187
- Da Rio, N., Robberto, M., Hillenbrand, L. A., Henning, T., & Stassun, K. G. 2012, *ApJ*, 748, 14
- Da Rio, N., Robberto, M., Soderblom, D. R., et al. 2010, *ApJ*, 722, 1092
- Daemgen, S., Correia, S., & Petr-Gotzens, M. G. 2012, *A&A*, 540, A46
- Dahm, S. E. 2005, *AJ*, 130, 1805
- Edwards, S., Strom, S. E., Hartigan, P., et al. 1993, *AJ*, 106, 372
- Eisner, J. A., Arce, H. G., Ballering, N. P., et al. 2018, *ApJ*, 860, 77
- Fang, M., Hillenbrand, L. A., Kim, J. S., et al. 2020, arXiv e-prints, arXiv:2009.11995
- Fang, M., Kim, J. S., van Boekel, R., et al. 2013a, *ApJS*, 207, 5
- Fang, M., van Boekel, R., Bouwman, J., et al. 2013b, *A&A*, 549, A15
- Fang, M., van Boekel, R., Wang, W., et al. 2009, *A&A*, 504, 461(Paper I)
- Fang, M., Kim, J. S., Pascucci, I., et al. 2017a, *AJ*, 153, 188
- Fang, Q., Herczeg, G. J., & Rizzuto, A. 2017b, *ApJ*, 842, 123
- Fedele, D., van den Ancker, M. E., Henning, T., Jayawardhana, R., & Oliveira, J. M. 2010, *A&A*, 510, A72
- Feiden, G. A. 2016, *A&A*, 593, A99
- Gizis, J. E. 2002, *ApJ*, 575, 484
- Goodwin, S. P. 2013, *MNRAS*, 430, L6
- Greenstein, J. L., & Struve, O. 1946, *PASP*, 58, 366
- Greve, A. 2010, *A&A*, 518, A62
- Guarcello, M. G., Damiani, F., Micela, G., et al. 2010, *A&A*, 521, A18
- Gully-Santiago, M. A., Herczeg, G. J., Czekala, I., et al. 2017, *ApJ*, 836, 200
- Guo, Z., Herczeg, G. J., Jose, J., et al. 2018, *ApJ*, 852, 56
- Hasenberger, B., Forbrich, J., Alves, J., et al. 2016, *A&A*, 593, A7
- Herbig, G. H., & Bell, K. R. 1988, *Third Catalog of Emission-Line Stars of the Orion Population : 3 : 1988*
- Herbig, G. H., & Terndrup, D. M. 1986, *ApJ*, 307, 609
- Herbst, W., Bailer-Jones, C. A. L., Mundt, R., Meisenheimer, K., & Wackermann, R. 2002, *A&A*, 396, 513
- Herczeg, G. J., & Hillenbrand, L. A. 2014, *ApJ*, 786, 97
- . 2015, *ApJ*, 808, 23
- Hernández, J., Calvet, N., Perez, A., et al. 2014, *ApJ*, 794, 36
- Hillenbrand, L. A. 1997, *AJ*, 113, 1733
- Hillenbrand, L. A., Bauermeister, A., & White, R. J. 2008, in *Astronomical Society of the Pacific Conference Series*, Vol. 384, 14th Cambridge Workshop on Cool Stars, Stellar Systems, and the Sun, ed. G. van Belle, 200
- Hillenbrand, L. A., & Carpenter, J. M. 2000, *ApJ*, 540, 236
- Hillenbrand, L. A., Hoffer, A. S., & Herczeg, G. J. 2013, *AJ*, 146, 85
- Hillenbrand, L. A., Strom, S. E., Calvet, N., et al. 1998, *AJ*, 116, 1816
- Hughes, J., Hartigan, P., Krautter, J., & Kelemen, J. 1994, *AJ*, 108, 1071
- Husser, T.-O., Wende-von Berg, S., Dreizler, S., et al. 2013, *A&A*, 553, A6
- Jeffries, R. D., Littlefair, S. P., Naylor, T., & Mayne, N. J. 2011, *MNRAS*, 418, 1948
- Jeffries, R. D., Oliveira, J. M., Naylor, T., Mayne, N. J., & Littlefair, S. P. 2007, *MNRAS*, 376, 580
- Johns-Krull, C. M., & Valenti, J. A. 1996, *ApJL*, 459, L95
- Johnson, H. L. 1965a, *ApJ*, 141, 923
- Johnson, H. M. 1965b, *ApJ*, 142, 964
- Joy, A. H. 1945, *ApJ*, 102, 168

- Keenan, P. C., & McNeil, R. C. 1989, *ApJS*, 71, 245
- Kirkpatrick, J. D., Henry, T. J., & McCarthy, Donald W., J. 1991, *ApJS*, 77, 417
- Kounkel, M., Hartmann, L., Loinard, L., et al. 2017, *ApJ*, 834, 142
- Kounkel, M., Covey, K., Suárez, G., et al. 2018, *AJ*, 156, 84
- Kraus, A. L., Herczeg, G. J., Rizzuto, A. C., et al. 2017, *ApJ*, 838, 150
- Kraus, A. L., Ireland, M. J., Martinache, F., & Hillenbrand, L. A. 2011, *ApJ*, 731, 8
- Krautter, J., Wichmann, R., Schmitt, J. H. M. M., et al. 1997, *A&AS*, 123, 329
- Lada, C. J., Muench, A. A., Haisch, Jr., K. E., et al. 2000, *AJ*, 120, 3162
- Lee, T. A. 1968, *ApJ*, 152, 913
- Looper, D. L., Burgasser, A. J., Kirkpatrick, J. D., & Swift, B. J. 2007, *ApJL*, 669, L97
- Lucas, P. W., Roche, P. F., Allard, F., & Hauschildt, P. H. 2001, *MNRAS*, 326, 695
- Luhman, K. L. 1999, *ApJ*, 525, 466
- . 2004, *ApJ*, 617, 1216
- . 2006, *ApJ*, 645, 676
- . 2007, *ApJS*, 173, 104
- Luhman, K. L., Herrmann, K. A., Mamajek, E. E., Esplin, T. L., & Pecaú, M. J. 2018, *AJ*, 156, 76
- Luhman, K. L., Mamajek, E. E., Shukla, S. J., & Loutrel, N. P. 2017, *AJ*, 153, 46
- Luhman, K. L., Rieke, G. H., Young, E. T., et al. 2000, *ApJ*, 540, 1016
- Luhman, K. L., Stauffer, J. R., Muench, A. A., et al. 2003, *ApJ*, 593, 1093
- Luhman, K. L., & Steeghs, D. 2004, *ApJ*, 609, 917
- Lyo, A.-R., Lawson, W. A., & Bessell, M. S. 2004, *MNRAS*, 355, 363
- Mamajek, E. E., Lawson, W. A., & Feigelson, E. D. 1999, *ApJL*, 516, L77
- Mamajek, E. E., Meyer, M. R., & Liebert, J. 2002, *AJ*, 124, 1670
- Manara, C. F., Fedele, D., Herczeg, G. J., & Teixeira, P. S. 2016, *A&A*, 585, A136
- Manara, C. F., Frasca, A., Alcalá, J. M., et al. 2017a, *A&A*, 605, A86
- Manara, C. F., Testi, L., Rigliaco, E., et al. 2013, *A&A*, 551, A107
- Manara, C. F., Testi, L., Herczeg, G. J., et al. 2017b, *A&A*, 604, A127
- McJunkin, M., France, K., Schneider, P. C., et al. 2014, *ApJ*, 780, 150
- Megeath, S. T., Gutermuth, R., Muzerolle, J., et al. 2012, *AJ*, 144, 192
- Mészáros, S., Allende Prieto, C., Edvardsson, B., et al. 2012, *AJ*, 144, 120
- Morris, B. M. 2020, *ApJ*, 893, 67
- Muench, A. A., Alves, J., Lada, C. J., & Lada, E. A. 2001, *ApJL*, 558, L51
- Muench, A. A., Lada, E. A., Lada, C. J., & Alves, J. 2002, *ApJ*, 573, 366
- Mužić, K., Scholz, A., Geers, V. C., Jayawardhana, R., & López Martí, B. 2014, *ApJ*, 785, 159
- Neckel, T., Klare, G., & Sarcander, M. 1980, *Bulletin d'Information du Centre de Données Stellaires*, 19, 61
- Nguyen, D. C., Brandeker, A., van Kerkwijk, M. H., & Jayawardhana, R. 2012, *ApJ*, 745, 119
- O'dell, C. R., Wen, Z., & Hu, X. 1993, *ApJ*, 410, 696
- Parenago, P. P. 1954, *Trudy Gosudarstvennogo Astronomicheskogo Instituta*, 25, 3
- Pascucci, I., Testi, L., Herczeg, G. J., et al. 2016, *ApJ*, 831, 125
- Pecaú, M. J., & Mamajek, E. E. 2013, *ApJS*, 208, 9
- . 2016, *MNRAS*, 461, 794
- Preibisch, T., Guenther, E., Zinnecker, H., et al. 1998, *A&A*, 333, 619
- Reid, I. N., Cruz, K. L., Kirkpatrick, J. D., et al. 2008, *AJ*, 136, 1290
- Riaz, B., Gizis, J. E., & Harvin, J. 2006, *AJ*, 132, 866
- Ricci, L., Robberto, M., & Soderblom, D. R. 2008, *AJ*, 136, 2136
- Riddick, F. C., Roche, P. F., & Lucas, P. W. 2007a, *MNRAS*, 381, 1077
- . 2007b, *MNRAS*, 381, 1067
- Rigliaco, E., Natta, A., Testi, L., et al. 2012, *A&A*, 548, A56
- Robberto, M., Soderblom, D. R., Scandariato, G., et al. 2010, *AJ*, 139, 950
- Robberto, M., Beckwith, S. V. W., Panagia, N., et al. 2005, *AJ*, 129, 1534
- Rugel, M., Fedele, D., & Herczeg, G. 2018, *A&A*, 609, A70
- Sacco, G. G., Franciosini, E., Randich, S., & Pallavicini, R. 2008, *A&A*, 488, 167
- Shkolnik, E. L., Liu, M. C., Reid, I. N., Dupuy, T., & Weinberger, A. J. 2011, *ApJ*, 727, 6
- Skrutskie, M. F., Cutri, R. M., Stiening, R., et al. 2006, *AJ*, 131, 1163
- Slesnick, C. L., Hillenbrand, L. A., & Carpenter, J. M. 2004, *ApJ*, 610, 1045
- Smith, N., Bally, J., Shuping, R. Y., Morris, M., & Kassis, M. 2005, *AJ*, 130, 1763

- Soderblom, D. R., Hillenbrand, L. A., Jeffries, R. D., Mamajek, E. E., & Naylor, T. 2014, in *Protostars and Planets VI*, ed. H. Beuther, R. S. Klessen, C. P. Dullemond, & T. Henning, 219
- Somers, G., & Pinsonneault, M. H. 2015, *ApJ*, 807, 174
- Song, I., Zuckerman, B., & Bessell, M. S. 2004, *ApJ*, 600, 1016
- Sterzik, M. F., Alcalá, J. M., Covino, E., & Petr, M. G. 1999, *A&A*, 346, L41
- Torres, C. A. O., Quast, G. R., da Silva, L., et al. 2006, *A&A*, 460, 695
- van Altena, W. F., Lee, J. T., Lee, J. F., Lu, P. K., & Uppgren, A. R. 1988, *AJ*, 95, 1744
- Venuti, L., Prisinzano, L., Sacco, G. G., et al. 2018, *A&A*, 609, A10
- Venuti, L., Stelzer, B., Alcalá, J. M., et al. 2019, *A&A*, 632, A46
- Wahhaj, Z., Cieza, L., Koerner, D. W., et al. 2010, *ApJ*, 724, 835
- Walker, M. F. 1983, *ApJ*, 271, 642
- Webb, R. A., Zuckerman, B., Platais, I., et al. 1999, *ApJL*, 512, L63
- Weights, D. J., Lucas, P. W., Roche, P. F., Pinfield, D. J., & Riddick, F. 2009, *MNRAS*, 392, 817
- Weilbacher, P. M., Monreal-Ibero, A., Kollatschny, W., et al. 2015, *A&A*, 582, A114
- White, R. J., & Basri, G. 2003, *ApJ*, 582, 1109
- White, R. J., & Hillenbrand, L. A. 2004, *ApJ*, 616, 998
- Wichmann, R., Sterzik, M., Krautter, J., Metanomski, A., & Voges, W. 1997, *A&A*, 326, 211
- Wolff, S. C., Strom, S. E., & Hillenbrand, L. A. 2004, *ApJ*, 601, 979
- Zapatero Osorio, M. R., Béjar, V. J. S., Pavlenko, Y., et al. 2002, *A&A*, 384, 937
- Zuckerman, B., & Song, I. 2004, *ARA&A*, 42, 685
- Zuckerman, B., Webb, R. A., Schwartz, M., & Becklin, E. E. 2001, *ApJL*, 549, L233

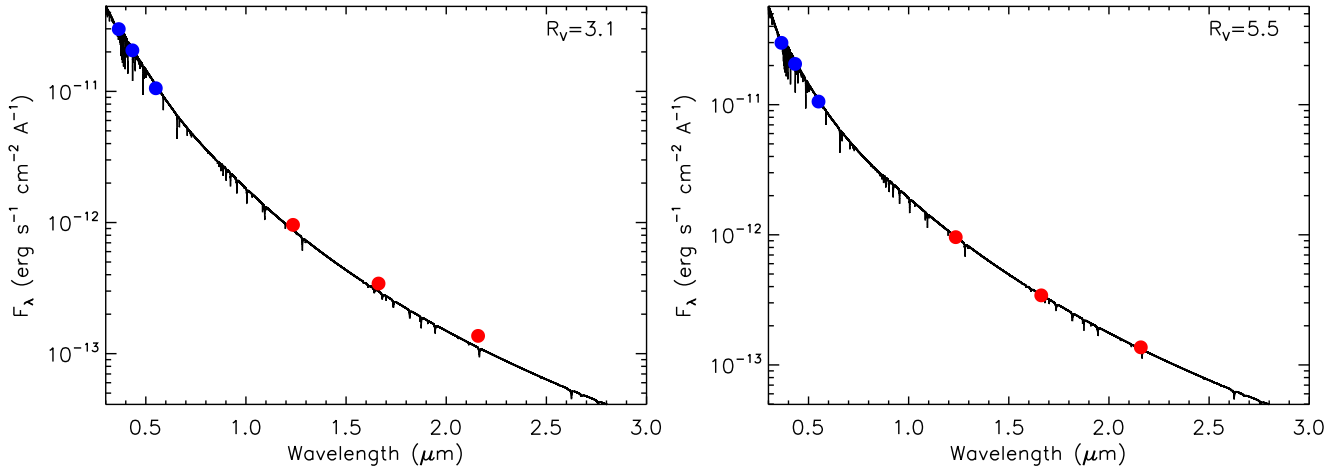


**Figure 14.** SED of HD 37042 in analyzed our sample in this paper. Filled circles are photometric data from *UBV* bands (blue, Neckel et al. 1980) and 2MASS *JHK<sub>s</sub>* bands (red, Skrutskie et al. 2006). The *UBV* band photometry are just used for plotting, and have not been used for the SED fitting. The dark solid line show best-fit model atmosphere with  $R_V=3.1$  (left panel) and 5.5 (right panel).

## APPENDIX

### A. FLUX RE-CALIBRATION

We refine the calibration of the MUSE data using the O-type star HD 37042 in the field. We obtain the BOSZ Kurucz model atmosphere (Mészáros et al. 2012) with  $T_{eff}$  from 8000 K to 35000 K, and surface gravity  $\log g$  from 3.5 to 5.0, and fit the MUSE spectra of HD 37042 using the model atmospheres which are rotationally broadened and degraded to the MUSE spectral resolution. The best-fit model is obtain by minimizing the  $\chi^2$ , and give  $T_{eff}=29000$  K and  $\log g=4.5$ . We then fit the broad-band photometry from *Gaia* and 2MASS of HD 37042 using the aforementioned best-fit model with two free parameters, extinction and stellar angular radius as in Fang et al. (2009) and Fang et al. (2013a). We use the extinction law from extinction law of Cardelli et al. (1989), adopting two total to selective extinction values ( $R_V=3.1$  and 5.5). The best-fit model atmospheres with  $R_V=3.1$  and  $A_V=0.76$  or  $R_V=5.5$  and  $A_V=1.03$  are show in Fig. 14. The one with  $R_V=5.5$  can fit the broad-band photometry from optical bands to near-infrared bands, and used for the flux-calibration correction.

In Fig. 15, we compare the best-fit model with  $R_V=5.5$  with the MUSE spectra of HD 37042. The comparison show that the MUSE spectra calibrated in (Weilbacher et al. 2015) underestimate the flux by  $\sim 5\%$ . We fit the flux ratio between the MUSE spectra and the best-fit model atmosphere with 5-order poly function, avoiding the regions that we affected by the telluric absorption, and use it as a correction for the MUSE spectra of our targets; see Fig. 15(b). During the fitting process, we avoid the regions that are affected by the telluric absorption.

### B. PRE-MAIN SEQUENCE SPECTRAL TEMPLATES

In Table 3, we list the WTTSs with X-shooter spectra and their spectral types in the literature. In this work, we mainly refer to the results from Pecaut & Mamajek (Pecaut & Mamajek 2013, 2016), Manara (Manara et al. 2013, 2017a), and Luhman (Luhman & Steeghs 2004; Luhman 2007; Luhman et al. 2017). In the following, we discuss the techniques for the spectral classification in them.

Pecaut & Mamajek (2013, 2016) classify the spectra using spectral standards for main-sequence stars and giants and their G/K types are tied closely to the classification system of Keenan & McNeil (1989) and their M types are consistent with the classification system of Kirkpatrick et al. (1991). Among their spectral standards, we note one star GJ 701. This star is assigned as an M0.0 V in (Pecaut & Mamajek 2013). In Figure 16, we compare the spectrum of GJ 701 with those of other M-type from Kirkpatrick et al. (1991). The comparisons suggest that GJ 701 should be around M1.0V-M1.5V. This explains why RECX 4 is classified as M0 in (Pecaut & Mamajek 2013) and M1.75 in Luhman & Steeghs (2004). For the spectral type earlier than M0 and later than M1, the spectral types from (Pecaut & Mamajek 2013) are generally consistent with the results in the literature. Luhman & Steeghs (2004);

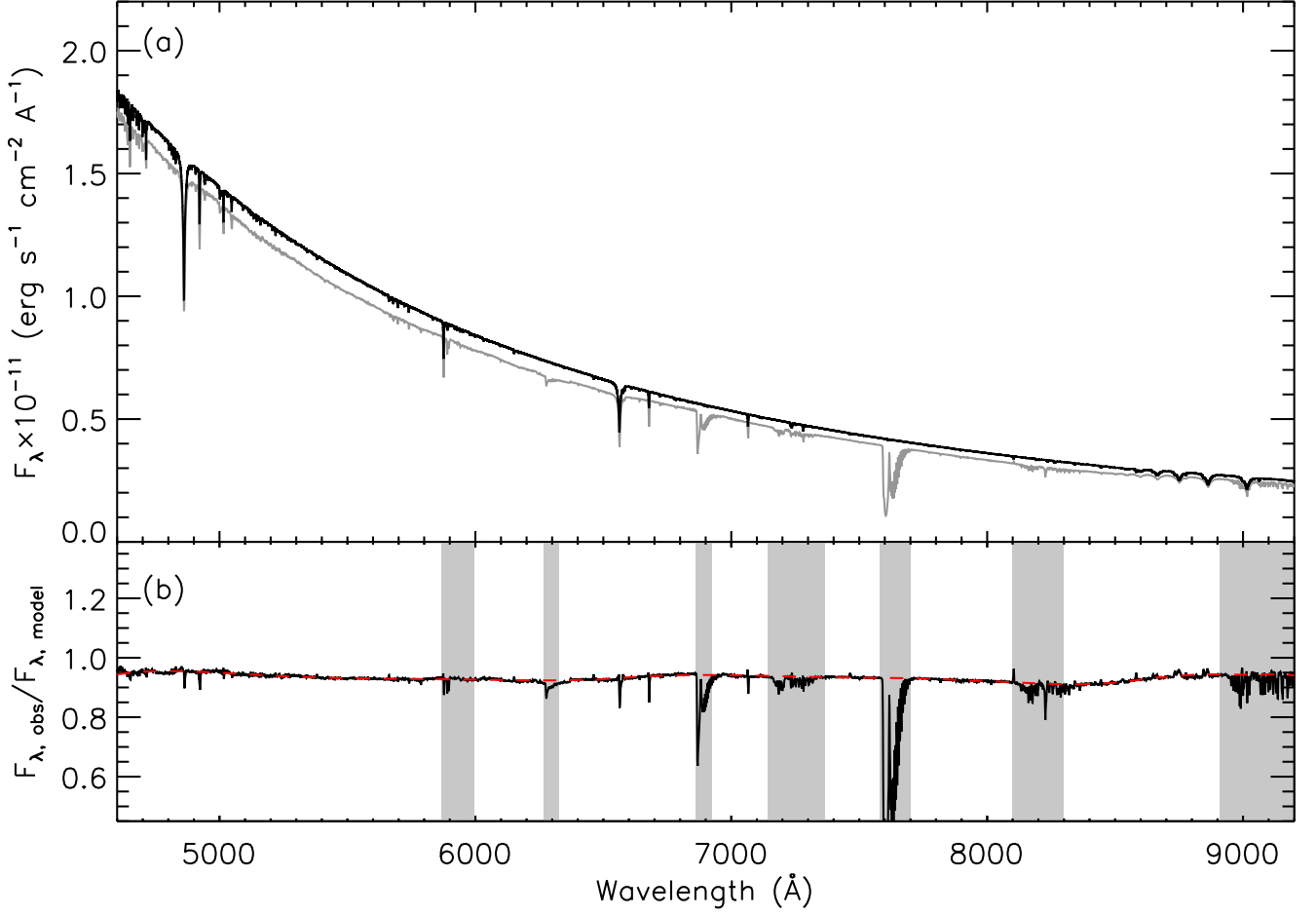


**Figure 15.** (a) Comparison of the best-fit model (black) with the MUSE spectrum (gray) of HD 37042. (b) Flux ratio between the MUSE spectrum of HD 37042 and the best-fit model. The red dash line is used for the flux-calibration correction for the MUSE spectra of our targets. The gray color filled regions mark the wavelength ranges which are affected by the telluric absorption.

Luhman (2007); Luhman et al. (2017) construct a spectral type sequence for young M dwarfs. For spectral types earlier than M5, they based on the Kirkpatrick classification system, and for the ones later than M5, they combine the spectra from field dwarfs and giant stars.

The majority of the X-shooter spectra are collected from Manara et al. (2013, 2017a). In Manara et al. (2013), they classify the spectra using the strengths of TiO, VO, CaH, etc. in the spectral region between 5800 and 9000 Å. In Manara et al. (2017a), they do the spectral classification based on the scheme developed in Herczeg & Hillenbrand (2014) for ones earlier than K5, and the ones from Jeffries et al. (2007) for K6 and later K type. For M types, Manara et al. (2017a) use the mean values derived using the methods in Riddick et al. (2007b), Jeffries et al. (2007), and Herczeg & Hillenbrand (2014). The three methods are all based on the strengths of molecular bands, and the typical differences in the spectral types from the three methods is about 0.5 subclasses.

While most of literature SpTs for most of sources agree with each other within 1 subclass, there are some sources with very large differences in literature SpT ( $> 2$  subclasses), e.g. TWA 15A. To help determine the used spectral types of the sources, we re-classify the spectral types using two methods: one is from Fang et al. (2017a), and the other is to fit the X-shooter spectra with the M-type spectral templates constructed by Luhman (Luhman 1999; Luhman et al. 2003; Luhman 2004, 2006). The former one is based on the relations between the strengths of molecular bands and the spectral types, and can provide the reliable spectral classification for late-K to M type stars. The latter one is only for M-type stars and to calibrate spectral types of the X-shooter spectra to the M-type spectral sequence defined

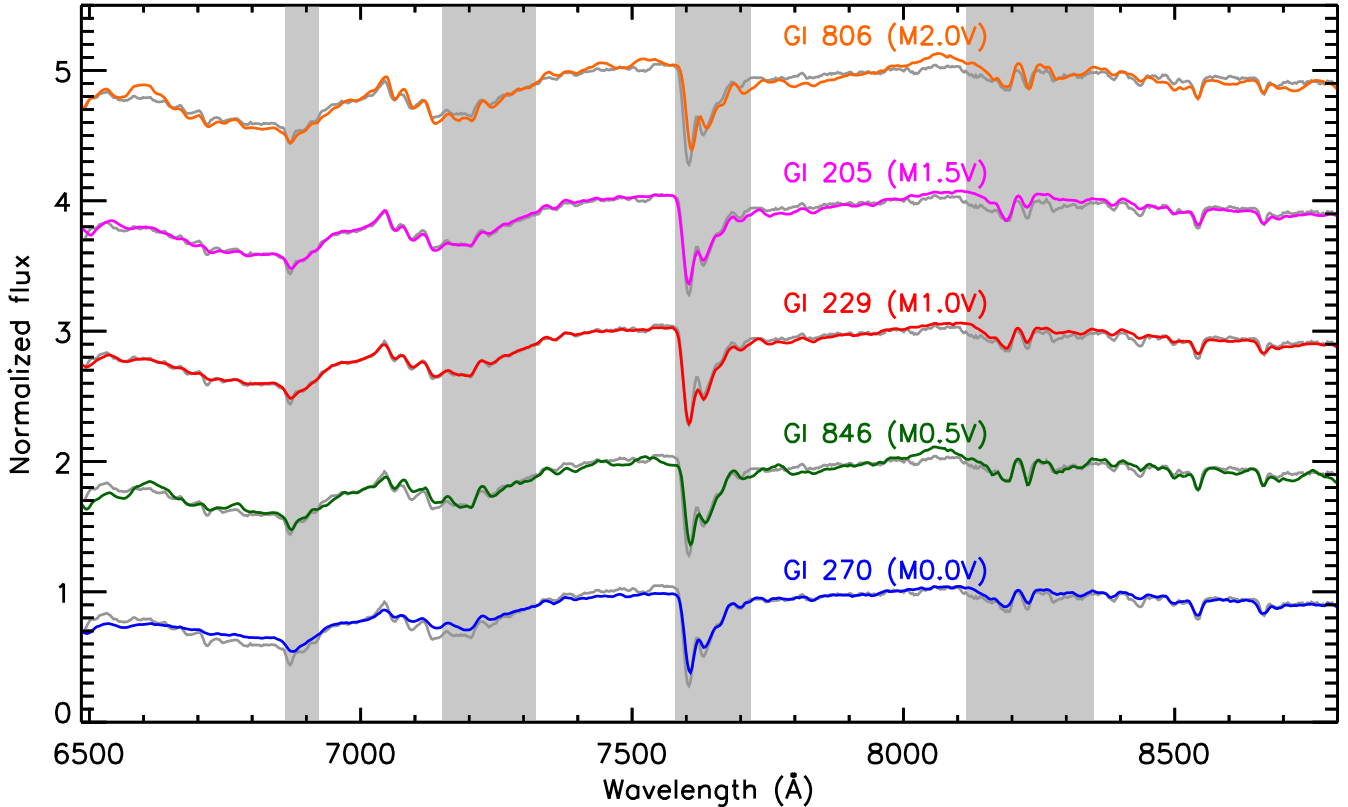


**Figure 16.** A comparison of the spectrum of Gl 701 (gray) with those from other M-type stars. In order to correct for the uncertainty in the flux calibration for each spectrum, we obtain the ratios between the spectra of Gl 701 and each comparison star at different wavelengths, and then fit the ratios using 3-order polynomial functions. The spectrum of each comparison star is multiplied by the best-fit polynomial function, and shown in the figure. The gray color filled regions mark the wavelength ranges which are affected by the telluric absorption. Gl 701 has been used as a M0.0V template in Pecaut & Mamajek (2013), but should be around M1.0V-M1.5V type.

by Luhman. The results from the two methods are also listed in Table 3 in Appendix B. With the new results, we can determine the spectral types of the sources with large differences in literature SpT. For instance, TWA 14A have spectral types ranging from M1.5 to M3.5 in the literature, and with the new spectral types in this work we assign M3.25 to this source.

For the K4-K6 type X-shooter templates, the spectral types in the literature agree with each other very well, and we assign the literature SpT to them. For the early-K and G types, we take the spectral types which are generally consistent with the ones from Manara et al. (2013, 2017a) and Pecaut & Mamajek (2013). For these sources, there could be 1-5 subclass differences in the spectral types of individual sources. The differences could be due to the different methods used in the spectral classification. Reconciliation of this discrepancy is beyond the scope of this work. Furthermore, the majority of our sample are later than K5 type. Thus, this uncertainties on the early-K and G types do not affect any main results in this work.



**Table 3.** The parameters for WTTSS

ID	Name	RA (J2000)	DEC (J2000)	Region	SpT <sup>α</sup>	SpT <sup>β</sup>	SpT <sup>γ</sup>	Other SpT	Ref	SpT <sup>δ</sup>	SpT <sup>ε</sup>	Used SpT	A <sub>V</sub> (mag)
1	RECX 1	08 36 56.24	-78 56 45.7	η Cha	K5		K6	K4, K4, K7, K7	1, 2, 3, 34			K6	0
2	RECX 3	08 41 37.03	-79 03 30.4	η Cha	M3.5		M3.25	M3, M3	2, 3	M3.2±0.3	M3.25	M3.25	0
3	RECX 4	08 42 23.77	-79 04 03.0	η Cha	M0		M1.75	K7, M1.5	2, 3	M1.1±0.6	M1.75	M1.75	0
4	RECX 6	08 42 38.77	-78 54 42.8	η Cha			M3	M2, M3	2, 3	M3.0±0.2	M3.0	M3.0	0
5	RECX 10	08 44 31.90	-78 46 31.2	η Cha	K9		M1	K7/M0, K7, M0.5	1, 2, 3	K9.0±1.0	M0.5	M0.5	0
6	RECX 12	08 47 56.77	-78 54 53.2	η Cha			M3.25	M2, M2, M3	1, 2, 3	M3.3±0.3	M3.0	M3.25	0
7	J0836	08 36 10.73	-79 08 18.4	η Cha	M5.5		M5.5	M5.5, M5.5	3, 4	M5.7±0.2	M5.5	M5.5	0
8	J0838	08 38 51.50	-79 16 13.7	η Cha	M5.25		M5.25	M5, M5	3, 4	M5.5±0.1	M5.5	M5.25	0
9	TWA 2A	11 09 13.80	-30 01 39.9	TWA	M1.5	M2	M2.25	M0.5, M2, M1.5, M2.2	5, 6, 7, 28	M2.1±0.5	M2.5	M2.25	0
10	TWA 3B	11 10 27.81	-37 31 53.2	TWA	M4			M4.5	33	M4.1±0.2	M4.0	M4.0	0
11	TWA 6	10 18 28.70	-31 50 02.9	TWA		K7	M0.0	K7, M0, M0.0	5, 6, 28	K7.2±0.5		K7.0	0
12	TWA 7	10 42 30.06	-33 40 16.6	TWA	M3	M3	M3.25	M1, M2, M3.2	5, 6, 28	M3.2±0.2	M3.25	M3.25	0
13	TWA 8A	11 32 41.27	-26 51 56.0	TWA	M3			M3, M3, M3	6, 32, 33	M3.1±0.5	M3.0	M3.0	0
14	TWA 8B	11 30 11.94	-26 35 33.3	TWA	M5.5			M5, M5.2, M5.5, M5.5	5, 28, 32, 33	M5.5±0.2	M5.5	M5.25	0
15	TWA 9A	11 48 24.22	-37 28 49.2	TWA	K7	K5		K5, K5, K7, K6	5, 6, 8, 28	K6.3±0.7		K7.0	0
16	TWA 9B	11 48 23.73	-37 28 48.5	TWA		M3		M1, M3.5, M3.4	5, 8, 28	M3.6±0.3	M3.5	M3.5	0
17	TWA 14	11 13 26.22	-45 23 42.7	TWA	K8	M0.5		M0, M0.6, K8, M1.9	7, 10, 28	M0.5±0.6	M1.25	M0.5	0
18	TWA 15A	12 34 20.65	-48 15 13.5	TWA		M3.5		M1.5	10	M3.3±0.4	M3.25	M3.25	0
19	TWA 15B	12 34 20.47	-48 15 19.5	TWA		M3		M2.2, M2	7, 10	M3.3±0.4	M3.0–M3.25	M3.25	0
20	TWA 25	12 15 30.72	-39 48 42.6	TWA	K9	M0	M0.75	M0, M1, M0.5	11, 6, 28	K9.8±0.9	M0.25	M0.5	0
21	TWA 26	11 39 51.14	-31 59 21.5	TWA		M9	M8.5	M8, M8, M9	12, 13, 14	M8.5±0.4	M8.0	M8.5	0
22	TWA 29	12 45 14.16	-44 29 07.7	TWA		M9.5	M9.25	M9.5	13	M9.2±0.4	M8.5	M9.5	0
23	Sz 94	16 07 49.60	-39 04 28.8	Lupus		M4		M4	15	M3.6±0.4	M3.5	M3.5	0
24	Sz 107	16 08 41.80	-39 01 37.0	Lupus		M5.5		M5.5	15	M5.5±0.1	M5.5	M5.5	0
25	Sz 121	16 10 12.20	-39 21 18.1	Lupus		M4		M3	15	M4.1±0.3	M4.0–M4.25	M4.0	0
26	Sz 122	16 10 16.42	-39 08 05.1	Lupus		M2		M2	15	M2.1±0.4	M2.25	M2.25	0
27	Par-Lup3-1	16 08 16.03	-39 03 04.3	Lupus		M6.5		M7.5, M6.25	16, 17	M6.3±0.9	M6.5–M7.0	M6.5	1.4 <sup>d</sup>
28	Par-Lup3-2	16 08 35.78	-39 03 47.9	Lupus		M5		M6	16	M5.1±0.2	M5.0	M5.0	0
29	RXJ1526.0-4501	15 25 59.65	-45 01 15.7	Lupus	K0	G9		G7, G8, G5	6, 18, 20			K0.0	0
30	RXJ1508.6-4423	15 08 37.74	-44 23 17.0	Lupus	G6	G8		G8, G1.5, G8,	6, 18, 20			G6	0
31	RXJ1515.8-3331	15 15 45.36	-33 31 59.8	Lupus	K0	K0.5		K0, K0, K1, K0	6, 19, 20, 30			K0.5	0.2 <sup>g</sup>
32	RXJ1538.6-3916	15 38 38.36	-39 16 54.1	Lupus	K4	K4		K4	20			K4.0	0
33	RXJ1540.7-3756	15 40 41.17	-37 56 18.5	Lupus	K6	K6		K6	20			K6.0	0
34	RXJ1543.1-3920	15 43 06.25	-39 20 19.5	Lupus		K6		K6	20			K6.0	0
35	SO 879	05 39 05.42	-02 32 30.3	σ Ori		K7		K7, K6.5, K7	21, 24, 31	K7.0±0.8		K7.0	0.2 <sup>g</sup>
36	SO 925	05 39 11.41	-02 33 32.8	σ Ori		M5.5		M5, M5.5	22, 23	M5.5±0.1	M5.5	M5.5	0
37	SO 999	05 39 20.25	-02 38 25.8	σ Ori		M5.5		M5.5, M4	23, 24	M5.4±0.1	M5.0–M5.5	M5.25	0
38	SO 797	05 38 54.92	-02 28 58.4	σ Ori		M4.5		M4.5	23	M4.7±0.2	M4.75–M5.0	M4.75	0
39	SO 641	05 38 38.58	-02 41 55.9	σ Ori		M5		M5, M5.5	23, 27	M5.2±0.2	MM5.0–5.5	M5.25	0
40	RXJ0438.6+1546	04 38 39.07	+15 46 13.6	Taurus		K2	K1	G6, K2, K2	25, 29, 30			K2.0	0.2 <sup>f</sup>
41	J160550.5-253313	16 05 50.64	-25 33 13.6	UpSco	G7	K1		K1, G7	6, 26			K1.0	0.2 <sup>g</sup>
42	J160843.4-260216	16 08 43.41	-26 02 16.8	UpSco	G7	K0.5		G9, G7	6, 26			K0.0	0.4 <sup>g</sup>
43	LM717	11 08 02.34	-76 40 34.3	Cha I		M6.5	M6			M6.4±0.3	M6.25	M6.5	0.3 <sup>e</sup>
44	J11195652-7504529	11 19 56.52	-75 04 52.9	Cha I		M7	M7.25			M6.8±0.8	M5.75	M6.5	0

<sup>α</sup> Spectral types are from Pecaut & Mamajek (2013) and Pecaut & Mamajek (2016); <sup>β</sup> Spectral types are from Manara et al. (2013) and Manara et al. (2017a); <sup>γ</sup> Spectral types are from Luhman & Steeghs (2004), Luhman et al. (2017), and Luhman (2007); <sup>δ</sup> Spectral types are classified using the scheme in Fang et al. (2017a); <sup>ε</sup> Spectral types are classified using the spectral templates from Luhman.

A<sub>V</sub>: <sup>d</sup> derived from  $J - H$  color, <sup>e</sup> derived from  $J - H$  and  $J - K_S$  colors, <sup>f</sup> derived from the  $r - J$  color; <sup>g</sup> derived from the  $V - K_s$  color. The used intrinsic colors are from Fang et al. (2017a) or Pecaut & Mamajek (2013).

**References**—1. Covino et al. (1997), 2. Mamajek et al. (1999), 3. Lyo et al. (2004), 4. Song et al. (2004), 5. Webb et al. (1999), 6. Torres et al. (2006), 7. Shkolnik et al. (2011), 8. White & Hillenbrand (2004), 9. Sterzik et al. (1999), 10. Zuckerman et al. (2001), 11. Zuckerman & Song (2004), 12. Gizis (2002), 13.Looper et al. (2007), 14. Reid et al. (2008), 15. Hughes et al. (1994), 16. Comerón et al. (2003), 17. Muzić et al. (2014), 18. Mamajek et al. (2002), 19. Wichmann et al. (1997), 20. Krautter et al. (1997), 21. Zapatero Osorio et al. (2002), 22. Barrado y Navascués et al. (2003), 23. Rigliaco et al. (2012), 24. Hernández et al. (2014), 25. Kraus et al. (2017), 26. Preibisch et al. (1998), 27. Caballero et al. (2006), 28. Herczeg & Hillenbrand (2014), 29. Nguyen et al. (2012), 30. Wahhaj et al. (2010), 31. Sacco et al. (2008), 32. White & Hillenbrand (2004), 33. Venuti et al. (2019), 34. Riaz et al. (2006).